

**Effects of Fiber Architecture and Through-the-Thickness Stitching on
Permeability and Compaction of Textile Preforms**

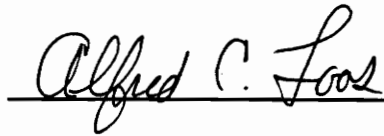
by

Kandathil Eapen Verghese

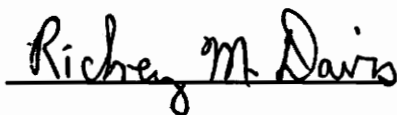
Thesis submitted to the Faculty of the
Virginia Polytechnic Institute and State University
in partial fulfillment of the requirements for the degree of
Master of Science

in

Materials Science and Engineering



Alfred C. Loos, Chair



Richey M. Davis



Ronald G. Kander

February, 1996

Blacksburg, Virginia

C.2

LD
5655
V855
1996
V474
C.2

ABSTRACT

The present work is a detailed study of the parameters that are involved in the characterization of fabric systems. These fabric systems are used as reinforcements in composite structures. Processes such as Resin Transfer Molding and Resin Film Infusion Molding that are used to manufacture composite structures, depend heavily on the responses of these reinforcements for their success. Fabric systems have undergone rapid changes over the years and have reached extremely advanced and complex forms. Near net shape preforms have become popular, and techniques such as multi-axial warp knitting and 3-D braiding are used to accomplish this. Further, the combination of these preforms with manufacturing processes such as Resin Transfer Molding and Resin Film Infusion Molding have resulted in the fabrication of complex composite components. The viability of these techniques for mass production has resulted in wide spread attention over recent years.

The problem of estimating the resistance of a given textile preform to the flow of resin or any fluid medium is characterized by its permeability. This quantity is dependent on the pore architecture and is therefore system dependent. The permeability of a preform changes with fiber volume fraction due to the changes in pore architecture. It is therefore critical to understand this quantity apriory, in order to ensure efficient fabrication of composite structures.

The complex nature of the pore architecture, makes permeability assessment an extremely difficult issue. Repeatability of test runs can become a difficult task as small inherent changes in the preform, can result in differences in pore structure and therefore result in different permeabilities. This study therefore tries to address this issue by incorporating a special study on the effects of statistics in permeability measurements. High costs of material handled, leads to limited testing and therefore small data bases. It is therefore important to take care while selecting the descriptive population distribution. The Student's t Test was used in this study to generate 50% confidence bands around the steady-state permeability data obtained on tests run using Type 162 E-glass fabric. The results were then compared with a similar advancing front permeability test. The results were found to be extremely encouraging.

The following work also involves the detailed study of compaction behavior of both multi-axial warp knit and braided preforms. Power law regression fit curves were obtained on the data in order to describe the change in fiber volume fraction with respect to applied external pressure, over a range of fiber volume fractions. Since the advent of composites, weak interfacial properties such as delamination and impact resistance have caused considerable concern in the community. Recently, through the thickness reinforcing techniques such as stitching have gained importance as being an inexpensive solution to this apparent problem. The present work involves the study of the effects of stitching density on compaction and permeability. Preforms with four stitching densities were tested along with a similar batch of unstitched preform, and regression curves were fitted to the data obtained. The effects of braiding angle in 2-D, triaxially braided preforms was also studied as a part of trying to understand this

ancient yet extremely interesting form textile manufacturing. Effects of thickness in 2-D, triaxially braided preforms was also examined. A small amount of work was also done to study the effects of sizing/finishing on compaction and permeability. Both, 7781, E-glass and AS4 Graphite fabric were tested.

ACKNOWLEDGMENTS

The author wishes to thank the following people for their contribution to this work

- Dr. A. C. Loos for his encouragement, advice and most of all confidence in my abilities. Without his support this work would not have been possible.

- Drs. R. M. Davis and R. G. Kander for taking time out of their busy schedules to serve on my committee.

- Anand Rau for his many insightful and stimulating comments into both research and life in general. His friendship and advice in trying times will always be greatly appreciated.

- John Fingerson for initially training me to do permeability tests and later helping me throughout the course of this research.

- Archie, Bill Shaver, R. A. Simonds, Joseph T. Price-O'Brien for their support and cooperation.

- CIT, National Science Foundation and McDonnell Douglas Aerospace for their support.

- My parents and family whose love, support, and guidance through the years, have helped me become who I am. Words fail miserably in trying to convey my deep sense of regard and appreciation.

- Last, but not the least, the Lord Almighty, whose blessings have always supported and nurtured my goals and principles in life.

Table of Contents

Abstract	ii
Acknowledgments	v
Table of Contents	vi
List of Figures	ix
List of Tables	xiv
Chapter 1	
Introduction	1
Chapter 2	
Literature Review	5
2.1 Permeability	5
2.1.1 Relationships	6
2.2 Compaction	14
2.3 In-plane Permeability	15
2.4 Through-the-thickness Permeability	18
2.5 Factors which Influence Permeability	20
2.5.1 Wettability and Capillary Effects	20
2.5.2 Sizing Effects	23
2.5.3 Damage Tolerance and Stitching Effects	24

Chapter 3

Fabric Characterization	28
3.1 Materials	28
3.1.1 Fabrics	28
3.1.2 Preforms	30
3.1.3 Fluid	32
3.2 Test Fixtures	32
3.2.1 15 cm ² Steel Fixture	32
3.2.2 5 cm ² Steel Fixture	33
3.2.3 NASA Brass Fixture	37
3.3 Material Parameters	37
3.3.1 Compaction	37
3.3.2 Steady State Permeability	44
3.3.3 Advancing Front Permeability	51

Chapter 4

Analysis of Permeability Measurements	53
4.1 Confidence Bounds on Steady-State Permeability	54
4.2 Advancing front Permeability	59
4.3 Discussion	63

Chapter 5

Results	64
5.1 Comparison of Test Fixtures	64

5.2 Thickness Effects in Multi-axial Warp Knit Preform	66
5.3 Effects of Batch Variation in Multi-axial Warp Knit Preforms	70
5.4 Through-the-Thickness Stitching Effects	73
5.5 Braided Preforms	109
5.5.1 Braiding Angle Effects	109
5.5.2 Thickness Effects	111
5.6 Sizing Effects on Permeability	117
5.6.1 AS-4 Carbon Fiber	121
5.6.2 Glass Fiber	121
Chapter 6	
Conclusions and Future Work	131
References	135
Vita	140

LIST OF FIGURES

Figure3.1	Sketch of the cavity of the 15cm ² steel fixture	34
Figure3.2	Photograph of the 15cm ² steel fixture	35
Figure3.3	Schematic of the through-the-thickness fixture	36
Figure3.4	Photograph of the 5cm ² steel fixture	38
Figure3.5	Schematic of the NASA brass fixture	39
Figure3.6	Photograph of the NASA brass fixture	40
Figure3.7	Compaction pressure as a function of fiber volume fraction of F-72 finished 7781 E-glass fabric	43
Figure3.8	Through-the-thickness permeability as a function of fiber volume fraction of F-72 finished 7781 E-glass fabric	48
Figure3.9	Schematic of the in-plane fixture	49
Figure3.10	In-plane permeability as a function of fiber volume fraction of F-72 finished E-glass fabric, warp direction	50
Figure4.1	Flow rate as a function of pressure gradient for 162 E-glass fabric in the fill direction	55
Figure4.2	Fill direction steady state permeability for 162 E-glass fabric	56
Figure4.3	Fill direction permeability for 162 E-glass, along with the statistical confidence bounds	58
Figure4.4	Schematic diagram of the 1-D line source to line sink fluid infiltration condition	60

Figure4.5	Inlet pressure versus Infiltration time for E-glass fabric in the fill direction	62
Figure5.1	Fiber volume fraction as a function of compaction pressure of a 3k AS-4 fabric. Comparison of data obtained from different fixtures	65
Figure5.2	Through-the-thickness permeability as a function of fiber volume fraction of a multi-axial warp knit preform. The preforms were from batch`95 with a 0.5" stitch spacing and a 1/8" stitch pitch. Comparison of NASA brass and 5cm ² steel fixtures	67
Figure5.3	Through-the-thickness permeability as a function of fiber volume fraction of a multi-axial warp knit preform. The preforms were from batch`95 with a 0.2" stitch spacing and a 1/8" stitch pitch. Comparison of NASA brass and 5cm ² steel fixtures	68
Figure5.4	Fiber volume fraction versus compaction pressure for multi-axial warp knit preform. Tests performed on NASA brass fixture with batch`94 preforms	69
Figure5.5	Through-the-thickness permeability as a function of fiber volume fraction for multi-axial warp knit preforms. Tests conducted on the NASA brass fixture with batch`94 preforms	71
Figure5.6	Compaction pressure as a function of fiber volume fraction for a 70-ply multi-axial warp knit preform. Tests performed on the NASA brass and 15cm ² steel fixtures	72
Figure5.7	Along the stitching permeability as a function of fiber volume fraction for 70 ply multi-axial warp knit preforms. Tests conducted on 15cm ² steel fixture	74
Figure5.8	Through-the-thickness permeability as function of fiber volume fraction for 70-ply multi-axial warp knit preform. 0.5":1/8" stitched preform. Tests conducted on NASA brass fixture	75
Figure5.9	Through-the-thickness permeability as a function of fiber	

	volume fraction for 70-ply multi-axial warp knit preforms. Tests were conducted on the 5cm ² steel fixture	76
Figure5.10	Fiber volume fraction as a function of compaction pressure for multi-axial warp knit preforms with different stitch densities	81
Figure5.11	In-plane permeability as a function of fiber volume fraction for multi-axial warp knit preforms measured along the stitching direction	83
Figure5.12	In-plane permeability as a function of fiber volume fraction for multi-axial warp knit preforms measured along the stitching direction	84
Figure5.13	Bar graph comparison of in-plane permeability of preforms with a 0.5" stitch spacing at specific fiber volume fractions	85
Figure5.14	Bar graph comparison of in-plane permeability of preforms with a 0.2" stitch spacing at specific fiber volume fractions	86
Figure5.15	In-plane permeability as a function of fiber volume fraction for preforms with different stitch spacing and a stitch pitch of 1/6". Tests were conducted along the stitching direction	87
Figure5.16	In-plane permeability as a function of fiber volume fraction for preforms with different stitch spacing and a stitch pitch of 1/8". Tests were conducted along the stitching direction	88
Figure5.17	Fiber volume fraction versus compaction pressure. Comparisons between preforms with different stitch spacing and a stitch pitch of 1/6"	89
Figure5.18	In-plane permeability as a function of fiber volume fraction for multi-axial warp knit preforms with a stitch spacing of 0.5" measured normal to the stitching direction	92
Figure5.19	In-plane permeability as a function of fiber volume fraction for multi-axial warp knit preforms with a stitch spacing of 0.2" measured normal to the stitching	

	direction	93
Figure5.20	Bar graph comparison of in-plane, normal to the stitching direction permeability of preforms with a 0.5" stitch spacing at specific fiber volume fractions	94
Figure5.21	Bar graph comparison of in-plane, normal to the stitching direction permeability of preforms with a 0.2" stitch spacing at specific fiber volume fractions	95
Figure5.22	Through-the-thickness direction permeability as a function of fiber volume fraction for multi-axial warp knit preforms	96
Figure5.23	Through-the-thickness direction permeability plots of multi-axial warp knit preforms at specific fiber volume fractions	97
Figure5.24	Optical micrograph of the area around a stitch of a preform with 0.5" stitch spacing and 1/8" stitch pitch	99
Figure5.25	Optical micrograph of the area around a stitch of a preform with 0.2" stitch spacing and 1/8" stitch pitch	100
Figure5.26	Optical micrograph of the area around a stitch looking from the bottom of a preform with 0.5" stitch spacing and 1/8" stitch pitch	101
Figure5.27	Optical micrograph of the area around a stitch looking from the bottom of a preform with 0.2" stitch spacing and 1/8" stitch pitch	102
Figure5.28	Photograph taken on the Nikon Epiphot around a stitch of a preform with 0.5" stitch spacing and 1/8" stitch pitch	103
Figure5.29	Photograph taken on the Nikon Epiphot around a stitch of a preform with 0.2" stitch spacing and 1/8" stitch pitch	104
Figure5.30	Photograph taken on the Nikon Epiphot between two stitches of a panel with 0.5" stitch spacing and 1/8" stitch pitch	105

Figure5.31	Photograph taken on the Nikon Epiphot between two stitches of a panel with 0.2" stitch spacing and 1/8" stitch pitch	106
Figure5.32	Schematic diagram of the misalignment in the individual fiber tows caused by stitching	108
Figure5.33	Fiber volume fraction as a function of compaction pressure for preforms with 60 and 70 degree braiding angles	110
Figure5.34	In-plane permeability as a function of fiber volume fraction for the braided preforms measured along the stitching direction	113
Figure5.35	In-plane permeability as a function of fiber volume fraction for the braided preforms measured normal to the stitching direction	114
Figure5.36	Through-the-thickness permeability as a function of fiber volume fraction for the braided preforms	115
Figure5.37	Fiber volume fraction as a function of compaction pressure for thick and thin braided preforms. Braiding angle was 60 degrees	116
Figure5.38	In-plane permeability as a function of fiber volume fraction for thick and thin braided preforms , measured along the stitching direction	118
Figure5.39	In-plane permeability as a function of fiber volume fraction for thick and thin braided preforms , measured normal to the stitching direction	119
Figure5.40	Through-the-thickness permeability plot for the thick and thin braided preforms	120
Figure5.41	In-plane, warp direction permeability as a function of fiber volume fraction for 'W' sized and unsized AS4 fabric	122
Figure5.42	In-plane permeability as a function of fiber volume fraction for 'W' sized and unsized AS4 fabric, measured in the fill direction	123

Figure5.43 In-plane permeability as a function of fiber volume fraction for unsized AS4 124

Figure5.44 Fiber volume fraction as a function of compaction pressure for F-16 and F-72 finished 7781 E-glass fabric 125

Figure5.45 In-plane permeability plots for finished E-glass fabrics measured in the warp direction 126

Figure5.46 In-plane permeability plots for finished E-glass fabrics measured in the fill direction 127

Figure5.47 Through-the-thickness permeability as a function of fiber volume fraction for finished E-glass fabrics 128

LIST OF TABLES

Table 3.1	Fiber areal weights of fabrics and preforms	29
Table 4.1	Permeability power law regression fit constants	57
Table5.1	Densities of the stitched preforms	78
Table5.2	Constants for the compaction fit equation	80
Table5.3	Constants for the permeability fit equation	91
Table5.4	Constants for the permeability fit equation	112
Table5.5	Constants for the permeability fit equation	129

Chapter 1

INTRODUCTION

Over the years, several composite manufacturing techniques have been tried and tested. However, resin transfer molding (RTM) has shown greater promise than most others as being a good and effective mass production technique. One of the reasons for this increase in popularity is the ability to use near net shape techniques to manufacture complex shapes. Another reason for its success are the relative low investment costs involved. Today, both the automotive as well as aerospace industries are beginning to accept this process.

Resin transfer molding has several offshoots that essentially use the same basic principle, but also incorporate modifications. Reaction injection molding (RIM), combines multiple thermosetting monomers into a single chamber by high speed impingement mixing. The resultant mix is then hydraulically pumped into a closed mold whereupon the monomers react to form the hardened thermosetting polymer. Since this process does not include reinforcing fibers, structurally strong parts cannot be fabricated. To overcome this difficulty, reinforced reaction injection molding (RRIM) is used. However, the use of just 10-15% fiber volume fraction, limits the use of the resulting products. Structural reaction injection molding (SRIM) makes use of a fabric preform, and therefore results in the fabrication of stronger structural parts.

The vacuum assisted resin injection (VARI) process, makes use of vacuum along with injection pressure [1]. All the above techniques share common features which include use of liquid resin feed stock, that hardens through an exothermic chemical curing process, and requires a matched mold.

Resin transfer molding involves injecting resin into a closed mold containing a pre-placed dry fabric reinforcement. The reinforcement could be arranged in any direction depending on design requirements. The mold faces are compressed against the preform in order to achieve the desired fiber volume fraction. A pressure pot or constant flow rate pump is used to deliver resin at the required pressure and temperature. Before injection, the resin is placed in a vacuum oven to remove entrapped gases which tend to form voids in the final part. Sometimes, vacuum is applied at the outlet during actual injection in order to assist both the flow of a low viscosity resin into the preform as well as reduce the probability of creating voids. Once the resin has completely infiltrated the preform, the cure cycle is initiated in order to cure the resin. After the cure cycle is complete, the component is released from the mold. More recently, resin film infusion (RFI) molding has been gaining popularity in the aerospace industry to manufacture complex near net shape parts such as wing structures. The technique uses a degassed film of resin that is placed on the tool. The preform is then placed on top of this film and the assembly is then placed inside a mold. A vacuum bag is placed over the mold and a strong vacuum is drawn. The vacuum together with the mechanical force applied onto the preform to get it to the desired fiber volume fraction, forces the resin to move through the thickness of the

preform to saturate it. The resin saturated preform is then cured. One of the main objectives of this research is to address the relationship between preform compaction and permeability. Permeability, is a measure of the resistance offered by a preform to fluid flow through it. It is extremely important to estimate this, as the resistance changes dramatically with external compaction and can therefore change the required injection pressure significantly. Both the inplane and through-the-thickness permeabilities of the preform were investigated.

A statistical analysis was performed to determine the confidence limits on the permeability data. The small density of population that one is able to generate from the inherent nature of the test as well as the prohibitive costs involved in repetitive testing. The section tries to impress the existence of small inherent variations in the fabric that are beyond the control of the user that makes repeatability of test results an area of importance. Confidence limits therefore become a necessity while trying to report permeability data. The statistical results obtained for E-glass fabric when input into the standard 1-D model to predict infiltration times, has proven to be of great success when compared to actual panel production times. Chapter 4, deals with the discussion of these results.

In recent years there has been considerable interest in the use of through-the-thickness reinforcement to enhance the interlaminar strength and damage tolerance of textile structural composites. One commonly used technique to achieve this is through-the-thickness stitching. An important part of this research is therefore, to

study the permeability and compaction, of preforms consisting of different stitching densities. The preform was a multiaxial warp knit fabric, made up of AS4 Carbon fiber, stitched in the through-the-thickness direction. Stitching density is altered by either changing the stitch spacing or stitch pitch. Results from all of the above mentioned tests have been presented in chapter 5. The chapter also presents permeability and compaction data obtained from 2-D braided preforms with different braid angles and thickness. Finally, tests were performed with different test fixtures to study the effects of sample size on the permeability. The results of these tests are discussed at the beginning of chapter 5.

Over the years, much research has been focused on the interface between the fiber and matrix. In order to improve the properties of the interface, different finishes are applied to the fibers or sizings are used to coat the fiber. Permeability and compaction results of E-glass fabrics with different finishes and 'W' sized and unsized carbon fabric systems are reported.

Chapter 2

LITERATURE REVIEW

Resin Transfer Molding (RTM) came into existence due to two important factors in the late 1970's. The first one was the oil embargo that created a shortage in the supply of petrochemicals, which in turn resulted in the sharp increase in prices of polyester resins, glass, peroxides and other related materials that were being used at that time by the Fiberglass Reinforced Polyester (FRP) industry. The second was the new governmental regulations on styrene emissions not only at the place of work but also in the exhausted air. Several advantages such as light weight molds, lower tooling costs, and overall energy savings ensured the early growth of the process and today it is considered to be the most viable process for the manufacture of high performance composite structures and has therefore become of great interest to both the aerospace as well as the automotive industries. Over the past couple of years, work has been focused on trying to understand issues such as mold design, optimum inlet, outlet and vent placement, preform permeability, preform compaction, fiber resin interaction; e.g., contact angle, capillary pressure and surface tension. Several research groups have also made attempts to try and model the actual process either numerically or analytically.

2.1 PERMEABILITY

The following section details the various governing relationships that are used in the study of permeability. Some of the following relationships are used more frequently than others. The section will also try to highlight the various models

that have been proposed in order to study this otherwise, extremely complex area of transport.

2.1.1 Relationships

The commonly used model for flow of resin through a reinforcement is one that was put forth by Darcy [2]. This model describes the flow of Newtonian fluids through porous media and it states that the flow rate (Q) through a constant area specimen is proportional to its cross sectional area (A), the pressure drop across the specimen (ΔP) and inversely proportional to the viscosity of the fluid (μ) and the length (L).

The equation is then given by

$$Q = \frac{S A \Delta P}{\mu L} \quad (2.1)$$

The above equation is known as the Darcy's Law, and (S) in the equation stands for the all important parameter, "Permeability". It is a constant for the fabric under a fixed compaction load and has dimensions of [m^2]. The differential form of Darcy's law for an anisotropic medium can be expressed as

$$v_i = - \frac{S_{ij} p_{,j}}{m} \quad (2.2)$$

where S_{ij} is the permeability tensor. There has however been some debate in the past couple of years on the validity of Darcy's Law. Gauvin and Chibani [3] have reported experimental RTM results, where the flow was not linearly

proportional to the pressure gradient. They assume that the reason for the discrepancies is that the resin does not behave like a Newtonian fluid. Molnar, Trevino and Lee [4] have also reported similar results while Fracchia and Tucker [5] and Gebart, Strombeck and Lundemo [6] have reported excellent agreement between experiments and Darcy's Law.

In composites manufacturing it is often required to know the influence of fiber volume fraction on the permeability as it is the fiber volume fraction (V_f) that determines the mechanical properties of the final product. This relationship described by the Kozeny-Carman equation

$$S = \frac{R^2 (1 - V_f)^3}{4k V_f^2} \quad (2.3)$$

where (k) is the so-called Kozeny constant [7]. This equation was initially developed for isotropic granular beds consisting of ellipsoids and it has been assumed to be valid for a fibrous porous medium where flow is along the fibers. The fiber volume fraction is determined by the following equation:

$$V_f = \frac{W}{\rho A h} \quad (2.4)$$

where ρ is the fiber density, W is the total mass of the fibrous network, h is the thickness and A is the flow area normal to the direction of flow.

The obvious inaccuracy in the transverse permeability of an aligned fiber bed calculated by the Kozeny Carman equation led to the modification of the above equation by Gutowski et al. [8]. Gutowski et al. [8] proposed the following model

$$S = \frac{R^2 \left(\sqrt{\frac{V'_a}{V'_f}} - 1 \right)^3}{4k' \left(\frac{V'_a}{V'_f} + 1 \right)} \quad (2.5)$$

where (V'_a) and (k') are the fiber volume fraction at which flow is completely cut off and the Kozeny constant in the transverse direction, respectively. The model was developed using a modified Kozeny-Carman equation and then defining the individual quantities in the equation by assuming a certain fiber geometry for transverse flow. The equation agrees with the standard Kozeny Carman equation when V'_a is equal to 1, but gives a much lower value for permeability when V'_a is less than 1. Hercules AS-4 and Hysol-Grafil XA-S (Courtaulds) graphite fiber systems were used in order to validate the proposed model.

Gebart, Strombeck and Lundemo [6] have developed equations that explain both the flow of fluid perpendicular and parallel to the fibers. The method used essentially involved defining a “representative cell”, which consisted a of periodic arrangement of fibers in a given region. The assumptions made are that the variation in area is slow so that the inertia effects can be neglected and that all the fibers are perfectly aligned with one another and are continuous. The equations are

$$S_{\perp quad} = \frac{16}{9p\sqrt{2}} \left(\sqrt{\frac{V_{fmax}}{V_f}} - 1 \right)^{\frac{5}{2}} R^2 \quad (2.6)$$

and

$$S_{\perp hex} = \frac{16}{9p\sqrt{6}} \left(\sqrt{\frac{V_{fmax}}{V_f}} - 1 \right)^{\frac{5}{2}} R^2 \quad (2.7)$$

where $S_{\perp quad}$ and $S_{\perp hex}$ are the permeabilities perpendicular to the fiber for quadratic and hexagonal packing, R is the fiber radius and V_{fmax} is the maximum fiber volume fraction. A modified Kozeny-Carman equation is used to determine the permeability parallel to the fiber direction and is written as

$$S = \frac{8R^2}{c} \frac{(1 - V_f)^3}{V_f^2} \quad (2.8)$$

where the constant c takes on values depending on the nature of packing or what is also known as the shape factor. For the quadratic packing sequence c is 57 and for hexagonal c is 53.

Kim et al. [9] have proposed an empirical model which is of the following form

$$K = A(BV_{\infty} - V_f)^4 \quad \text{for:} \quad \begin{cases} V_f \leq V_{\infty} \\ 1 \leq B \leq \frac{1}{V_{\infty}} \end{cases} \quad (2.9)$$

here A and B are constants for the model.

Recently, Skartsis, Kardos, and Khomami [10] reviewed the theoretical and experimental studies concerned with the flow of resin through an aligned porous medium and have concluded that the Kozeny-Carman equation does not accurately describe the permeability behavior even though the flow might be Newtonian and have attributed this to the existence of bed non-uniformities. They have also stated that the Kozeny constant is valid only for a narrow range of porosities, usually greater than 0.6.

Permeability of porous materials depends very strongly on the morphological structure. Due to the complexity of the fiber architecture and the lack of a standardized permeability test method, many researchers have attempted to determine the permeability either analytically or numerically.

Gauvin and Chibani [11] have done a considerable amount of detailed work on the modeling of permeability of non-woven fiber mats. They have tried to include the effects of shear flow and drag on the fluid as it passes over the individual fiber rovings. Their expressions for the losses stem from the equations of continuity and momentum. They have also used the Lamb's equation to compute the drag coefficient. They introduced a new parameter representing the surface density of a constitutive layer, which while depending on the roving diameter, also depended on the rovings pattern. They did find excellent agreement in the values obtained from their model and experiments.

Greve and Soh [12] performed some of the early work on measuring the permeability of anisotropic media. Their work consisted of both analytically modeling anisotropic infiltration as well as performing experiments to actually confirm the results. The modeling essentially made use of the equation for continuity and the Darcy's Law, in conjunction with the relevant coordinate transformations in order to correctly fit the elliptical profile of the flow front through the anisotropic porous medium. They were able to present results that showed that the effective isotropic permeability was the geometric mean of the principal permeabilities. Their experimental results matched well with the model prediction.

Parnas and Phelan [13] were able to successfully take into account the effects of heterogeneities in preforms. They classified the heterogeneities into two categories, the first one being due to the structure of the fiber bundles itself and the second one being due to the boundaries such as edges etc. They were able to use the Brinkman equation to estimate the effects of the boundary heterogeneities. They also found that the heterogeneities due to the fiber bundle structure was actually responsible in the creation of voids and therefore higher effective permeabilities.

Phelan [14] also used the Brinkman equation to model axial and transverse flow through square arrays of solid and porous cylinders. These cylinders are analogous to fiber bundles. Calculations showed that the flow rate can be enhanced by the cylinder permeability. Preliminary experimental results also indicated that permeability could affect the fluid mechanics of the flow around the fiber.

Sadiq, Parnas and Advani [15] recently published experimental results of fluid flow in an ideal fiber bed consisting of cylindrical rods, either aluminum or

nylon, in a square arrays which verified the air entrapment mechanism assumed in the model published by Parnas and Phelan [13]. Their experiments showed that the voids formed when the resin flow front tended to encompass the fiber bundles and then kept them stable. The fluid was injected into the mold transverse to the rods. Lower volume fractions inside the tows produced smaller voids. The experimental permeability was higher than that of the solid rods with the same diameter.

Berdichevsky and Cai [16] used their self consistent model to evaluate the permeability of an aligned fiber bundle. The major idea in any self consistent model is to substitute the effects of the tow on one fiber by the effect of some continuum medium with unknown properties on this fiber. The properties are to be such that some consistency conditions be satisfied in order to generate the necessary equations for determining these properties. The consistency conditions used by Berdichevsky and Cai, were the standard equivalence of the average flow near the fiber to that in the fiber mat condition, and the added consistency of energy dissipation condition. Their model gives formulas for both longitudinal and transverse permeabilities as a function of the fiber volume fraction. The normalized longitudinal permeability is expressed as

$$S_x^* = \frac{1}{8V_f} \left[\ln \frac{1}{V_f^2} - (3 - V_f)(1 - V_f) \right] \quad (2.10)$$

where V_f is the fiber volume fraction. Likewise, the expression for the normalized transverse permeability is given by

$$S_z^* = \frac{1}{8V_f} \left[\ln \frac{1}{V_f^2} - \frac{1 - V_f^2}{1 + V_f^2} \right] \quad (2.11)$$

In addition to the above, their finite element simulation considered the effect of four idealized packing structures on the permeability. The packings were square, hexagonal, hollow square and hollow hexagonal. The plots comparing the results obtained using the self consistent model and the finite element solutions, showed that knowledge of the fiber structure was also important in addition to the volume fraction or porosity in order to predict the permeability correctly.

Finally a unified model, composed of both the self-consistent method and the finite element simulation, was proposed which evaluates the permeability as a function of two variables, the ultimate fiber volume fraction similar to that defined by Gutowski [8], and the actual fiber volume fraction. This model accurately portrays the physics of flow passing through obstacles, and therefore, different fiber packing arrangements can be considered.

Astrom, Pipes, and Advani [17] developed flow rate versus pressure gradient relationships for flow of Newtonian fluids through spherical and cylindrical beds. For the flow past spherical beds they have used the Carreau viscosity model in conjunction with the capillary flow assumption. The inertia terms were neglected in the equation of motion and the capillary region was assumed to be circular. The average velocity equation thus obtained was then used with the appropriate hydraulic radius for spherical beds in order to obtain the required relationship. For flow past cylindrical beds the same approach was used, however a correction in the hydraulic radius was made to accommodate the change in geometry.

Lastly, Gauvin, Kerachni and Fisa [18] have studied the effects of mat surface density, and have developed a model which takes into account the variations in the surface density. They reported that variations in mat surface density tend to

change the local permeability, which in turn cause fairly large variations in the mold fill times. Their work highlights the fact that it is impossible to develop a unified permeability model and that studying the permeability on a case by case basis is a more accurate method.

2.2 COMPACTION

The response of a porous medium to the application of load is perhaps the starting step to understanding it's resistance to flow of fluids. There has not been a significant amount of work that has focused on compaction, reported in the literature. Most research groups have neglected the compaction effects and focused mostly on permeability. However, the two parameters cannot be uncoupled.

Batch and Cuminsky [19] published extensive work in the area of fabric compaction. They have found that a random fiber mat is easily compressible and has a larger thickness change during mold closing than an unidirectional fabric. The fiber volume fraction varies depending on the amount and type of each layer in a given cross section. In multilayered composites, each layer compresses under the same pressure, hence the change in layer thickness during mold closing decreases as elasticity decreases. They have proposed a model that combine the advantages of both the FENE spring model and the model suggested by Gutowski [8]. The fiber bed is considered to be a stiffening set of non-linear springs and then, N the compaction stress normal to the fiber mat is written

$$N = K(V_f) (V_f - V_o) \quad (2.12)$$

where, V_0 is the initial fiber volume fraction. The fiber elastic constant, K is defined as

$$K = K_0 \quad \text{for } V_f < V_{f, \text{const}} \quad (\text{Hookean regime}) \quad (2.13)$$

$$K = K_0 \frac{1-\eta}{\eta} \frac{1/V_0 - 1/V_f}{1/V_f - 1/V_\infty} \quad \text{for } V_f \geq V_{f, \text{const}} \quad (2.14)$$

(non Hookean regime)

where η is the packing inefficiency and $V_{f, \text{const}}$ is the fiber volume fraction at which the transition from the Hookean to the non Hookean regime takes place. They have also found that for random and aligned fibers, V_0 and V_∞ are large and also the deformation is almost entirely in the non Hookean regime.

Pearce and Summerscales [20] have drawn some interesting points in their studies. They found that unrestrained compaction of fabric results with little lateral spreading, but results in dissipation of stored strain energy through fiber rearrangement. Also a power law regression can be fitted to the initial loading cycle and that the exponent of this equation is lower for a single layer as opposed to a stack of fabric. Fabric-fabric interaction provides a greater constraint compared with fabric-platen interaction. Compaction load dissipation follows an exponential relationship with time and the percentage residual load on the fibers is linearly dependent on the fiber volume fraction.

2.3 IN-PLANE PERMEABILITY

This section will discuss the experimental work done to characterize in-plane permeability behavior of various fiber assemblies. It is important to understand

that fiber systems with almost the same fiber diameter and porosity may have very different permeabilities. Factors such as flow direction, weave type, stitching etc. change in permeability.

Earlier work done by Adams, Miller, and Rebenfeld [21] measured in-plane warp and fill permeability values for three fabric types:

- (1) biaxially woven monofilament
- (2) bi - and triaxially woven multifilament and
- (3) several nonwoven fabrics

For the first type, the in-permeability values were higher for the fabrics with either the larger mesh or the twill weave pattern due to the larger pore structure of these materials.

For the second type, the in-permeability showed anisotropy when two plies were layered with the weave direction. The anisotropy was removed when the two layers were stacked in a cross ply arrangement one on top of the other. The authors also concluded that in a highly random oriented fiber lay up, the permeability would tend to become isotropic.

Lam and Kardos [22] conducted tests on different unidirectional fiber ply stacks. They found that the in-plane permeability decreased as the alternating plies were laid down at greater angles. The 0° - 90° lay-ups had the lowest permeability. This was then attributed to the increase in the tortuosity as the plies were rotated further off-axis.

Adams, Russel, and Rebenfeld [23] performed numerous tests on anisotropic fiber beds and developed equations that can be used to determine the permeability tensor of a homogenous, anisotropic porous medium using the center

port radial infiltration technique. They tried to highlight the difference between anisotropy and spatial variation and cited examples to bring out the difference. Their work involved analyzing the flow front position as a function of time during a radial injection and using the data to determine the components of the permeability tensor. This approach can be used to determine the components of the in-plane permeability tensor of anisotropic preforms.

The existence of two kinds of pores, namely the macroscopic and microscopic was noted. The macro level pores exist between adjacent filaments of each weave and the micro level pores exist at the filament-filament cross over. They conducted work on heterogeneous preforms and have shown that the permeability could be enhanced by replacing low permeability layers with higher permeability layers. Placing the high permeability layers near the center of the preform resulted in a higher permeability for the preform. The increase was attributed to the transverse flow from the high to low permeability layers. This was in turn thought to be a result of a pressure gradient generated as the fluid moved further ahead in the more permeable layer as opposed to the low permeability layer.

Work reported by Molnar, Trevino and Lee [24] focused on measuring the permeability of three types of glass fiber mats:(1) continuous random mat; (2) stitched bidirectional mat and (3) stitched unidirectional mat.

For unidirectional mats the X-direction was along the fiber. For the bidirectional mat the X-direction was perpendicular to the stitching direction while Y-direction was along the stitching direction. For random mat, the X-direction was along the direction of flow. Their research showed that the X-direction permeability was the same as the Y-direction for the random mat. The X-direction permeability for the random mat was similar to that of the bidirectional at low porosity and similar to the unidirectional at higher porosities. The X-direction permeability of the

bidirectional mat was found to be higher than the unidirectional mat. It was also found that the Y-direction permeability of the random mat was the highest, followed by the bidirectional and then the unidirectional mats. For all the mats however, the permeability decreased with decrease in porosity.

Recent work has been conducted by Wang, Wu, and Lee [25]. They performed center port, radial infiltration tests on three types of fiber mats

- (1) continuous random fiberglass mat;
- (2) stitched bidirectional fiberglass mat; and
- (3) 8-harness woven graphite mat.

It was seen that although the bidirectional mat was made up of two unidirectional mats placed in a cross ply arrangement, there was a net elliptical flow front. This was attributed to the difference in the gaps between the bundles in the top and bottom layers. They were also able to notice that the ellipse was oriented to a certain angle in the 8-harness fabric, and this was found to be due to the existence of a certain crimp angle. Their work also showed that the random fiber mat exhibited the highest permeability. The permeability of the 8-harness mat was found to be the least and this was attributed to its tight woven structure.

2.4 THROUGH-THE-THICKNESS PERMEABILITY

During RTM, resin tends to flow in both the in-plane as well as through the thickness directions. It is therefore important to understand the factors that influence the permeability in the transverse direction. One of the most important factors is the stacking sequence and preform assemblage.

Molnar, Trevino, and Lee [24] looked at the through the thickness permeability behavior for random and unidirectional mats. For a pure unidirectional mat, the close packing of the individual layers was found to greatly reduce the permeability. However, by adding random mats with higher permeability, the fluid was able to quickly reach the unidirectional layers. Once this layer was saturated, the flow was able to progress through the preform.

Loos and Weideman [26] characterized the through the thickness permeability behavior for preforms composed of Hexcel Hi-Tech multiaxial warp knit fabric and TTI IM7/8HS fabric. For the TTI material it was found that thickness had no effect on permeability. Tests were also performed on the Hexcel material using different stitching densities and it was seen that the heavily stitched material exhibited the greatest permeability and this was attributed to the stitching providing a low resistance pathway for fluid movement.

Recent work was reported by Wu, Wang, and Lee [27] on three fabric systems:

- (1) continuous strand random fiberglass;
- (2) stitched bidirectional fiberglass; and
- (3) 8-harness woven graphite fiber mat.

It was seen that for the 8-harness material, the inlet pressure is very high and this was then attributed to the tightly woven structure of the material. The study also showed that at very high flow rates, a nonlinear rise in pressure would be seen with flow rates. Their work also highlighted the effects of stacking on the through the thickness permeability. Different stacking sequences resulted in different permeabilities and this was then attributed to the fact that different stacking arrangements resulted in different compaction characteristics. Another reason for the variation was directed

to the fact that the interface region between the individual plies had different flow characteristics as compared to the bulk.

2.5 FACTORS WHICH INFLUENCE PERMEABILITY

The previous sections have reinforced the idea that permeability is largely dependent on the fiber orientation and flow direction. However, there are other factors that can influence the flow of resin through the reinforcement and they could be either physical or chemical in nature. These include the, degree of preform saturation, capillary pressure, wetting behavior and material heterogeneity due to through the thickness stitching.

2.5.1 Wettability and Capillary Effects

In RTM, the plies are stacked in the desired orientation and the ply interfaces created can influence the in-plane and through-the-thickness permeabilities. Batch and Cuminsky [19] investigated this problem and presented three possible cases for the compression of a multi-ply preform. The cases were:

- (1) no interfacial effects;
- (2) interface has higher pore content than adjoining layers; and
- (3) interface has lower pore content than adjoining layers.

They also presented the following equation for the average fiber volume fraction, V_{avg} to describe all the three cases:

$$V_{avg} = \left(\sum_{i=1}^n \frac{W_i}{V_{f,i}} + \sum_{j=1}^{n-1} \frac{W_{inter,j}}{V_{inter,j}} \right)^{-1} \quad (2.15)$$

where:

W_i is the weight fraction of layer i after removal of the portion contained in the layer;

$W_{inter, j}$ is the weight fraction of each interlayer j ;

$V_{f, i}$ is the fiber volume fraction of layer i ; and

$V_{inter, j}$ is the fiber volume fraction of interlayer j .

They also found that the interlayer packing at the interface can influence the behavior in three ways:

- (1) interlayer packing changes axial permeability due to high fiber volume fraction at the interface;
- (2) interlayer packing affects the fiber volume fractions and thicknesses of each layer in the cavity; and
- (3) interlayer restricts transverse flow from layer to layer.

Another factor that influences the permeability is capillary pressure. This occurs at the air/fluid interface. Several researchers have tried to incorporate the capillary pressure term into the integrated form of the Darcy's Law and used the advancing front permeability measurement technique. Gutowski et al.[28] used the following expression for the net pressure to calculate the advancing front permeability.

$$\Delta P + \frac{\sigma \cos\theta}{m} \quad (2.16)$$

where the second term denotes the capillary pressure and includes the surface energy, σ , the wetting angle, θ , and the mean hydraulic radius, m . The mean hydraulic radius is defined as the ratio of the free volume and the wetted area and is represented by the expression:

$$m = \frac{d_f}{4} \left(\frac{1 - V_f}{V_f} \right) \quad (2.17)$$

where V_f is the fiber volume fraction and d_f is the fiber diameter. They found that the permeability value in the case of the advancing front test was always greater than the steady state permeability due to channeling.

Ahn, Seferis and Berg [29] derived an expression for the capillary pressure based on the porosity of the preform which is expressed as:

$$P_c = \frac{F}{D_f} \frac{(1 - \phi)}{\phi} \sigma \cos \theta \quad (2.18)$$

where D_f is the fiber diameter, ϕ is the porosity, and F is the form factor.

The form factor depends on the fiber alignment in the direction of flow. For flow along the fiber direction in an unidirectional preform, the form factor is equal to 4. For flow perpendicular to the fibers, it is equal to 2. Often the form factor is determined experimentally. Peterson and Robertson [30] have noted in their work that the capillary pressure increases with increasing fiber volume fraction and decreasing fiber diameter.

Dave and Houle [31] in their work on preform saturation and its effect on preform permeability have suggested that for flow through unsaturated porous media, the permeability is not a constant but is defined as:

$$S = S_e = S_i S_r \quad (2.19)$$

where S_e is the effective permeability. The intrinsic permeability, S_i depends on

the fabric geometry and was defined by the Kozeny-Carman equation. The relative permeability S_r varies from 0 to 1 depending on the fabric saturation.

Dave and Houle [31] stated that saturation in an initially dry preform depends on the capillary number, C_a , which was defined as:

$$C_a = \frac{\mu V}{\gamma_{lv}} \quad (2.20)$$

where μ is the viscosity, γ_{lv} is the surface tension of the resin and V is the velocity. Surface tension is an important factor as it determines the wettability of the reinforcing fibers by the resin. A high surface tension increases the difficulty in removing voids during infiltration. Work done by Williams, Morris and Ennis [32] showed an increase in the apparent value of the Kozeny constant as the surface tension of the liquid increased.

Wettability has been defined as the ability of a liquid to spread itself over a surface [33]. Complete wetting is critical for the manufacture of quality composite parts. In addition, full wet out helps to improve the mechanical properties of the composite. The contact angle between the resin and the fiber is an indication of the wettability of the liquid. The greater the contact angle, the lower the wettability of the liquid on the solid surface.

2.5.2 Sizing Effects

Ever since the beginning of composites, the issue of the interface between the fiber and the matrix has been of great interest. The adhesion level generally determines the performance quality of the composite. Several mechanisms

have been proposed to explain the adhesion phenomenon. Surface chemistry, surface topography, weak boundary layer and others are some of the different theories that have been mentioned. Today, the process of sizing fibers has received a lot of attention. Madhukar and Drzal, have published a four part paper series [34,35,36] in which they have discussed results obtained on a highly tailored system. Their work dealt with three different Hercules fiber systems namely the unsized AU4, the proprietary sized AS4 and the lightly sized epoxy coated AS-4C. A model epoxy system consisting of diglycidyl ether of Bisphenol-A (DGEBA) and an aromatic diamine curing agent, meta-phenylene diamine (mPDA) was used as the matrix material. Their work has shown that there exists a marked relationship between the mode of failure and the level of adhesion between the fiber and the matrix. AU-4 exhibited low values of interfacial strength and shear failure near the fiber surface. The AS-4 however showed higher values of interfacial shear strength and the locus of failure was interfacial without failure through the fiber surface. The surface coated AS-4C showed significant matrix cracking indicating a transition in the mode of failure. In as much as their work has shown the importance of sizing in order to improve the properties of the interface, not much has been done to try and understand the effects of sizing on the basic manufacturing parameters.

2.5.3 Damage Tolerance and Stitching Effects

More recent work has been directed towards improving the damage tolerance of composite parts. The low resistance to "in-plane" compression load failure and low interlaminar shear strength of composites fabricated from unidirectional prepreg tape has lead to extensive research in the areas of textile preforms. Different alternatives have been sought after, amongst them are braiding, superior matrix materials and through-the-thickness reinforcements. Munjal and Maloney [37] have

discussed the use of braiding in order to manufacture preforms with improved performance. In their paper, braiding has been compared to other manufacturing methods namely, filament winding, pultrusion and tape lay up. In braiding, the 0° axial fibers can be laid down easily in order to improve stiffness and structural integrity as compared to filament winding. However, braiding of high performance fibers, such as high modulus graphite, aramid and glass have shown to pose certain processing problems such as fuzzing, fraying and breakage. Impact area has also been found to be minimal compared to conventional laminated composites. Compression after impact is also higher and does not degrade in this case. It has also been found that although the initial strength is about 5-10% lower than filament winding, percentage degradation is much less.

The use of high performance systems such as improved epoxies, thermoplastics and high strain fibers have proved to be extremely expensive in spite of improved properties. Work performed by NASA and McDonnell Douglas [38] however showed that the incorporation of through-the-thickness reinforcement in the form of conventional stitching could improve the inplane properties of composites at substantially low costs.

Morales [39] has investigated the use of three types of stitching fibers, graphite, glass, and Kevlar.

Twisting of the fibers to form stitching threads, results in a dramatic change in properties. Twisting has to be performed in order to make the cross section rounder and to hold the individual fibers tighter. The resulting thread will therefore not snag upon stitching. The tensile strength of graphite fibers reduced 56% from single fiber to thread configuration. There was a further reduction upon looping the fiber.

This then resulted in a net 82% reduction in the tensile strength from the thread to the

loop configuration. Glass showed a similar 67% drop in tensile strength whereas Kevlar only dropped by 35%. This work lead to a significant conclusion that favored the use of Kevlar as a suitable stitching material. Studies have also been conducted to show that the modified lock stitch or the chain stitch is best suited for the purpose of stitching composite preforms. The conventional lock stitch creates an area of stress concentration which is undesirable for composites

Morales also showed that with an increase in the density of stitching, the G_{IC} value also increased and the crack growth mechanism in stitched composites is different from that in the toughened resin systems. While the chemistry of the toughened resin system is the determining factor, it is the mechanical interlock existing in the stitched system that helps arrest crack growth.

Extensive work has been performed by Farley [40] to study the mechanism responsible for the reduced undamaged, compression strength in stitched composites. Panels made from AS4-3501-6 carbon-epoxy material was tested. The lay up consisted of 9 plies oriented at 0 and 90 degrees and was then stitched with either Toray T-900-1000 carbon or 1100 denier Kevlar-49 yarn. A stitch spacing of 0.64 cm and stitch pitch of 0.32 cm were used. In order to check whether kinking of the surface, inplane fibers around the stitching created the drop in the undamaged, compression strength, the stitches on the top and bottom surfaces were machined off resulting in a $[0_{0.5}/90/0/90/0/90/0/90/0_{0.5}]$ layup. The failure mode resulting from the short block compression tests remained the same in both cases, however, the compression strength of the unmachined specimens showed a 7-35% decrease in magnitude as compared to the machined specimens. It was believed that the location of the principal load carrying 0° fibers was important in order to compute the percentage increase in the compression strength. It was therefore proposed that

tufting, a process used in the carpet industry be used to stitch composite preforms [41].

More recently, Shim, Ahn and Seferis [42] have shown that stitching could result in the formation of surface pin holes on the laminate surface and internal void formation in the resin rich areas. It has also been found that internal voids were extremely difficult to control. This void formation was also found to be extremely anisotropic showing preference along the stitching direction.

Chapter 3

FABRIC CHARACTERIZATION

In this chapter the various materials used in this research along with a detailed explanation of the different manufacturing parameters and methods used to measure them are presented. Descriptions of test procedures, fixtures and equipment used to characterize the fabrics are given.

3.1 MATERIALS

This section details the different kinds of materials used in the current research. The different fabric types and fluid used in the permeability experiments are discussed. The areal weights of the various fabrics/preforms are presented in Table 3.1.

3.1.1 Fabrics

Four different types of fabric systems were used in the present investigation. They include:

- (1) 162 Plain Weave E glass
- (2) 7781, 8 harness satin weave, E glass with F16 and F72 finish
- (3) Unsized Plain Weave AS4
- (4) 'W' Sized Plain Weave AS4

Table 3.1: Fiber Areal Weights of Fabrics and Preforms

Fabric/Preform Type	Number of Plies/Tubes	Areal Weight in (g/m ²)
162 Plain Weave E Glass	12	4670
F 16 finished E Glass	16	4585
F 72 finished E Glass	16	4590
Unsize AS4	18	3480
'W' Sized AS4	18	3490
Multiaxial Warp Knit Unstitched	70	14270
Multiaxial Warp Knit:Batch`95 (0.5"Stitch Spacing & 1/6" Stitch Pitch)	70	14420
Multiaxial Warp Knit:Batch`95 (0.5"Stitch Spacing & 1/8" Stitch Pitch)	70	14480
Multiaxial Warp Knit:Batch`95 (0.2"Stitch Spacing & 1/6" Stitch Pitch)	70	14620
Multiaxial Warp Knit:Batch`95 (0.2"Stitch Spacing & 1/8" Stitch Pitch)	70	14700
Multiaxial Warp Knit:Batch`94 (0.5"Stitch Spacing & 1/8" Stitch Pitch)	70	13880
Multiaxial Warp Knit:Batch`94 (0.2"Stitch Spacing & 1/8" Stitch Pitch)	42	8410
0°±60° Braid	9 tubes	12700
	4 tubes	5030
	14 tubes	17440
0°±70° Braid	10 tubes	13140

Note: 1 tube is equal to 2 braid plies

The first type of fabric was used extensively for statistical analysis of steady-state and advancing front permeability measurements. The fabric was manufactured by Clark-Schwebel Fiberglass Corporation. There were 28 yarns in the warp direction and 16 yarns in the weft direction per square inch of the fabric.

The second type of fabric was a 7781, 8 harness satin weave E-glass. The fabric was manufactured by Hexcel Inc. The fabric was tested with two different finishes and had an end count of 57 x 54 ends per inch. The F-16 finish is composed of Volan and the F-72 finish is composed of Silane.

The third fabric was by Fabric Development Inc. There were 11 yarns in the warp direction and 12 yarns in the fill direction per square inch. The last fabric was similar in all respects to the third fabric except for the 'W' sizing that was applied to it.

3.1.2 Preforms

The preforms tested were a multiaxial warp knit preform and a 2-D braided material with different braiding angles and thickness.

This section will explain the basic configuration details of the multiaxial warp knit preform. Two batches of preform namely batch`94, received in 1994 and batch`95, received in 1995 were tested. The two batches had different areal weights. Both batches consisted of 7-ply quasi-isotropic $[+45^\circ/-45^\circ/0_2^\circ/90^\circ/0_2^\circ/-45^\circ/+45^\circ]$ base units. The important point to note here is that the 0° plies are grouped together and counted as one ply. These units are knitted together with light Nylon thread. The base units are then stacked together depending on the required number of plies and

then stitched together using Kevlar thread. The individual plies were made using AS4, 6k graphite fiber. AS4 is a commercially available PAN based carbon fiber manufactured by Hercules. The fiber has some proprietary sizing on it denoted by the letter 'S'. 6k represents the tow size, wherein every tow contains fibers equal to a thousand times the number specified, in this case 6000 fibers. The batch`94 consignment consisted of preforms 56-, 63-, 70-, 84-, 91-, 98- and 105-ply thick. Batch`95 consisted of 70-ply thick preforms The stacked preforms were then stitched together using 4-ply 1600 denier Kevlar needle thread with a low melt nylon coating. The bobbin thread was an uncoated 400 denier Kevlar. The stitching density however was categorized depending on the stitch spacing and pitch. Batch`94 consisted of preforms having stitch spacings of 0.5" and 0.2" and stitch pitch of 1/8". The batch`95 however, consisted of preforms with four different stitch patterns, they were the 0.5" spacing:1/6" pitch, 0.5" spacing:1/8" pitch, 0.2" spacing:1/6" pitch and 0.2" spacing:1/8" pitch. The resulting stitching densities measured as penetrations/inches² were 12, 16, 30 and 40, respectively. An identical batch of unstitched multiaxial warp knit preform was also tested.

The triaxially braided materials was made up of 12K, IM7 axial fiber and 6K, AS4 bias fiber braided at $\pm 60^\circ$ and $\pm 70^\circ$, and were stitched using Kevlar 29, 400 Denier, 3-ply thread at a pitch of 8-11 penetrations per inch. The $\pm 60^\circ$ and $\pm 70^\circ$ braids were made up of 9 tubes and 10 tubes of material, respectively. One tube is equal to two braid plies. A batch of $0\pm 60^\circ$ triaxially braided material with 4 and 14 tubes was also tested in order to evaluate thickness effects.

3.1.3 Fluid

The fluid used for measuring the permeability of the fabrics/preforms was corn oil. The oil had a viscosity of 0.054 Pa-s at 23°C. The viscosity of the oil as a function of temperature is given by the following equation,

$$\eta = (-2.0496 * T + 101.54) / 1000 \quad (3.1)$$

where, η = viscosity in Pa-s

T = temperature in °C

A Brookfield (model DV-III) programmable rheometer was used to test the viscosity of corn oil.

3.2 TEST FIXTURES

This section outlines the different test fixtures used during the present research.

3.2.1 15 cm² Steel Fixture

The fixture was primarily used for compaction and in-plane permeability tests. A sketch of the fixture is given in Figure 3.1. The cavity of the fixture is 15.44 cm x 17.98 cm. Four pressure transducers were mounted in the fixture. Three of them were flush mounted 5.08 cm apart into the base of the cavity and the fourth one was mounted onto the inlet face of the mold within the fluid groove as indicated in Figure

3.1. The fluid enters from one end and exits the other end of the fixture through fluid grooves in the base of the cavity. The inlet pressure is measured by a transducer mounted inside the inlet groove. The piston end of the fixture is connected to the load cell by a universal joint adapter. A square cross section ring is mounted on the piston in order to prevent oil leakage between the cavity and the piston. A linear variable displacement transducer (LVDT) is used to measure the mold gap once the fixture is closed. Figure 3.2 shows a photograph of the fixture.

3.2.2 5 cm² Steel Fixture

This fixture was used to perform transverse permeability tests. The fixture has a 5.08 cm x 5.08 cm cavity. The oil enters the cavity through a porous plate mounted in the base of the cavity and leaves through a similar porous plate mounted in the piston after traversing across the thickness of the preform. Figure 3.3 shows a schematic diagram of the fixture. A pressure transducer is used to measure the inlet pressure. The load is transferred from the load cell to the piston via a steel ball placed on top of the piston. An 'O' ring is used on the piston to prevent leakage. Figure 3.4 is a photograph of the fixture.

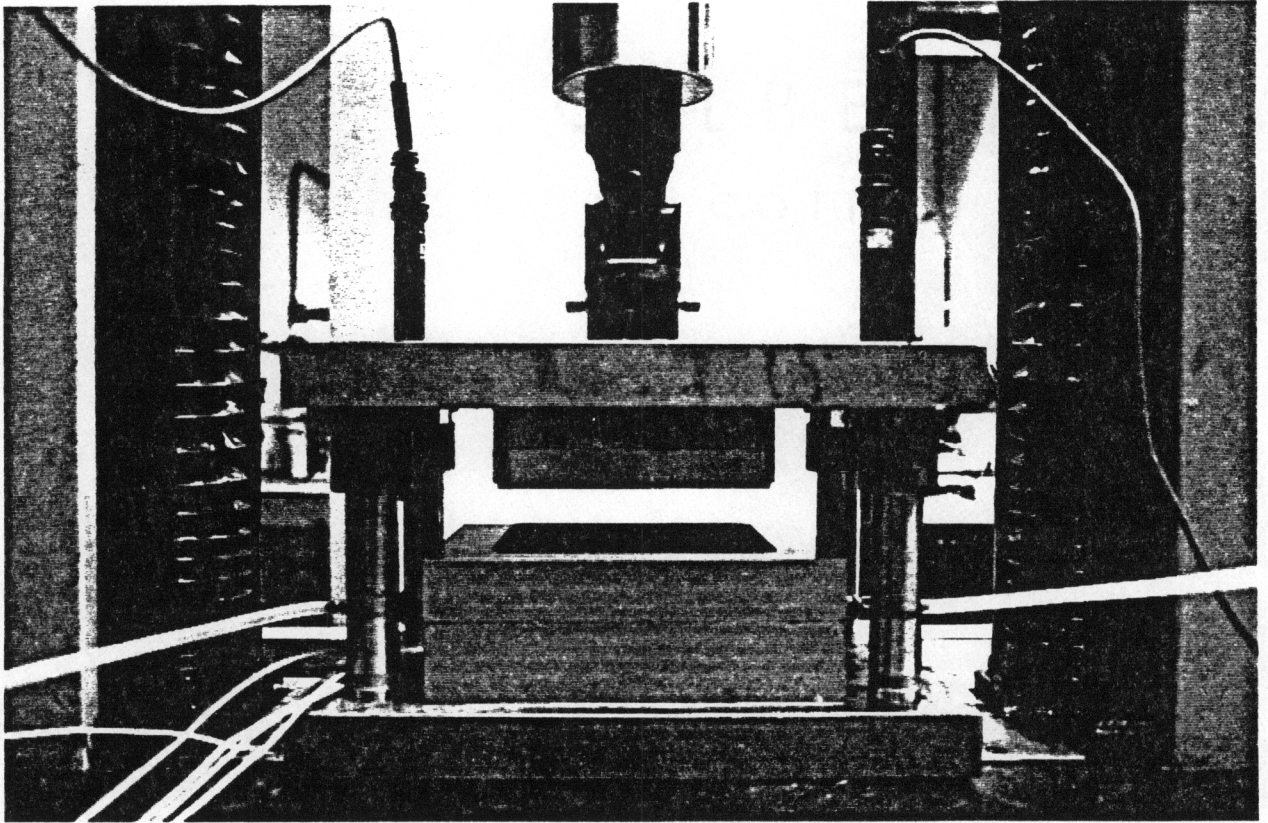


Figure 3.2: Photograph of the 15 cm² steel fixture

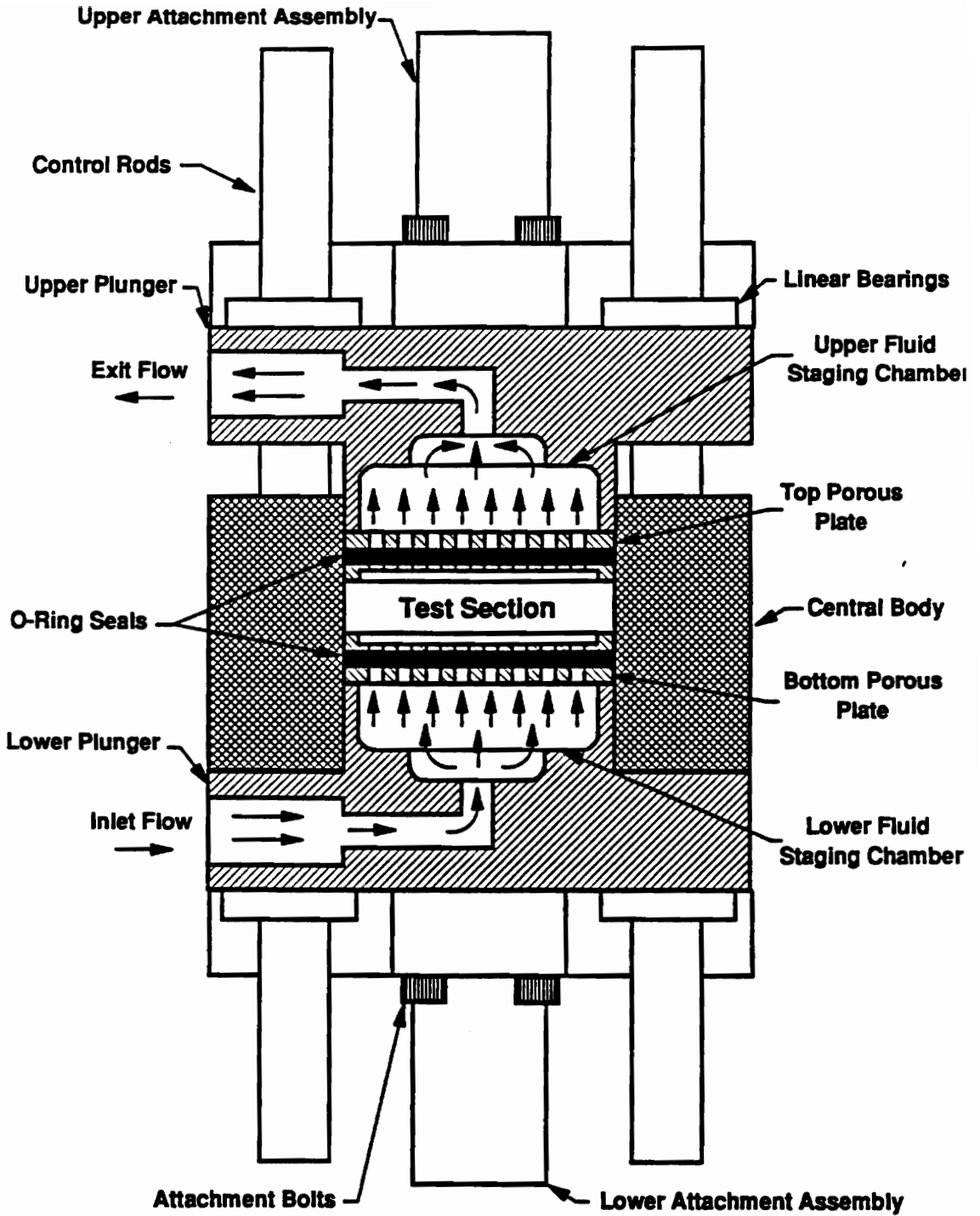


Figure 3.3: Schematic of the through-the-thickness fixture Reference[44]

3.2.3 NASA Brass Fixture

The NASA brass fixture was also used to perform transverse permeability tests. The fixture has a larger 15.24 cm x 15.24 cm cavity. The oil enters the cavity through a porous plate mounted in the bottom of the cavity and exits through a similar porous mounted on the piston. Figure 3.5 is a schematic diagram of the Brass fixture. The load is transferred from the load cell to the piston via a universal joint adapter. The mold gap is measured using either a vernier calipers or an LVDT. The inlet pressure is measured using a pressure transducer. Figure 3.6 is a photograph of the fixture.

3.3 MATERIAL PARAMETERS

In resin transfer molding and other injection molding processes, the material parameters that are of interest are, fabric/preform permeability and compaction. The permeability is measured in both in-plane, as well as, transverse or through-the-thickness. The in-plane permeability is measured in the warp and fill directions.

3.3.1 Compaction

This test involves the compacting of dry fabrics/preforms under applied

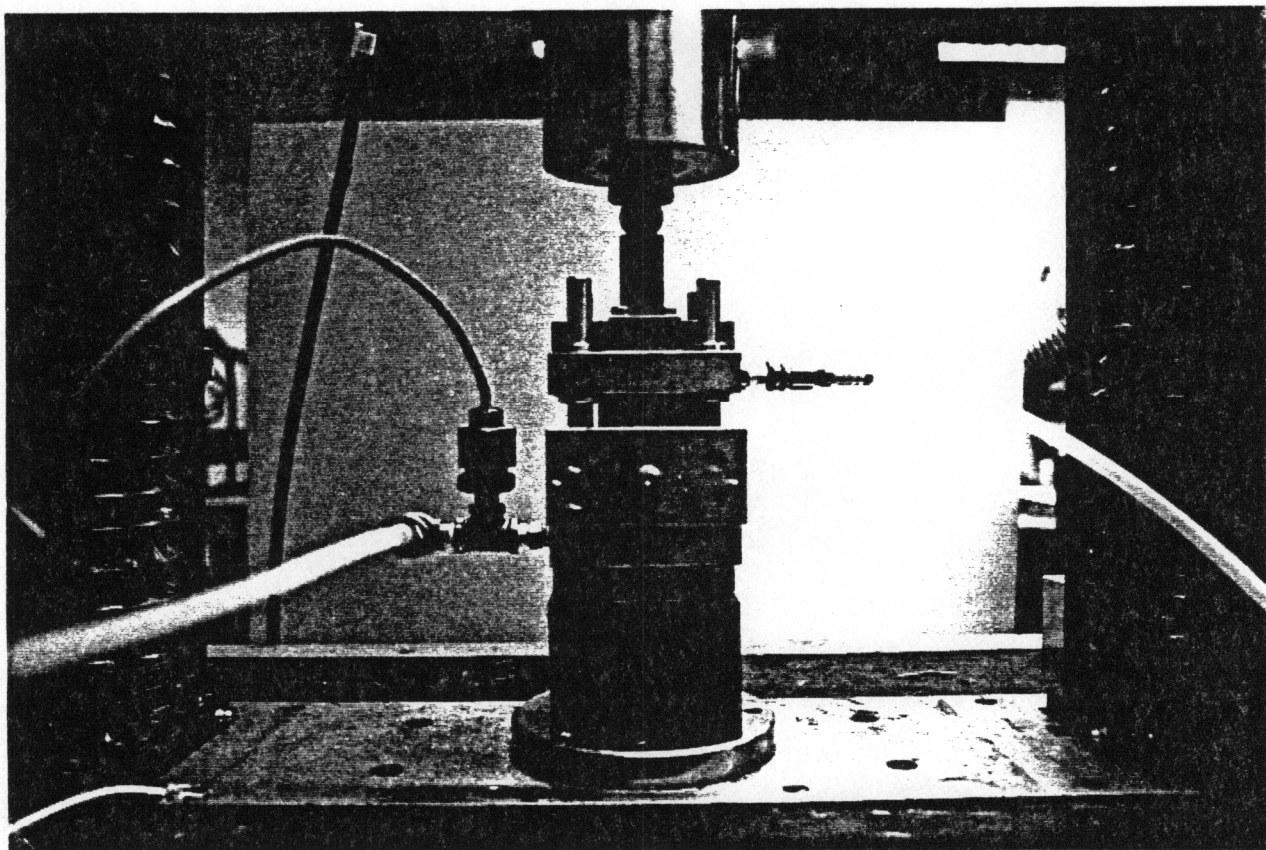


Figure 3.4: Photograph of 5 cm² Steel fixture

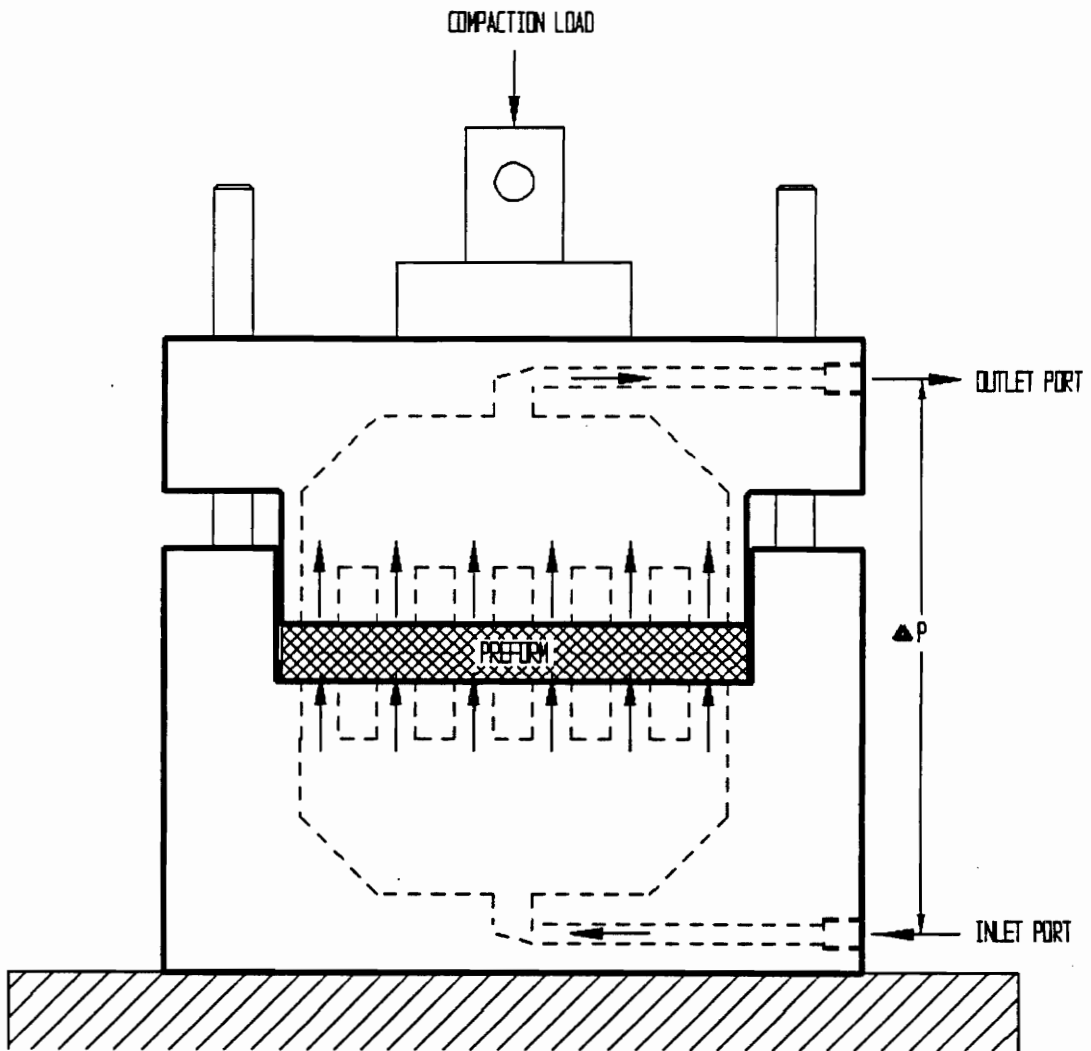


Figure 3.5: Schematic of the NASA Brass fixture [43]

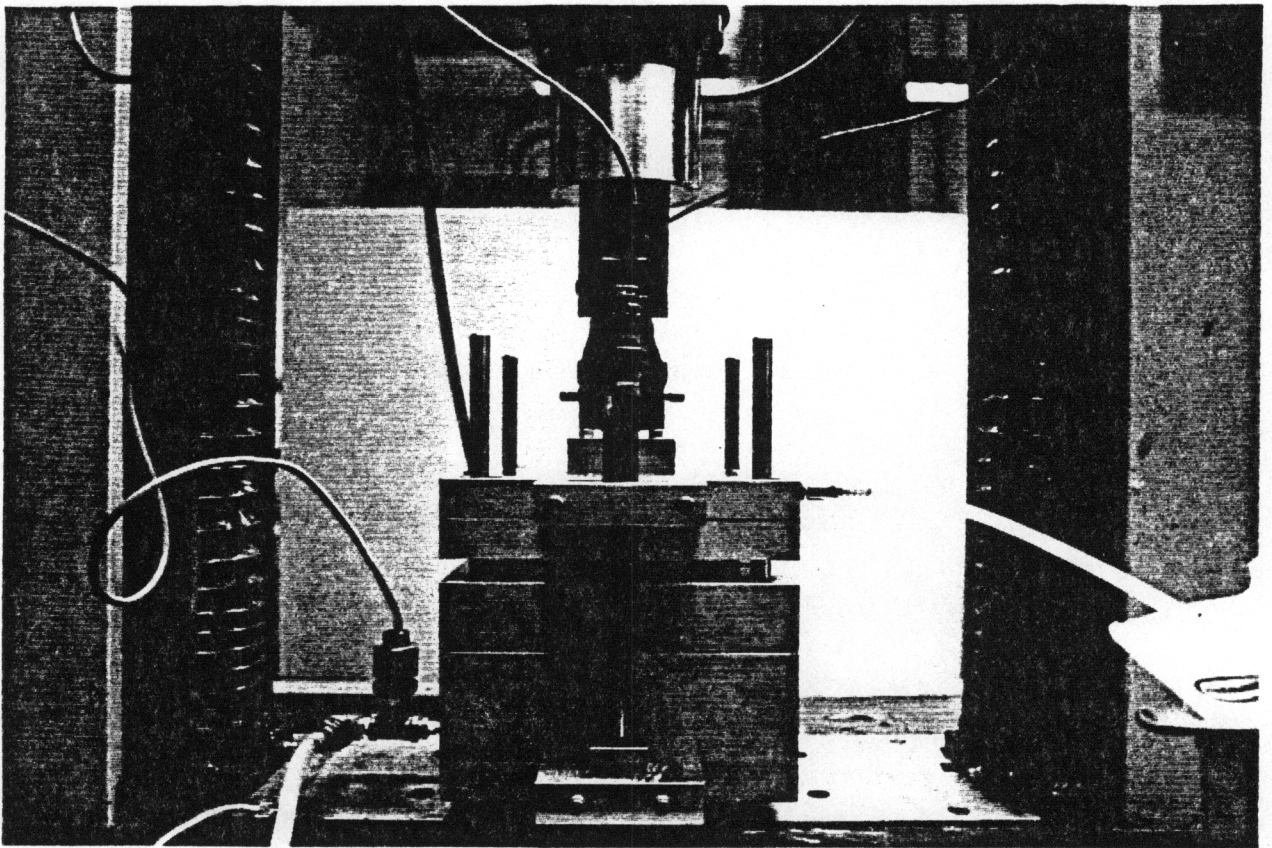


Figure 3.6: Photograph of the NASA Brass fixture

pressure and measuring the fiber volume fraction. This is the first test performed on a fabric as it reveals vital information regarding the initial fiber volume fraction and the amount of load that must be applied on the preform to achieve a certain fiber volume fraction.

Compaction tests were performed using the 15cm² steel fixture. The fixture was initially mounted onto the Instron (model number 1125) load frame and the two parts were held at the open position. The fabric was then rolled out and cut into plies 15.24 cm x 15.29 cm. This ensured a tight fit once placed inside the mold cavity. The fabric was then weighed in order to determine the areal weight. The areal weights of the fabrics/preforms tested during this research are given in Table 3.1. The fabric was then carefully placed ply by ply into the mold cavity. The LVDT on the fixture along with the load cell on the Instron were connected to Labview, the data acquisition system. The load frame was then switched on and the load cell and LVDT were calibrated and zeroed. The top of the mold, which is mounted onto the load cell, was then lowered until the load cell registered a load. The load frame was then stopped and the load was registered after it had stabilized. The upper platten was lowered at a constant rate until the next desired value of fiber volume fraction was reached. Once again the load was registered after reaching a steady value. This procedure was continued until the compaction loads for the entire range of fiber volume fractions were measured. Typically the range is from the point of initial contact to 65%. Once the test was complete, the upper platten of the mold was removed. The preform was then removed from the mold cavity and bagged. The load values obtained were then

divided by the preform cross sectional area to compute the pressure. The equation used to calculate the fiber volume fraction is given as

$$v_f = \frac{m}{\rho * A * h} \quad (3.2)$$

where,

ρ = fiber density (g/cc)

A = cross sectional area (cm²)

h = thickness of preform (cm)

m = mass of the preform (grams)

A typical plot of fiber volume fraction as a function of pressure is shown in Figure 3.7 for 16-ply of F 72 finished E-Glass. A power law regression curve is fit to the data

$$v_f = c (\text{compaction pressure})^d \quad (3.3)$$

where, c and d are the coefficients of the equation and represent the intercept and the rate of the curve. All compaction pressures are in units of kPa and the regression fit is valid only within the plotted range of pressures. The compaction test gives an estimate of the initial fiber volume fraction of the uncompacted preform. This is of particular interest when dealing with stitched preforms, as the density of stitching tends to change the initial fiber volume fraction. The importance of this information is evident when trying to conduct permeability tests where good contact of the preform with the faces of the mold are critical in order to prevent leakage.

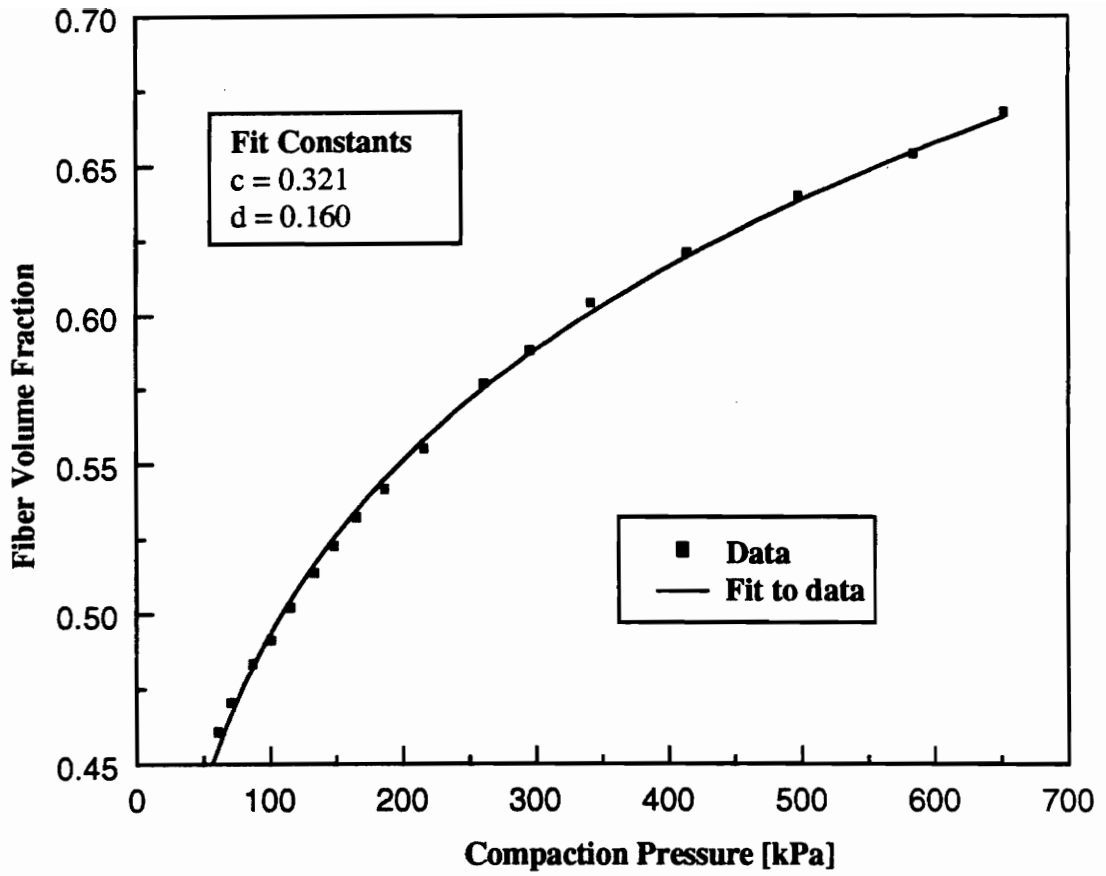


Figure 3.7: Compaction pressure as a function of fiber volume fraction of F-72 finished 7781 E-glass fabric.

3.3.2 Steady-State Permeability

Permeability of a porous medium is a measure of the resistance that it offers to the flow of fluid through it. A less permeable medium offers a greater resistance to flow than one that has a higher permeability. It is a constant that is determined only by the structure of the medium. Infact, it is the separation of the fluid properties from the porous medium properties that gives the permeability constant units of $[L^2]$. This section will discuss the tests that were performed and the equations that were used to measure permeability. For an orthotropic material, permeability measurements are made in three different material directions to determine the permeability tensor. The measurements are classified under two categories of tests depending on the direction of infiltration, in-plane and through-the-thickness or transverse.

Steady-state permeability is measured after the fluid has completely infiltrated and saturated the material. Darcy's law, proposed by Henry Darcy a French engineer in 1856, was used to compute it. The one-dimensional form of Darcy's law is written as follows

$$Q = \frac{SA}{\mu} \frac{\Delta P}{d} \quad (3.4)$$

where Q = flow rate of fluid (cc/min)

ΔP = pressure drop across the preform (Pa/m)

d = preform thickness (m)

S = Permeability (m^2)

μ = viscosity of the fluid (Pa-s) and

A = preform cross sectional area normal to the flow front (m^2)

Darcy's law in the above form is developed from first principles as an approximate macroscopic momentum balance equation.

Through-the-Thickness Permeability

Experimentally, the through-the-thickness permeability was measured using two fixtures, the 5cm² steel fixture and the NASA brass fixture. The fabric/preform was cut to the dimensions of the test cavity, weighed and the areal weight recorded. The piston end of the fixture, was then mounted onto the guide posts of the fixture and lowered slowly at first, in order to allow the "O"-ring to slip into the cavity and then rapidly until the desired initial fiber volume fraction was reached. Care must be taken not to lower the piston too rapidly, as the friction between the "O"-ring and the cavity edges may shear off the "O"-ring. Equation 3.2 was used to compute the fiber volume fractions at different mold gap distances. A constant flow rate pump was controlled from the computer and set to a desired flow rate. For all the tests, the fluid was made to infiltrate and saturate the fabric/preform. The accuracy of the pump was checked by allowing the fluid to flow into a graduated cylinder for a known amount of time. If the indicated flow rate delivered by the pump matched the measured value, the test proceeded, otherwise the pump was recalibrated. At each volume fraction of interest, the pressure drop for several flow rates were measured. The flow rate versus pressure gradient was plotted at each fiber volume fraction and a linear least squares

curve was fit to the data. Rewriting equation (3.4) the permeability can be determined as follows

$$S = \frac{\text{slope} * \mu}{A} \quad (3.5)$$

In the above equation, A the area normal to the flow and μ is the fluid viscosity. Tests were conducted over a range of fiber volume fractions and the resulting plot of permeability versus fiber volume fraction was obtained. A typical plot is shown in figure 3.8 for 16 plies of F 72 E-Glass for fiber volume fractions ranging from 51% to 65%. The data were fit to a power law least squares regression model similar to the one used in the compaction tests and is expressed as follows

$$S = a (V_f)^b \quad (3.6)$$

where, as before, a and b are the fit constants.

Once the test was completed, the direction of the load frame was reversed and the piston was removed from the mold cavity. The fabric/preform was then removed and bagged.

In-plane Permeability

Figure 3.9 shows a schematic diagram of the in-plane permeability fixture. The in-plane permeabilities were measured using the 15cm² steel fixture. A computer controlled, constant displacement Zenith pump was used to ensure constant flow rate injection. This pump was manufactured by Parker Hannifin Corp. As mentioned earlier in this chapter, corn oil was used as the injection fluid. The temperature of the oil was measured before starting the test in order to calculate the viscosity. A linear

variable displacement transducer (LVDT) was used to measure the mold height, and this along with the pressure transducers, the pump and the load cell, were all interfaced with the data acquisition system. In-plane permeability measurements were made in much the same manner as just explained for the through-the-thickness case. The fixture was prepared by mounting the four pressure transducers into the cavity and then attaching an LVDT to the mold. The transducers and the LVDT were all calibrated. The preform was cut 15.24cm x 15.29cm and then weighed to calculate the areal weight. The fabric/preform was then loaded into the mold cavity and the piston end was lowered slowly initially so that the piston descended smoothly into the cavity and then more rapidly until the desired fiber volume fraction was reached. Again care was taken not to lower the piston too fast to prevent shearing of the "O"-ring. In order to reduce the initial friction between the ring and cavity, commercially available WD-40 was sprayed on the ring. Once the desired fiber volume fraction was reached, the pump was switched on via the computer to a set flow rate and the fluid was allowed to saturate the fabric/preform. Labview was programmed to read the inputs from the pressure transducers, LVDT, load cell and pump to calculate the permeability in real time. Plots of permeability versus time, pressure versus time and load versus time could be viewed while the test was in progress. Figure 3.10 shows a typical plot of in-plane permeability in the warp direction for 16-ply of F 72 E Glass for fiber volume fractions ranging from 51% to 65%. Once the test was over, the load frame traverse direction was reversed and the piston was raised at a slow rate until it separates from the cavity. The saturated preform was then removed and bagged.

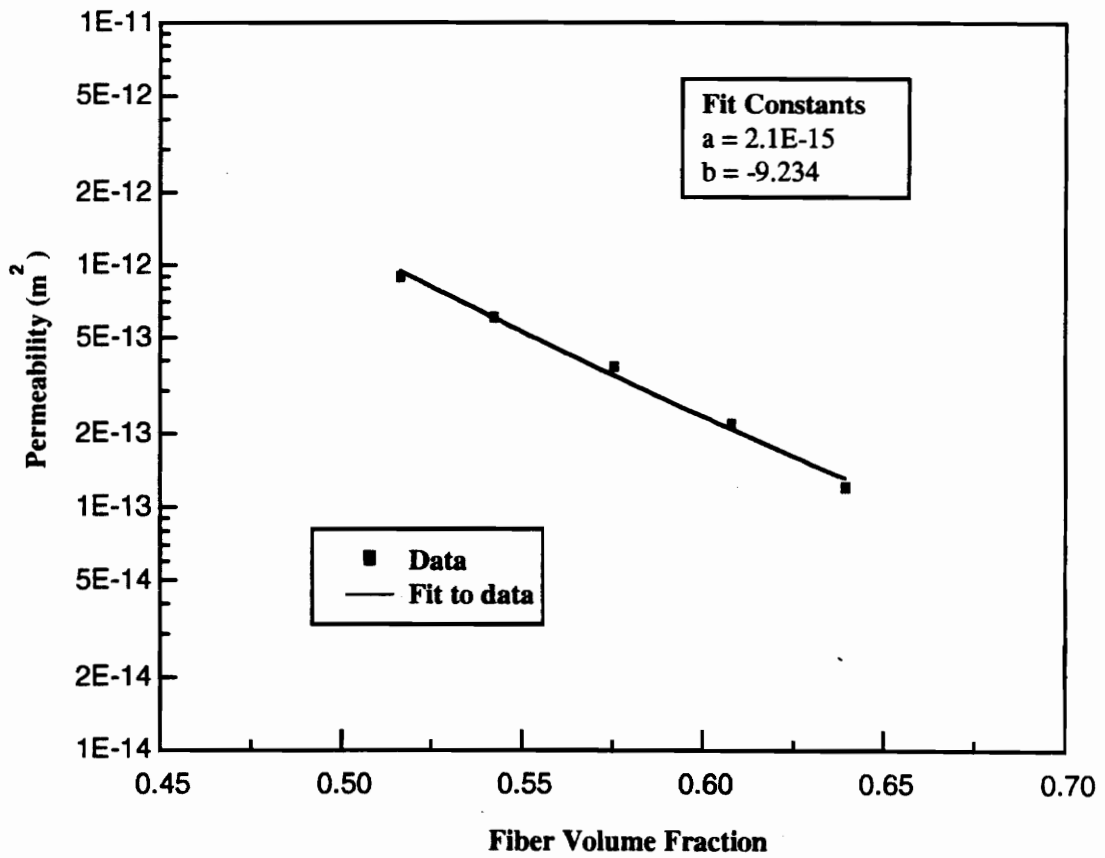


Figure 3.8: Through-the-thickness permeability as a function of fiber volume fraction of F-72 finished 7781 E-glass fabric

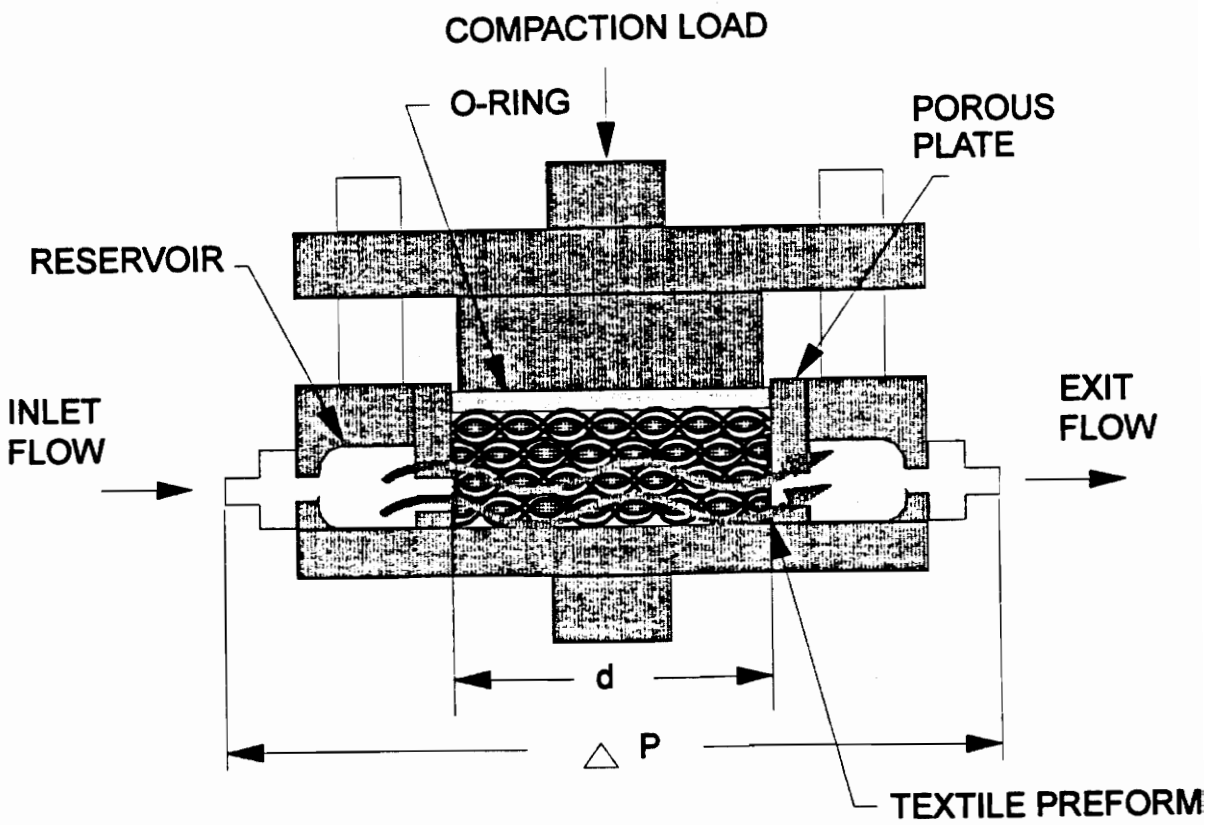


Figure 3.9: Schematic of the in-plane fixture

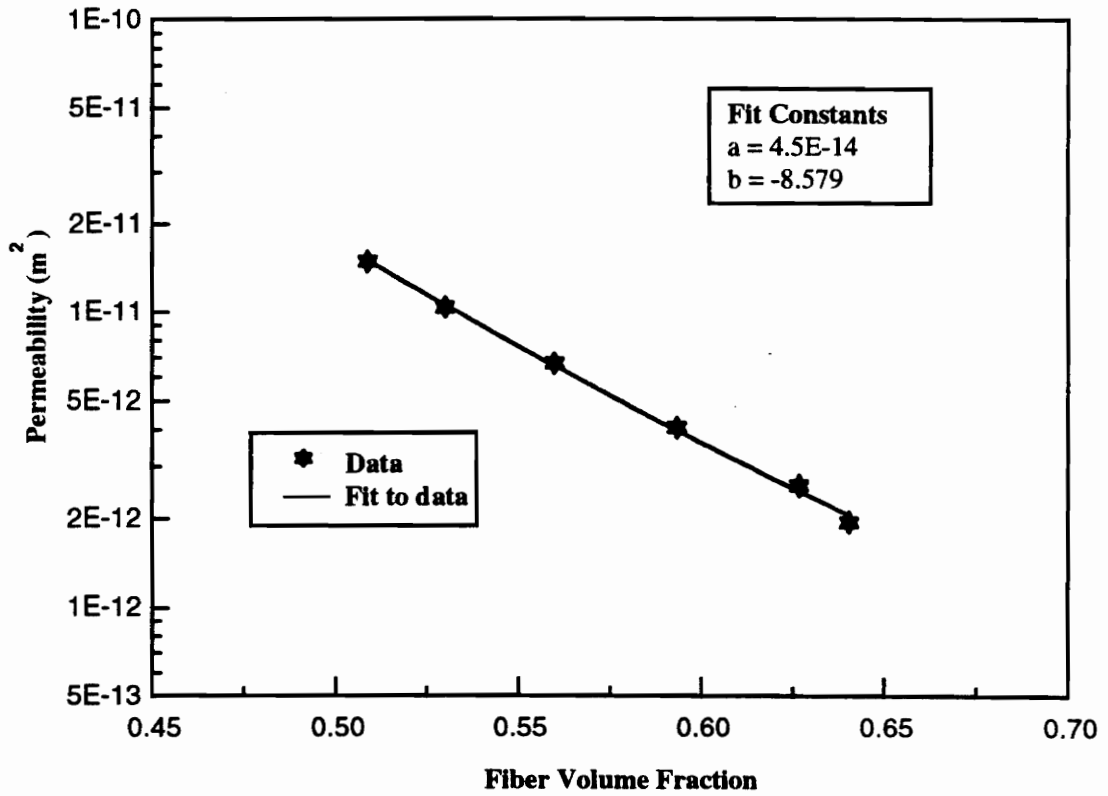


Figure 3.10: In-plane permeability as a function of fiber volume fraction of F-72 finished 7781 E-glass, warp direction

3.3.3 Advancing Front Permeability

The advancing front permeability was calculated using the pressure transducer data stored during the initial portion of the steady-state in-plane permeability test. The tests were performed on the 15cm² steel fixture. A sketch of the mold cavity was shown in Figure 3.1. Since the fluid is injected from a line source to a line sink, the shape of the flow front as the fluid permeates the dry fabric/preform, is assumed to be a straight line. As the flow front moves past a pressure transducer mounted in the cavity of the fixture, the transducer begins to respond. This then determines the exact time and flow front position. Similar pressure readings are registered as the flow front moves past the other transducers. The differential form of Darcy's equation was used to determine the advancing front permeability from the flow front position and time measurements under constant flow rate conditions. The differential form of Darcy's equation is written as

$$\frac{Q}{A} = -\frac{S}{\mu} \frac{dP}{dx} \quad (3.7)$$

For constant flow rate injection, Equation 3.7, can be rearranged to obtain a relationship between pressure and flow front position as follows

$$P = \frac{Q^* \mu}{S^* A} x \quad (3.8)$$

where P is the pressure in Pa and x is the front position in m.

On a plot of pressure drop versus flow front position, the slope of a linear least squares fit to the data can be used to determine permeability as follows

$$S = \frac{Q}{\text{slope}} \frac{\mu}{A} \quad (3.9)$$

The result obtained at a particular fiber volume fraction was then compared with the steady-state value of permeability. The major drawback of this form of permeability measurement is the inherent fiber volume fraction constraint. The test can be conducted only at one fiber volume fraction for a given sample of fabric/preform, as opposed to the steady state technique. The results are discussed in Chapter 4.

Chapter 4

ANALYSIS OF PERMEABILITY MEASUREMENTS

Permeability measurements are very complex to make and extreme care must be taken while performing the experiments. Problems that are commonly observed when measuring permeability include “channeling” where fabric/preform samples not cut to the exact dimensions of the mold cavity result in leakage of fluid along the edges of the preform, measuring equipment that may not be sensitive enough, and also inherent variations in the fabric [45]. All of these factors make repeatability of the measured permeability an important issue.

In flow simulation model predictions of infiltration time and injection pressure, values of the permeability tensor are required as input parameters [46]. These values are obtained at the appropriate fiber volume fraction by using the least squares regression fit to the permeability test data. The model results are then compared with experimentally obtained infiltration times and pressures. Often there are differences and in order to assess the significance of this discrepancy and to make comparisons more meaningful, the accuracy of the permeability measurements needs to be determined. Permeability may not be the only contributing factor to the discrepancy, but it certainly is an important one and therefore, a preliminary statistical study is presented in the followings sections.

4.1 CONFIDENCE BOUNDS ON STEADY-STATE PERMEABILITY MEASUREMENTS

The study involved taking into account the limited data sets that can be generated from steady-state permeability tests due to material and time constraints, and calculating upper and lower bounds of the permeability using a confidence coefficient. The standard Student's t-test [47] was used to achieve this as it was specially designed to handle small data sets.

Two steady-state in-plane permeability tests were conducted in the fill direction using Type 162 E-glass fabric. The test procedure has been outlined in Section 3.3.2. 16 plies of fabric were used and the areal weight of E-glass has been specified in Table 3.1. Figure 4.1 is a plot of the flow rate versus pressure gradient from one of the steady-state permeability tests. The plot indicates that the pressure gradient increases linearly with flow rate. This validates the assumption that the fabric is a porous medium and that Darcy's law can be applied to the fabric. A linear least squares regression curve was fit to each data set and the slope of the curve was used to calculate the permeability. The steady-state permeability as a function of fiber volume fraction is given in Figure 4.2. The permeability data were fit to a power law regression model given in Equation 3.6. The constants are reported in Table 4.1.

Next, the data were subjected to a standard Student's t-test and a confidence coefficient of 50% was chosen to calculate the upper and lower confidence bounds. The resulting constants are also given in Table 4.1. Figure 4.3 shows a plot of the

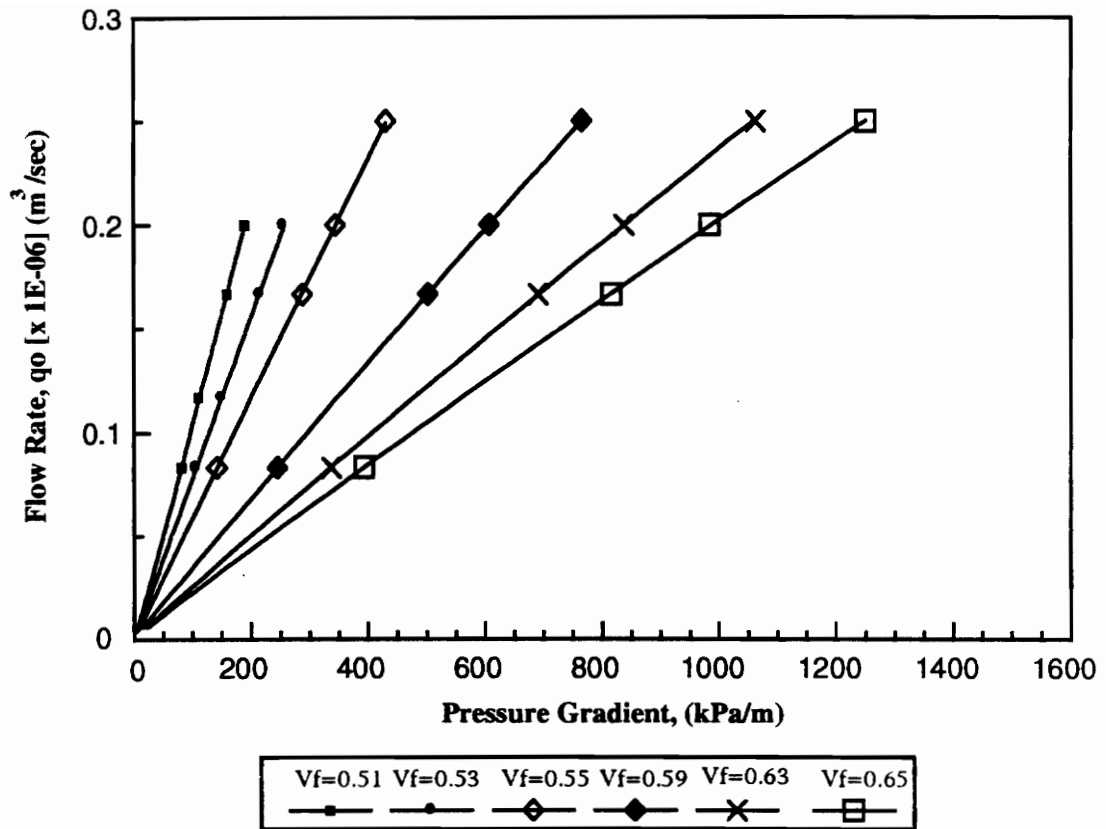


Figure 4.1: Flow rate as a function of the pressure gradient for 162 E-glass fabric in the fill direction. Symbols are data at the specified fiber volume fraction. Solid lines are linear least squares regression fits to each data set.

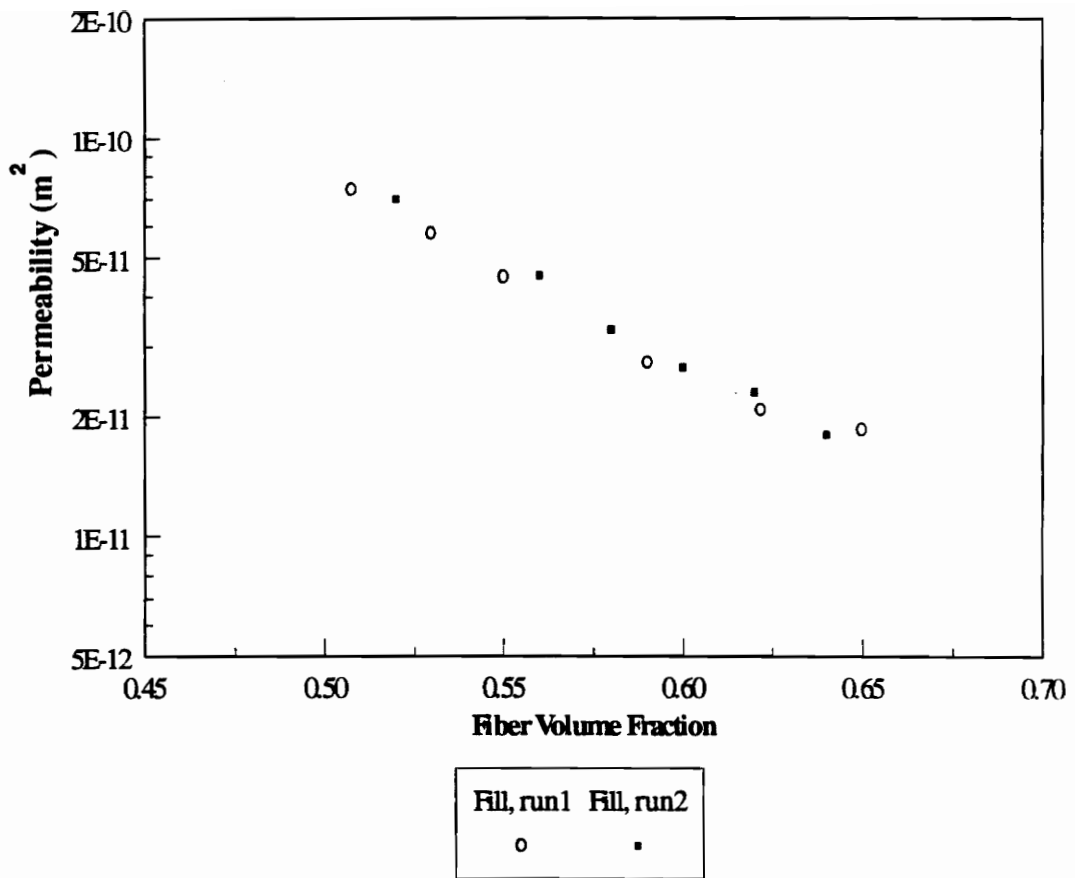


Figure 4.2: Fill direction permeability for 16 plies of 162 E-glass fabric.

Table 4.1: Permeability power law regression fit constants

Test Direction	a (m ²)	b
Mean Fill	1.3E-12	-5.88
Upper bound Fill	1.3E-12	-6.12
Lower bound Fill	1.3E-12	-5.63

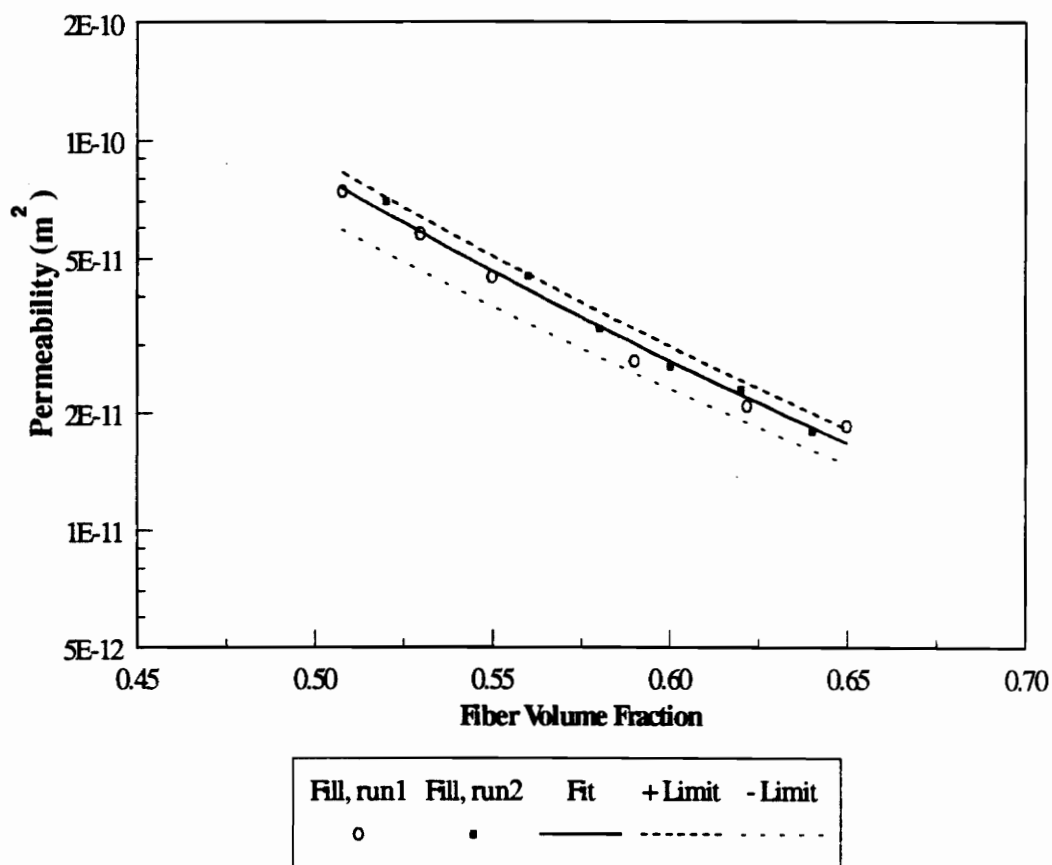


Figure 4.3: Fill direction permeability for 16 plies of 162 E-glass, along with the statistical confidence bounds.

upper and lower bounds on permeability for E-glass fabric. The original regression line, along with the data are also shown.

4.2 ADVANCING FRONT PERMEABILITY

Unlike the steady-state permeability method which measures the permeability of a saturated preform, the advancing front tests measure the permeability of the fluid infiltrating the dry preform. In actual resin transfer molding, since the fluid is infiltrating a dry preform, a comparison between the steady-state and advancing front permeability measurements is interesting. In order to achieve this, the steady-state permeability at a particular fiber volume fraction was input into a standard 1-D flow model to predict the injection pressure with respect to time during wet out of a dry preform. The constant flow rate case was used. The assumptions made in the development of the model were:

- 1) the fluid advances through the preform in a straight line front
- 2) the fluid viscosity is constant; and
- 3) the variation in permeability with position is negligible.

Figure 4.4 shows a schematic diagram of the 1-D flow geometry. The development of the model for the constant flow rate case can be found in [46]. However, the equations pertinent to the present study are as follows:

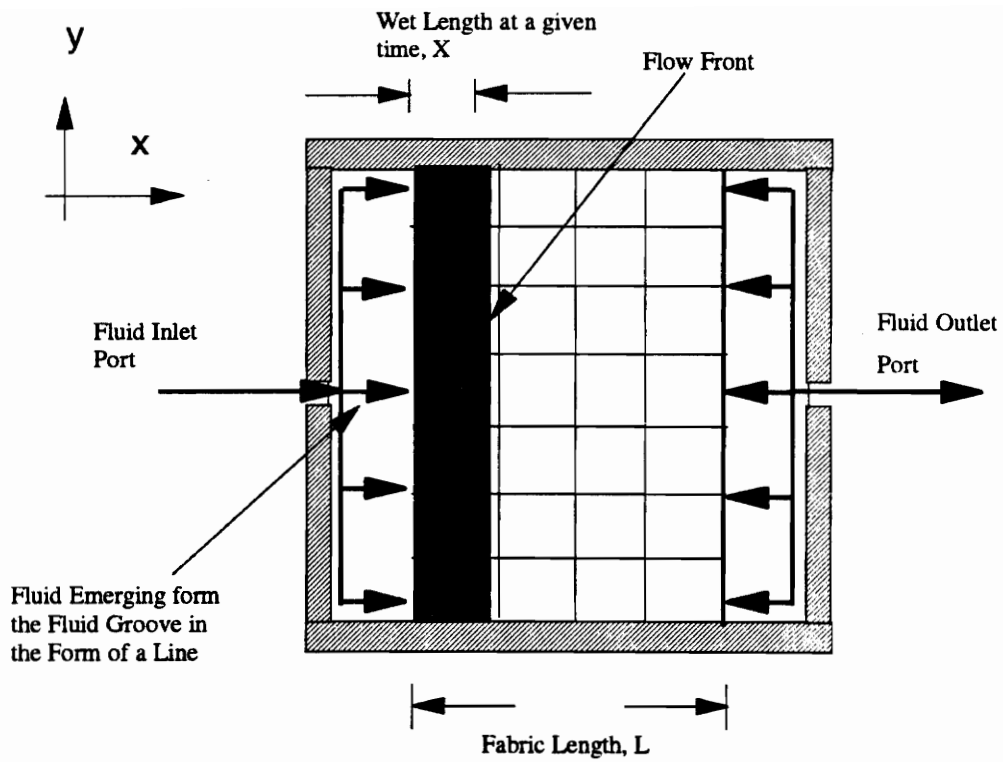


Figure 4.4: Schematic diagram of the 1-D line source to line sink fluid infiltration condition.

(a) Pressure distribution with respect to flow front position is given by

$$P_0 - P_b = \frac{q_0 \mu}{S_{xx}} x \quad (4.1)$$

where x is the flow front position, P_0 is the inlet pressure (at $x = 0$), P_b is the pressure at the flow front, q_0 is the flow rate, μ is the fluid viscosity, and S_{xx} is the permeability in the flow direction.

(b) Pressure distribution with respect to time is given by

$$P_0 - P_b = \frac{q_0^2 \mu}{S_{xx} \phi} t \quad (4.2)$$

where ϕ is the porosity of the preform, and t is the time.

The upper bound, mean and lower bound permeability values were calculated using their respective constants in Table 4.1 at a fiber volume fraction of 57.3%. The permeability values were then used in the 1-D model to predict the inlet pressure with respect to infiltration time. A constant flow rate of 5 cc/min was used in the calculations. Figure 4.5 shows a plot of the predicted inlet pressure with respect to infiltration time.

The comparison then involved conducting an advancing front permeability test on another batch of 16 plies of E-glass at 57.3% fiber volume fraction. A constant flow rate of 5 cc/min was selected for the test. The procedure for the test is outlined in Section 3.3.3. The pressure transducers in the 15cm² steel fixture were used to monitor both the position and the shape of the flow front.

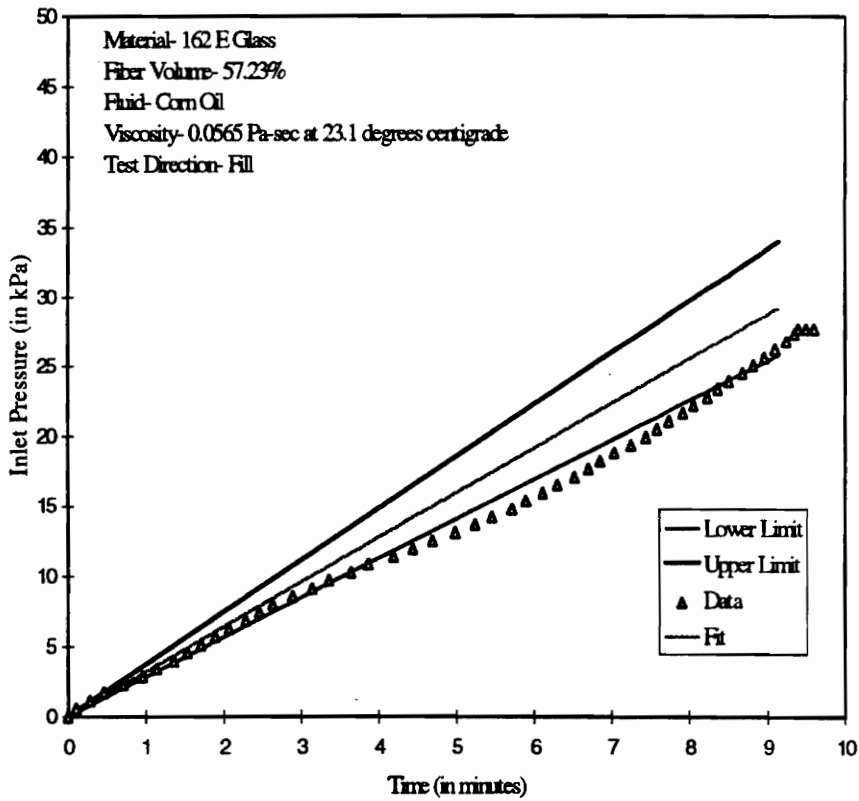


Figure 4.5: Inlet Pressure versus Infiltration time for E-glass in the fill direction.

The resulting data from the inlet pressure transducer as a function of time is shown in conjunction with the predicted curves in Figure 4.5.

4.3 DISCUSSION

Figure 4.5 indicates that the measured inlet pressure at the end of infiltration during the advancing front test lies close to the final inlet pressure calculated using the lower confidence bound of the steady-state permeability measurements. The pressure versus time data is non-linear unlike that predicted by the model. This could be due to deviation from the assumed 1-D, straight line fluid infiltration condition. In addition, the inlet pressure during infiltration is lower than that predicted by the model using the mean permeability and about half way through the test falls below the pressure calculated with the lower bound steady-state permeability. A statistical approach may therefore be more desirable for assessing the significance of the differences between model predictions and experimental observations.

Chapter 5

RESULTS

This chapter will present the results of permeability and compaction measurements obtained on the different fabric/preform systems during this research program. The effects of different fixtures, batches of preform, preform thickness, stitching density, braided preforms and sizing/finishing on compaction and permeability are presented.

5.1 COMPARISON OF TEST FIXTURES

Different test fixtures were used during the course of the research to obtain preform compaction and permeability as a function of fiber volume fraction. The following section presents data that compare compaction and permeability measurements obtained from different test fixtures.

Figure 5.1 shows a plot of fiber volume fraction as a function of compaction pressure of a 10-ply 'G' sized 3k AS4 fabric. The areal weight of the fabric is given in Table 3.1. The data from both the 15 cm² Steel fixture and the 5 cm² Steel fixture are almost the same except at high fiber volume fractions where the 15 cm² Steel fixture shows a higher compaction pressure compared to the 5 cm² Steel fixture.

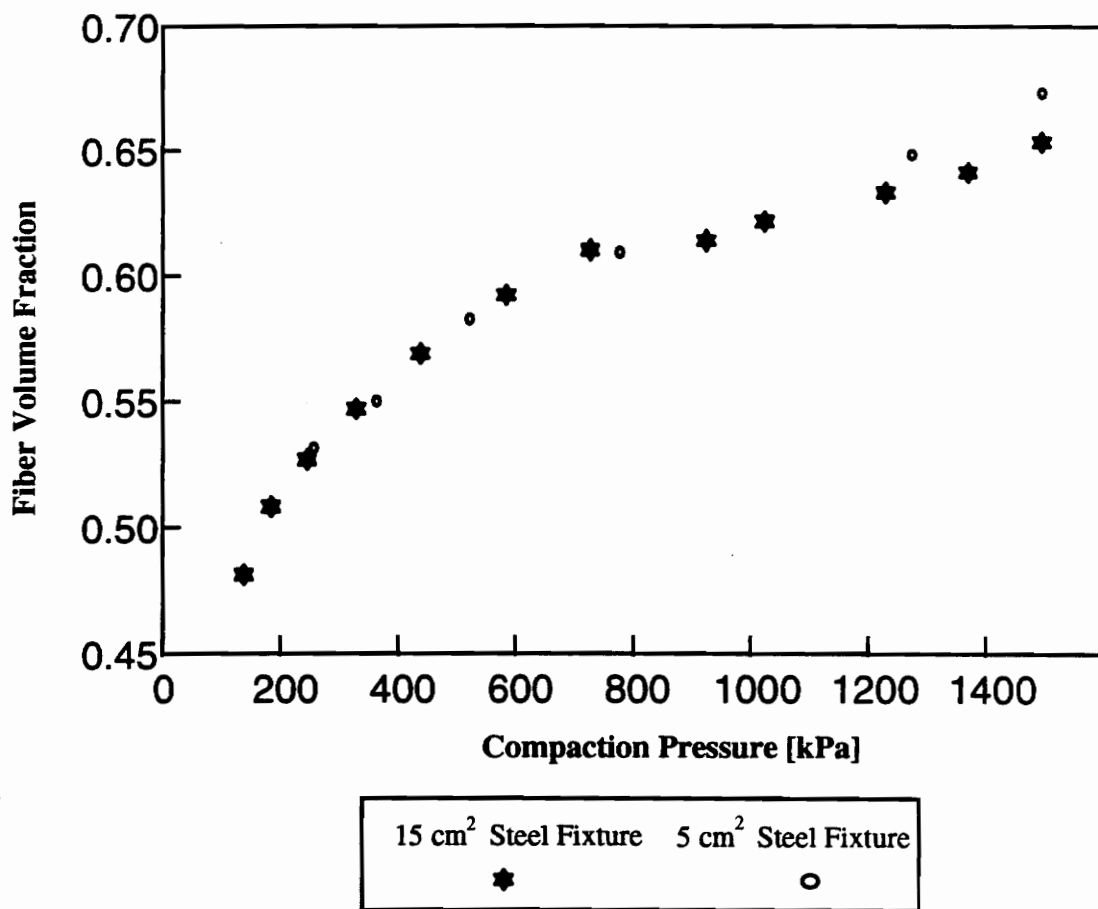


Figure 5.1: Fiber volume fraction as a function of compaction pressure of a 3k AS-4 fabric. Comparison of compaction data obtained from different fixtures.

Figure 5.2 is a plot of through-the-thickness permeability as a function of fiber volume fraction for multiaxial warp knit preforms. The preform had a stitch spacing of 0.5inch. and a stitch pitch of 1/8inch. and contained 70 plies. The areal weight is given in Table 3.1. The tests were performed with the NASA Brass fixture and the 5cm² Steel fixture. The results show that the change in permeability with fiber volume fraction is less pronounced in the NASA Brass fixture possibly due to leakage problems in the fixture around the “O”-ring.

The through-the thickness permeability of a 70-ply multiaxial warp knit preform as a function of fiber volume fraction is shown in Figure 5.3. The preform stitch spacing is 0.2” and the pitch is 1/8”. The NASA Brass fixture and the 5 cm² Steel fixture give similar permeability values for fiber volume fractions less then 60%. Above 60% fiber volume fraction, the smaller steel fixture gives a much lower permeability than the larger NASA Brass fixture.

5.2 THICKNESS EFFECTS IN MULTIAXIAL WARP KNIT PREFORMS

Batch `94, multiaxial warp knit preforms with different ply thickness were tested in order to assess the dependence of thickness on the compaction and permeability behavior of the preform. The preforms were from the 1994 batch and were stitched at a 0.5” spacing and 1/8” pitch. The NASA Brass fixture was used.

The fiber volume fraction as a function of compaction pressure is shown in Figure 5.4. The results show that up to a fiber volume fraction of 62%, the compaction is independent of the number of plies or thickness.. The number of plies

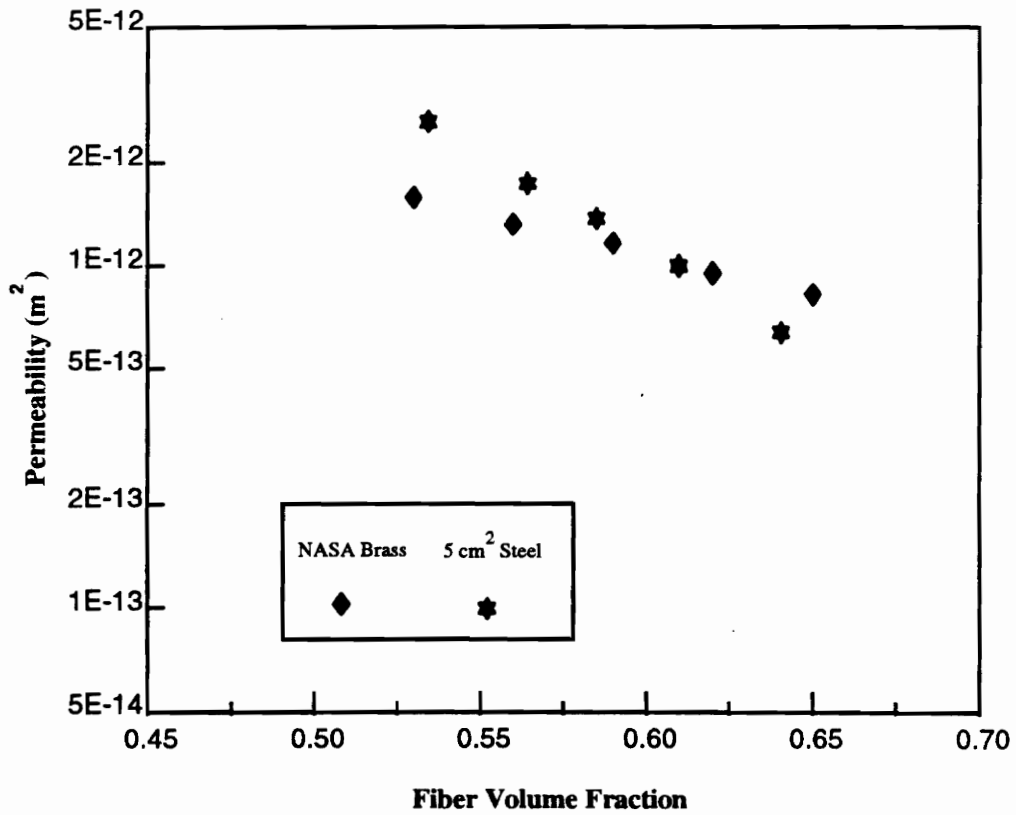


Figure 5.2: Through-the-thickness permeability as a function of fiber volume fraction of a multi-axial warp knit preform. The preforms were from batch '95 with a 0.5" stitch spacing and a 1/8" stitch pitch. Comparison of NASA Brass and 5 cm² steel fixtures.

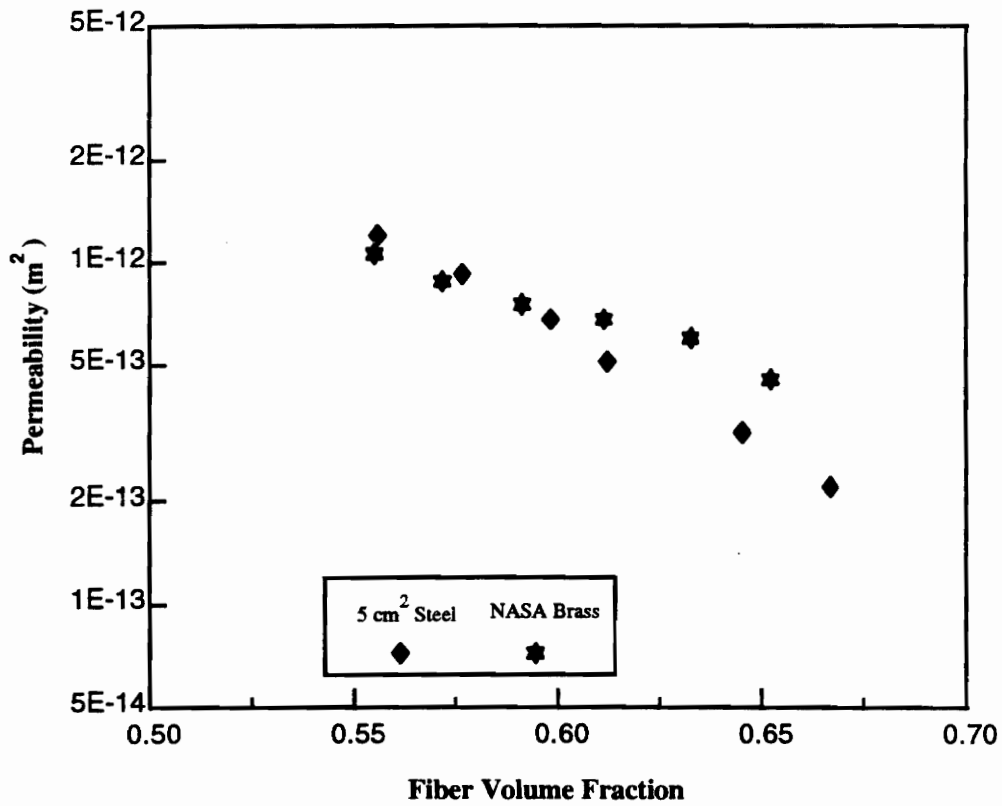


Figure 5.3: Through-the-thickness permeability as a function of fiber volume fraction of a multi-axial warp knit preform. The preforms were from batch`95 with a 0.2" stitch spacing and a 1/8" stitch pitch. Comparison of NASA Brass and 5 cm² Steel fixtures.

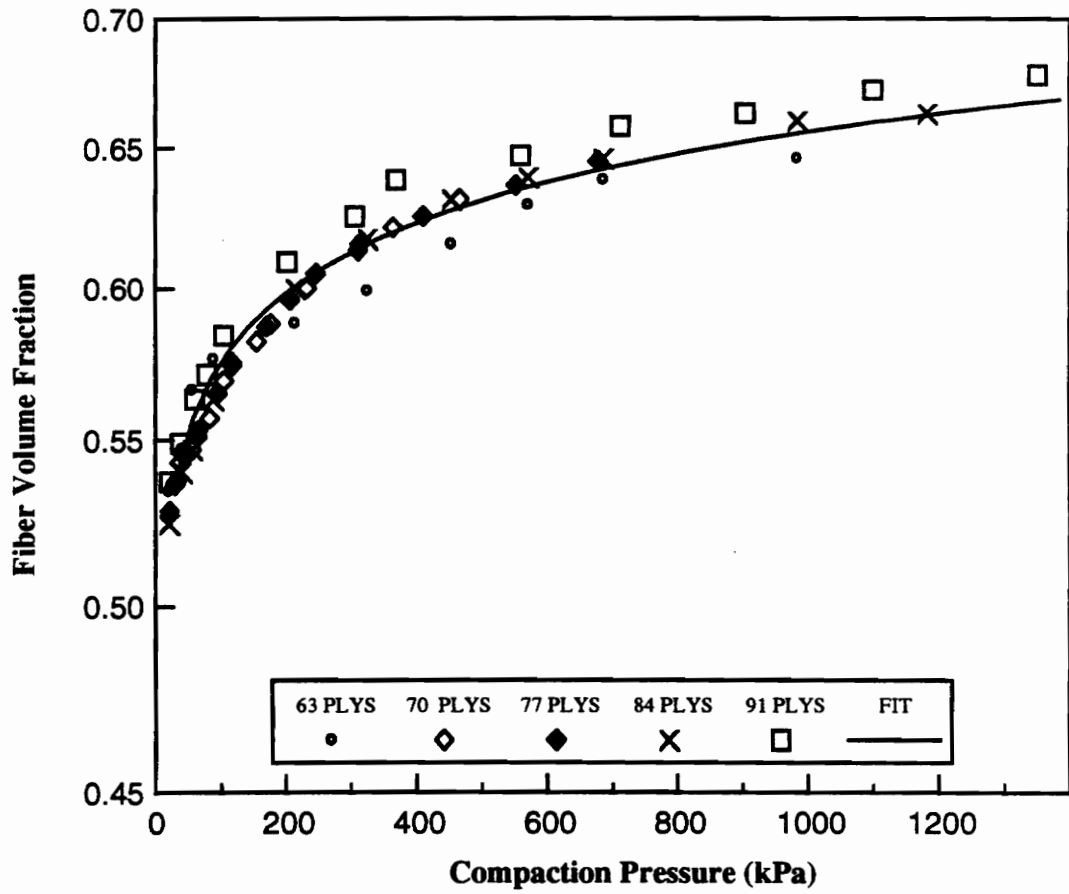


Figure 5.4: Fiber volume fraction versus Compaction Pressure for multi-axial warp knit preform. Tests performed on NASA Brass Fixture with batch`94 preforms.

ranged from 63 to 91. Weideman [44] observed the same phenomenon for preforms. Above 62% fiber volume fraction, the thicker preforms appear to achieve a higher volume fraction for a given compaction pressure. This trend may be due to the fact that the thicker preforms have a larger thickness change at the higher compaction pressures which can be measured more accurately.

Figure 5.5 shows the through-the-thickness permeability as a function of fiber volume fraction. There is virtually no dependence of the number of plies on the permeability behavior of the preform. The number of plies ranged from 63-112.

5.3 EFFECTS OF BATCH VARIATION IN MULTIAXIAL WARP KNIT PREFORMS

Two different batches of multiaxial warp knit preforms were tested. Both batches were made up of 70 plies and have been described in chapter 3. The areal weights of both batches are presented in Table 3.1.

A comparison between compaction behavior of the two preform batches is shown in Figure 5.6. The batch`94 preform was tested on the NASA brass fixture and the batch`95 preform was tested on the 15 cm² steel fixture. The preform stitch spacing and pitch were 0.5" and 1/8", respectively. The results from both the batches are almost identical, however the batch`94 preform indicates a consistently lower compaction pressure over the entire fiber volume fraction range. The possible reason for this might once again be because of fixture differences.

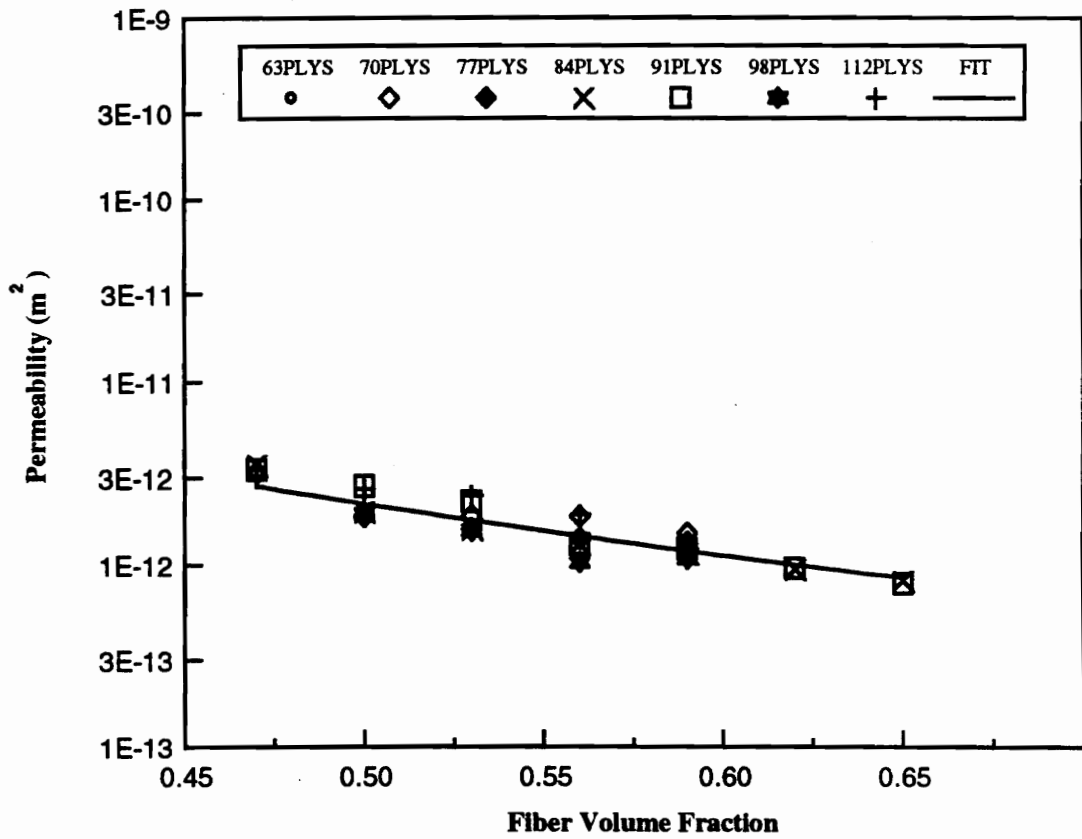


Figure 5.5: Through-the-thickness permeability as a function of fiber volume fraction for multi-axial warp knit preform. Tests conducted on the NASA Brass fixture with batch '94 preforms.

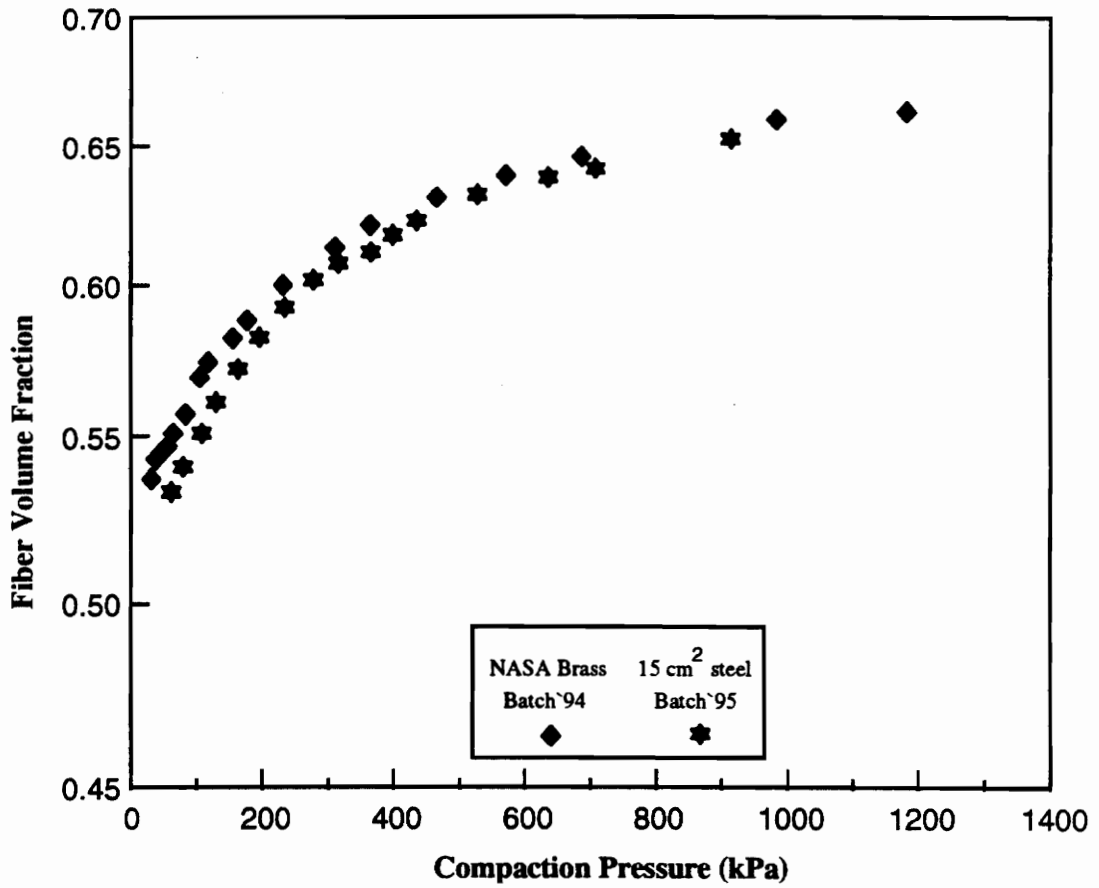


Figure 5.6: Compaction Pressure as a function of fiber volume for a 70-ply multi-axial warp knit preform. Tests performed on the NASA brass and 15 cm² steel fixtures

Figure 5.7 shows a plot of the in-plane, along the stitching direction permeability as a function of fiber volume fraction for both the batches of material. The stitch spacing and pitch are the same as before. The preforms were tested using the 15 cm² steel fixture. The batch'94 preforms have a higher permeability than the batch'95 preforms at all fiber volume fractions. At 60% fiber volume fraction, the batch '94 preform permeability is 66% higher than the batch '95 preform permeability. The results shown in Figure 5.7 may simply represent the variation in permeability that can be expected with different batches of preforms.

Figure 5.8 is a plot of through-the-thickness permeability as a function of fiber volume fraction for both batches of multiaxial warp knit preforms. The stitch spacing and pitch were 0.5" and 1/8", respectively and the number of plies was 70. The results show that both batches of preforms have similar permeabilities for the narrow range of fiber volume fractions where the data overlap.

Figure 5.9 is a plot of the through-the-thickness permeability as a function of fiber volume fraction for both batches of preforms. The stitch spacing was 0.2" and the stitch pitch was 1/8". The tests were performed on the 5 cm² steel fixture. The results once again show that through-the-thickness permeabilities are similar for both batches of materials.

5.4 THROUGH-THE-THICKNESS STITCHING EFFECTS

Multiaxial warp knitting is a way of holding together layers of unidirectional

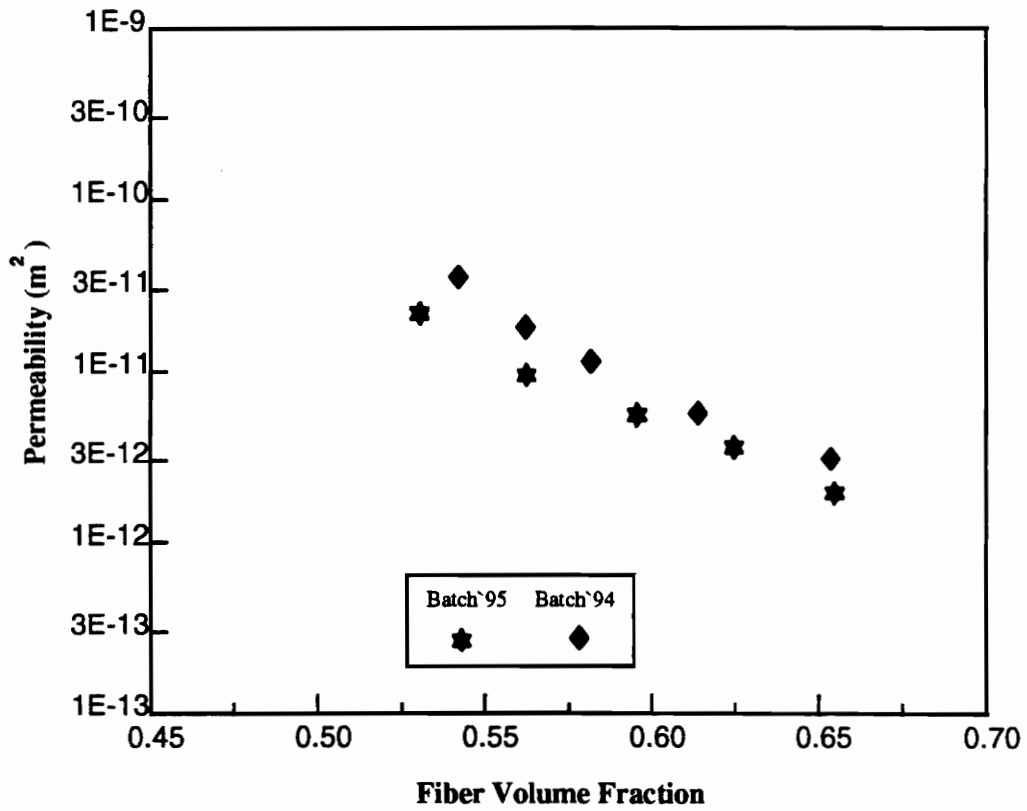


Figure 5.7: Along the stitching permeability as a function of fiber volume for 70 ply multi-axial warp knit preforms. Tests conducted on 15 cm² steel fixture

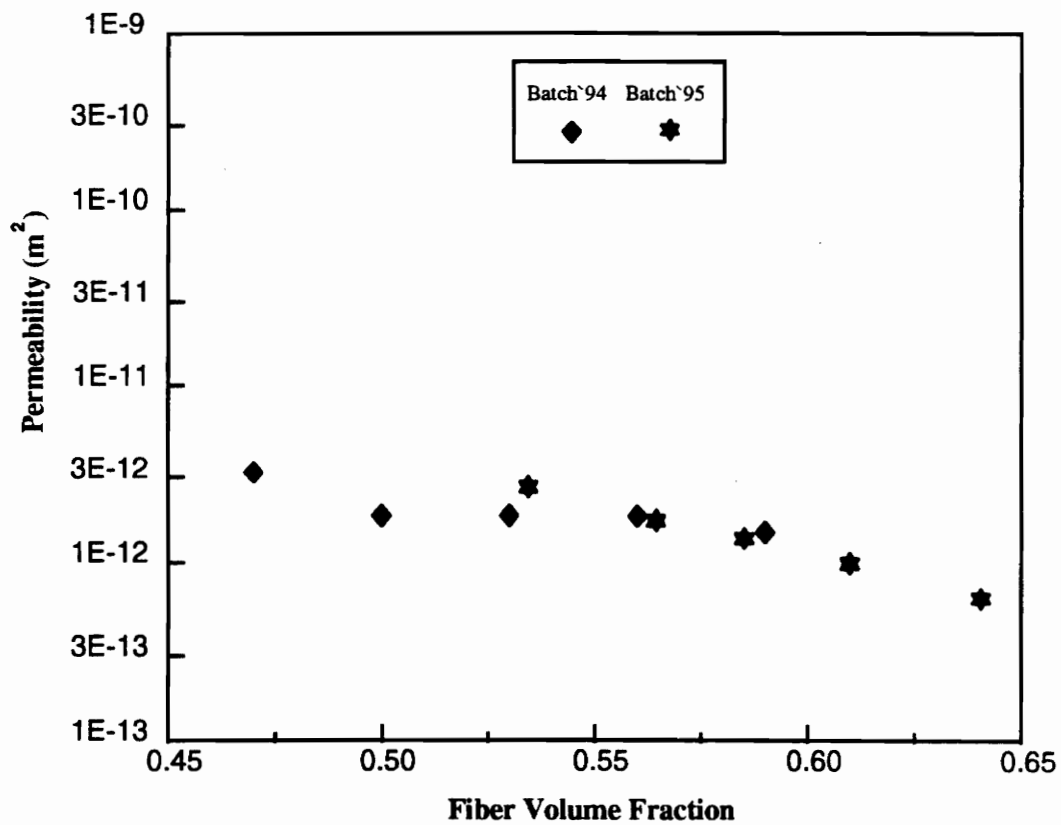


Figure 5.8: Through-the-thickness permeability as a function of fiber volume fraction for 70 ply multi-axial warp knit preform. 0.5":1/8" stitched preform. Tests conducted on NASA Brass fixture

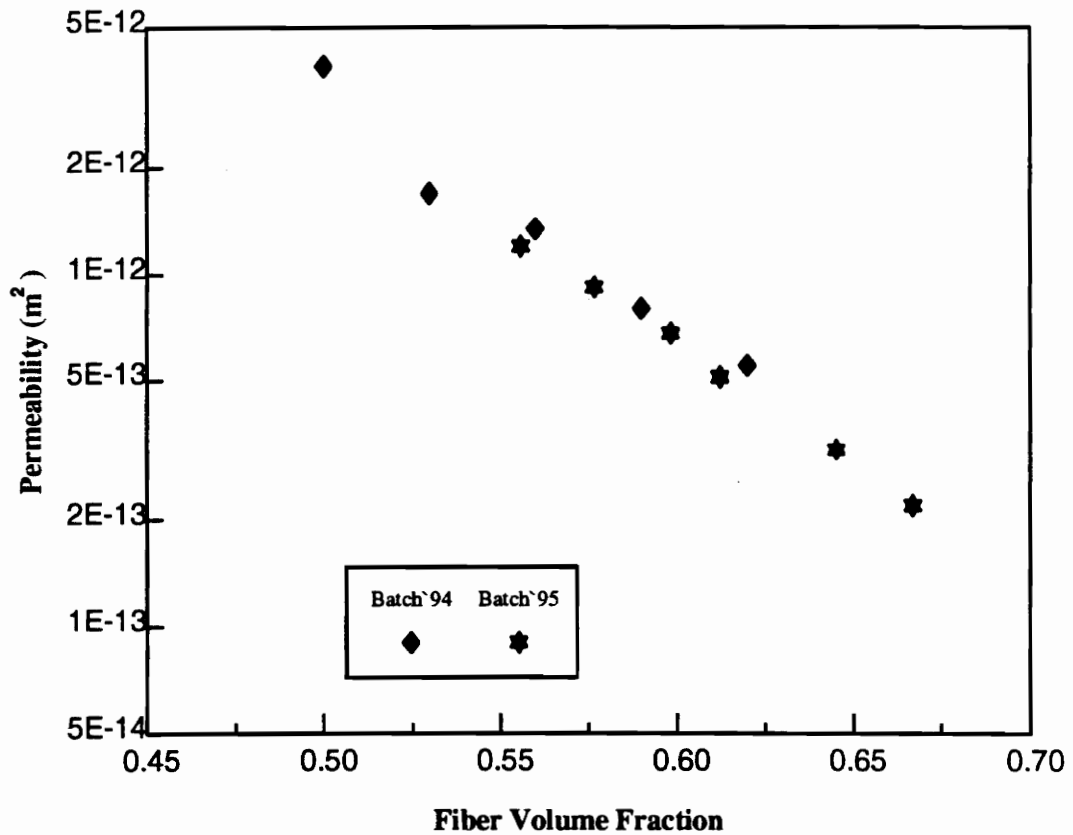


Figure 5.9: Through-the-thickness permeability as a function of fiber volume fraction for 70 ply multi-axial warp knit preforms. The stitch spacing and pitch were 0.2" and 1/8", respectively. Tests were conducted on the 5 cm² steel fixture.

reinforcing yarns that are oriented in several directions. This results in a multilayer structure with strength in many directions. A stiff yarn like carbon can be used as the reinforcing yarn, but a softer and more flexible yarn must be used to form the knitting loops. Preforms with through-the-thickness stitching require a modification to the value of preform density used in Equation 3.2 to calculate the fiber volume fraction. The computation was done by weighing a given sample of the stitched preform and then re-weighing the preform with the Kevlar stitching threads removed. The following rule of mixtures was used to estimate the density of the preform,

$$\rho_{preform} = \rho_{carbon} * v_{carbon} + \rho_{kevlar} * v_{kevlar} \quad (5.1)$$

where ρ = density of the specific component in g/m^3 and v = volume fraction of the specific component.

The density of carbon was taken to be $1.8g/m^3$ and that of Kevlar $1.44g/m^3$. Table 5.1 presents the weight of the stitched preform, weight of the Kevlar stitching, and the corrected preform density for the four different stitch densities.

The 15 cm^2 steel fixture was used for the compaction and in-plane permeability tests, and the 5 cm^2 steel fixture was used for the through-the-thickness permeability tests. The test procedures have been outlined in Section 3.3.1. The preforms were cut using a band saw so as to ensure good dimensional tolerance with the fixture cavities and weighed to compute their areal weights (see Table 3.1).

Table 5.1: Densities of the Stitched Preforms

Preform stitching parameters (spacing:pitch)	Weight of preform grams	Weight of Stitching grams	Density of Preform g/cm³
0.5":1/6"	337.7	2.72	1.796
0.5":1/8"	283.7*	2.94	1.795
0.2":1/6"	340.7	6.79	1.791
0.2":1/8"	342.5	8.85	1.788

Note:

* Preform size for this case was 12.7 cm x15.24 cm. For all other preforms it was 15.24cm x 15.29cm.

Figure 5.10 is a plot of fiber volume fraction as a function of compaction pressure for the preforms with different stitch densities. The constants of the power law regression model are presented in Table 5.2. The initial fiber volume fraction at zero load of the preforms are different and depend stitch density. The unstitched preform has the lowest initial fiber volume fraction and the 0.2":1/8" stitched preform has the highest. This is a result of the stitching tension which compacts the preform, and therefore, the higher the stitching density, the higher the initial fiber volume fraction. Typical compaction curves exhibit a linear portion at low fiber volume fractions and a non-linear portion at higher volume fractions. The linear part has been described as the Hookean part and the non-linear part as the non-Hookean part by Batch and Cumisky [20]. It is interesting to note that the linear part of the curve reduces as the density of stitching increases with a corresponding increase in the non-linear part. A possible reason for this may be that the stitching tends to constrain the movement of the individual carbon fiber tows, thereby reducing the ability of the fibers to redistribute the load through reorientation when compacted. It is important to perform the compaction test first, as useful insights into the initial fiber volume fraction of the preform and the amount of load that may be required to reach a desired fiber volume fraction can be ascertained.

The permeability tests were performed using the procedure outlined in Section 3.3.2. In order to minimize edge flow, the edges of the preform in contact with the walls of the fixture were smeared with silicone grease and then placed into the cavity of the

Table 5.2: Constants for the Compaction Fit Equation

Material Used	Number of Plies/Tubes	Constant 'c' ^{**} (in kPa)	Constant 'd' ^{**}
Multiaxial Warp Knit Preform [*] (Unstitched)	70	0.371	0.09
Multiaxial Warp Knit Preform [*] (0.5":1/6")	70	0.405	0.071
Multiaxial Warp Knit Preform [*] (0.5":1/8")	70	0.383	0.079
Multiaxial Warp Knit Preform [*] (0.2":1/6")	70	0.457	0.048
Multiaxial Warp Knit Preform [*] (0.2":1/8")	70	0.472	0.043
Braided Preform 0±60°	10 ^{***}	0.491	0.040
Braided Preform 0±60°, Thin	4 ^{***}	0.393	0.066
Braided Preform 0±60°, Thick	14 ^{***}	0.473	0.043
Braided Preform 0±70°	9 ^{***}	0.502	0.037
Glass Fabric 'F 16 Finish'	16	0.258	0.146
Glass Fabric 'F 72 Finish'	16	0.236	0.16

Note:

* Preforms are from Batch`95

** The fit equation used is Fiber Volume Fraction = c*(Applied Pressure)^d

*** 1 braid tube is equal to 2 braid plies

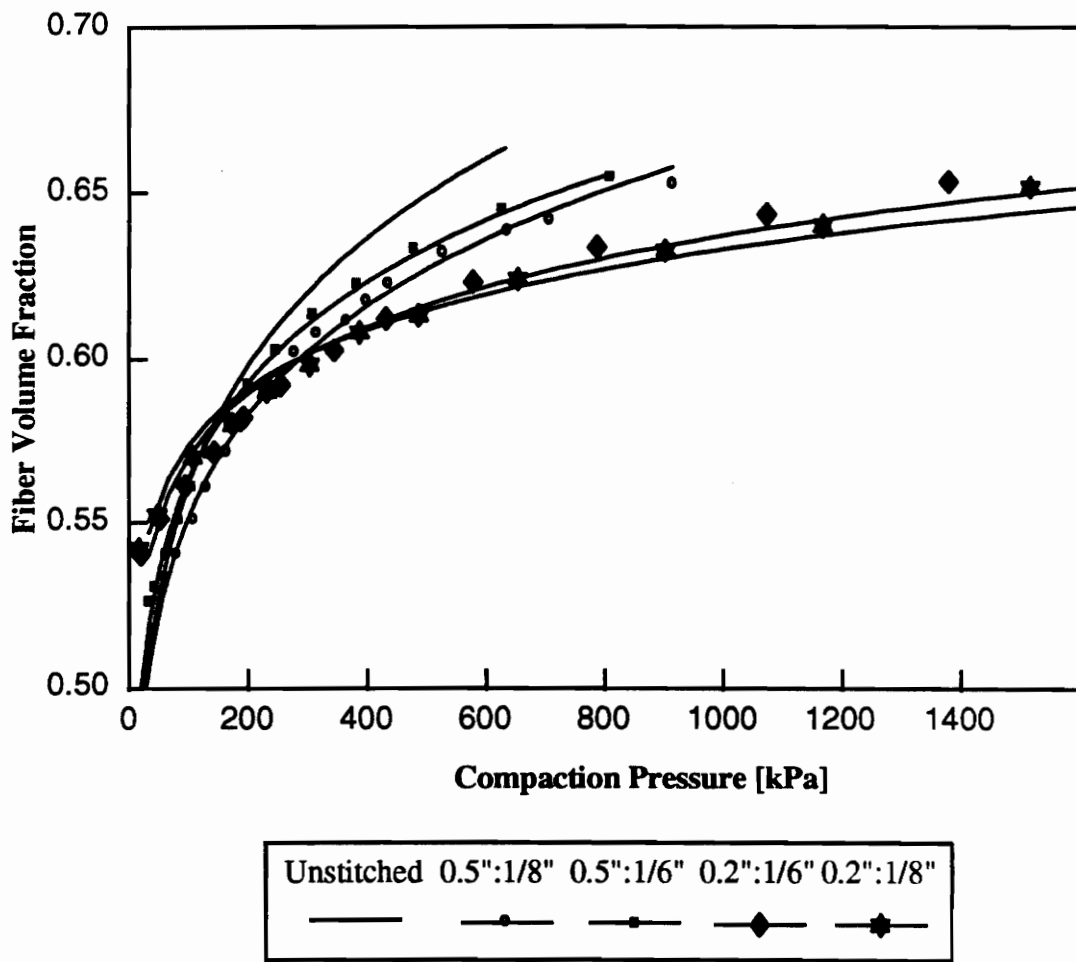


Figure 5.10: Fiber volume fraction as a function of compaction pressure for multi-axial warp knit preforms with different stitch densities.

fixture. Figures 5.11 and 5.12 are plots of in-plane permeability as a function of fiber volume fraction measured along the stitching direction. The figures compare the permeability behavior of preforms with stitch spacings of 0.5" and 0.2" to the unstitched preform. It is clear that stitching increases the in-plane permeability. Figure 5.13 is a bar graph plot comparing the values of in-plane permeability of preforms with a 0.5" stitch spacing at specific fiber volume fractions. Data was obtained from Figure 5.11. The preforms with the 1/8" stitch pitch have a slightly higher permeability than the preforms with the 1/6" stitch pitch. The in-plane along the stitching permeability of preforms with 0.2" stitch spacing at specific fiber volume fractions is shown in Figure 5.14. The data was obtained from Figure 5.12. For a given stitch spacing, the preforms with the higher number of stitches per inch have a higher permeability.

Figures 5.15 and 5.16 compare the in-plane permeability of preforms stitch with different spacing and a common stitch pitch. There does not seem to be any direct correlation between in-plane permeability and stitch spacing. Figure 5.17 shows the fiber volume fraction versus compaction pressure for preforms with a 1/6" stitch pitch. The compaction curves intersect each other at the same fiber volume fraction that the permeability curves intersect in Figure 5.15. Hence, for fiber volume fractions below 56.5%, the 0.2" stitch spacing preforms have a higher permeability than the 0.5" stitch spacing preforms. Above a fiber volume fraction of 56.5%, the opposite is true. The intersection of the permeability curves in Figure 5.16 at 60%

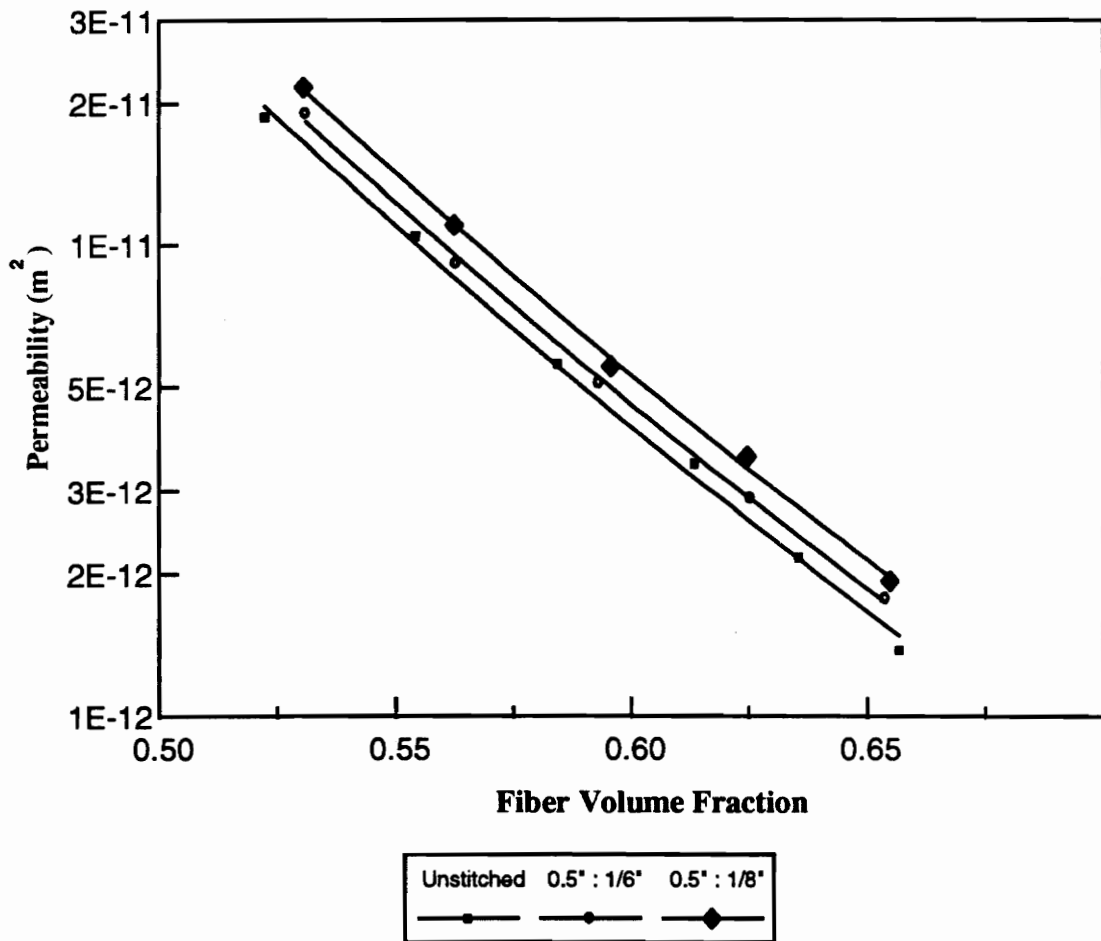


Figure 5.11: In-plane permeability as a function of fiber volume fraction for multi-axial warp knit preforms measured along the stitching direction.

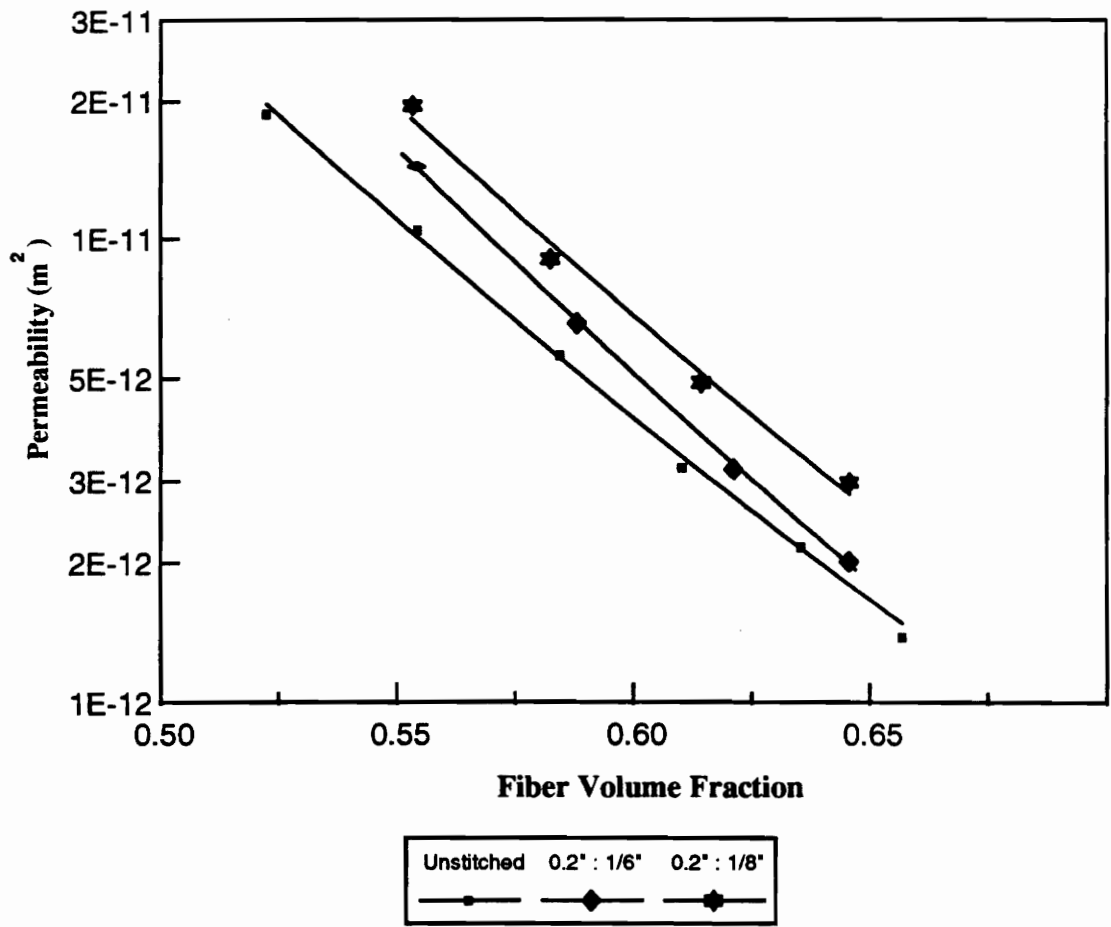


Figure 5.12: In-plane permeability as a function of fiber volume fraction for multi-axial warp knit preforms measured along the stitching direction.

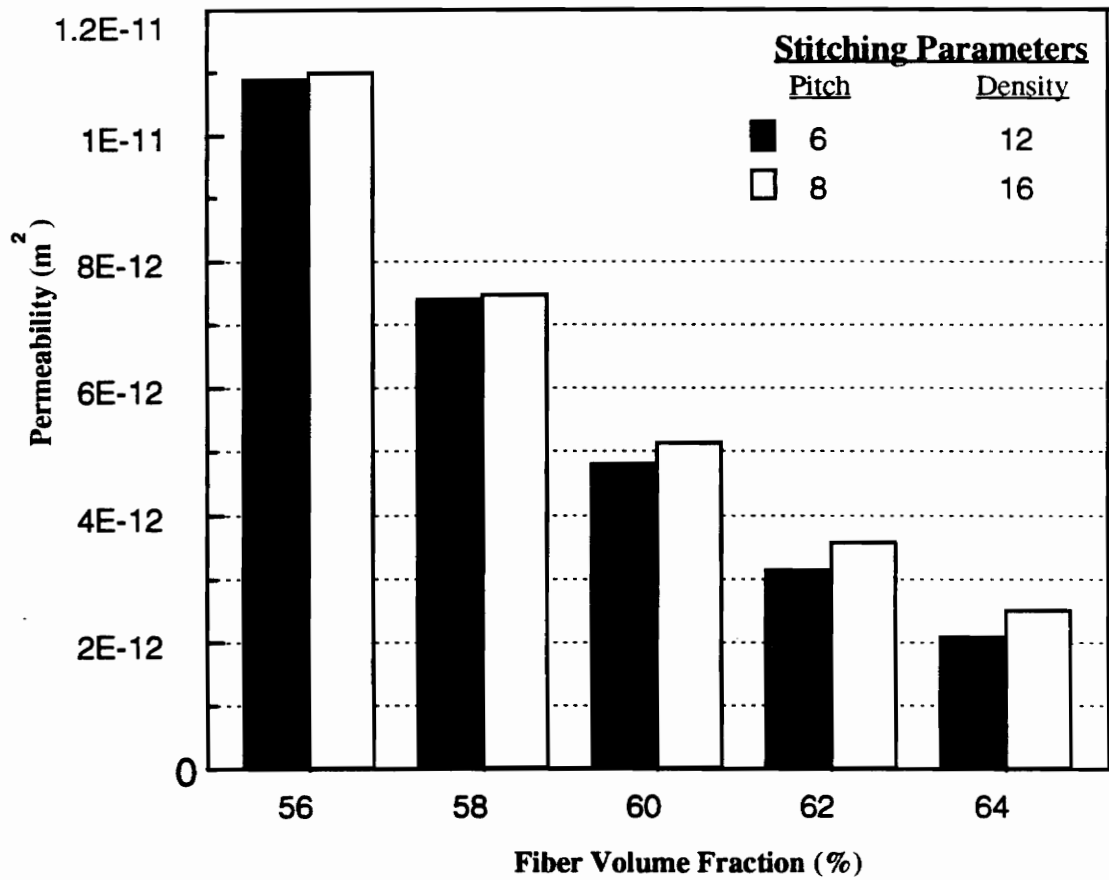


Figure 5.13: Bar graph comparison of in-plane, along the stitching direction permeability of preforms with a 0.5" stitch spacing at specific fiber volume fractions.

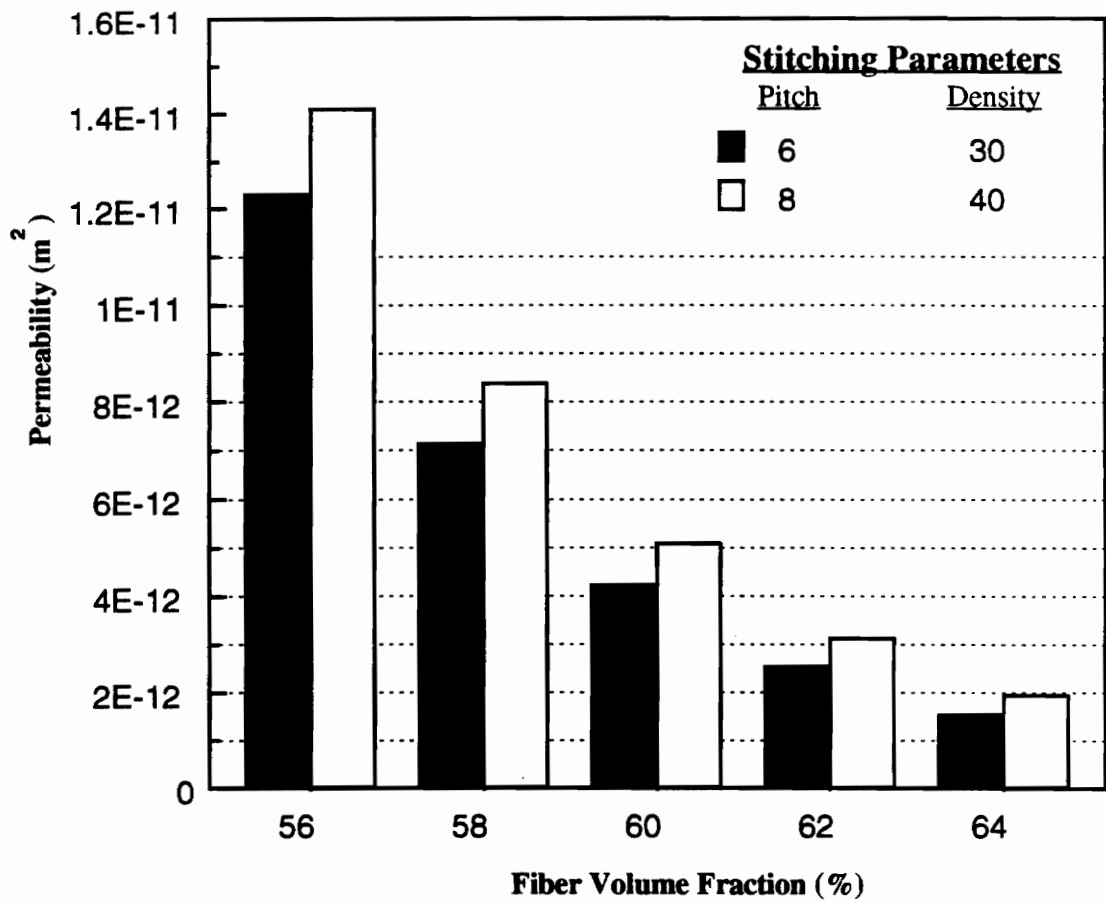


Figure 5. 14: Bar graph comparison of in-plane, along the stitching direction permeability of preforms with a 0.2" stitch spacing at specific fiber volume fractions.

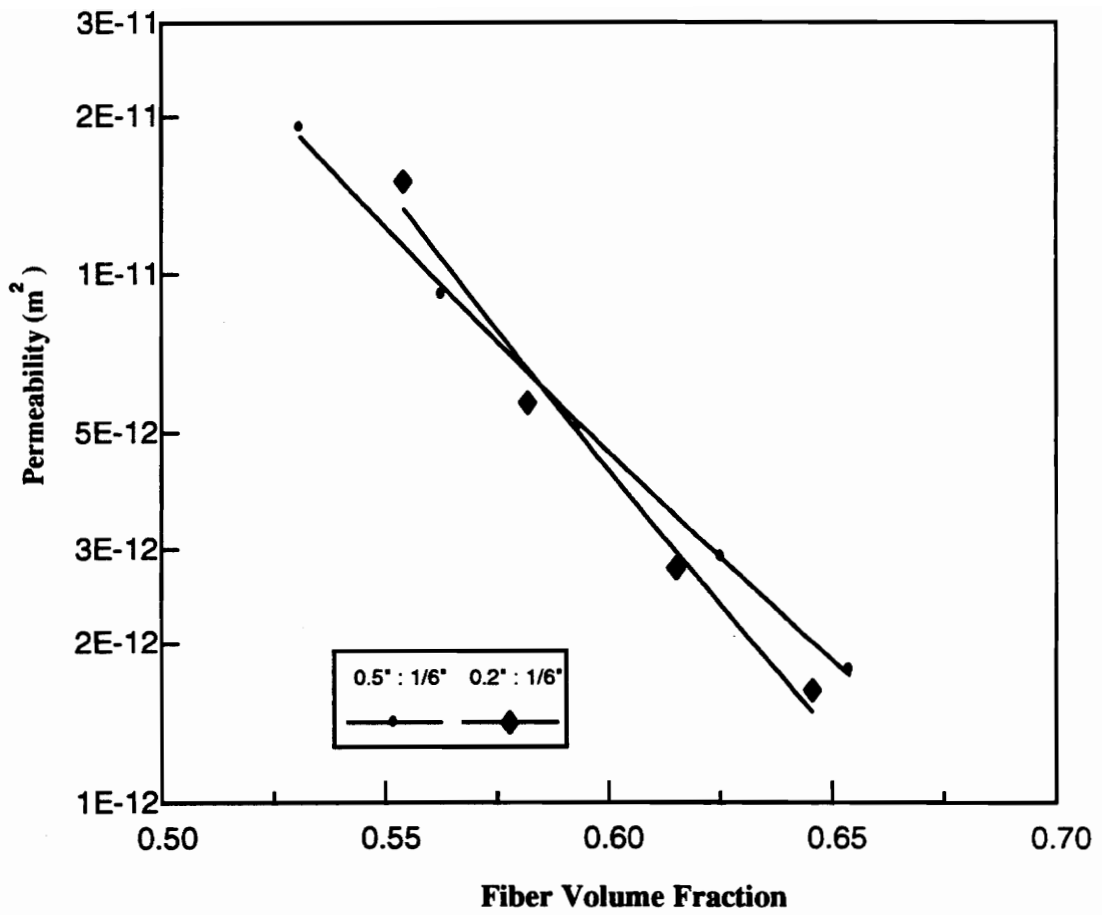


Figure 5.15: In-plane permeability as a function of fiber volume fraction for preforms with different stitch spacing and a stitch pitch of 1/6". Tests were conducted along the stitching direction.

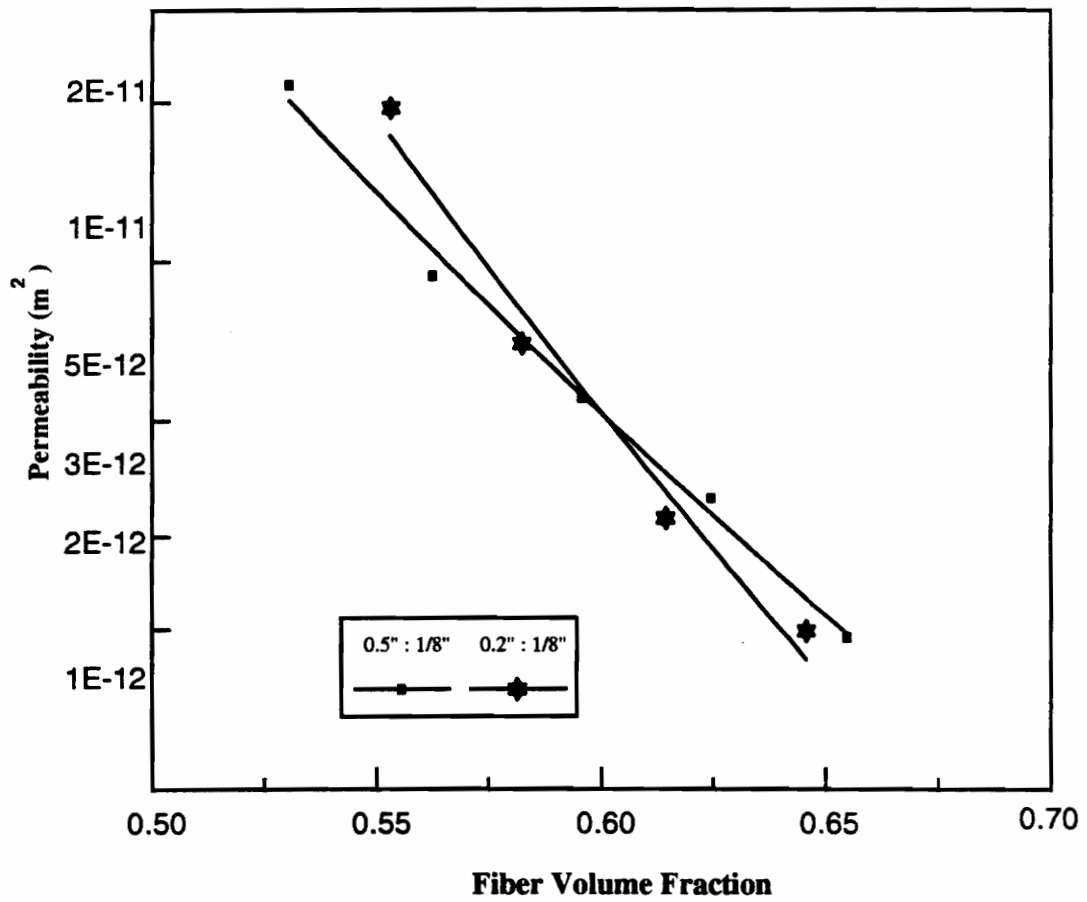


Figure 5.16:In-plane permeability plots as a function of fiber volume fraction for preforms with different stitch spacing and a stitch pitch of 1/8". Tests were conducted along the stitching direction.

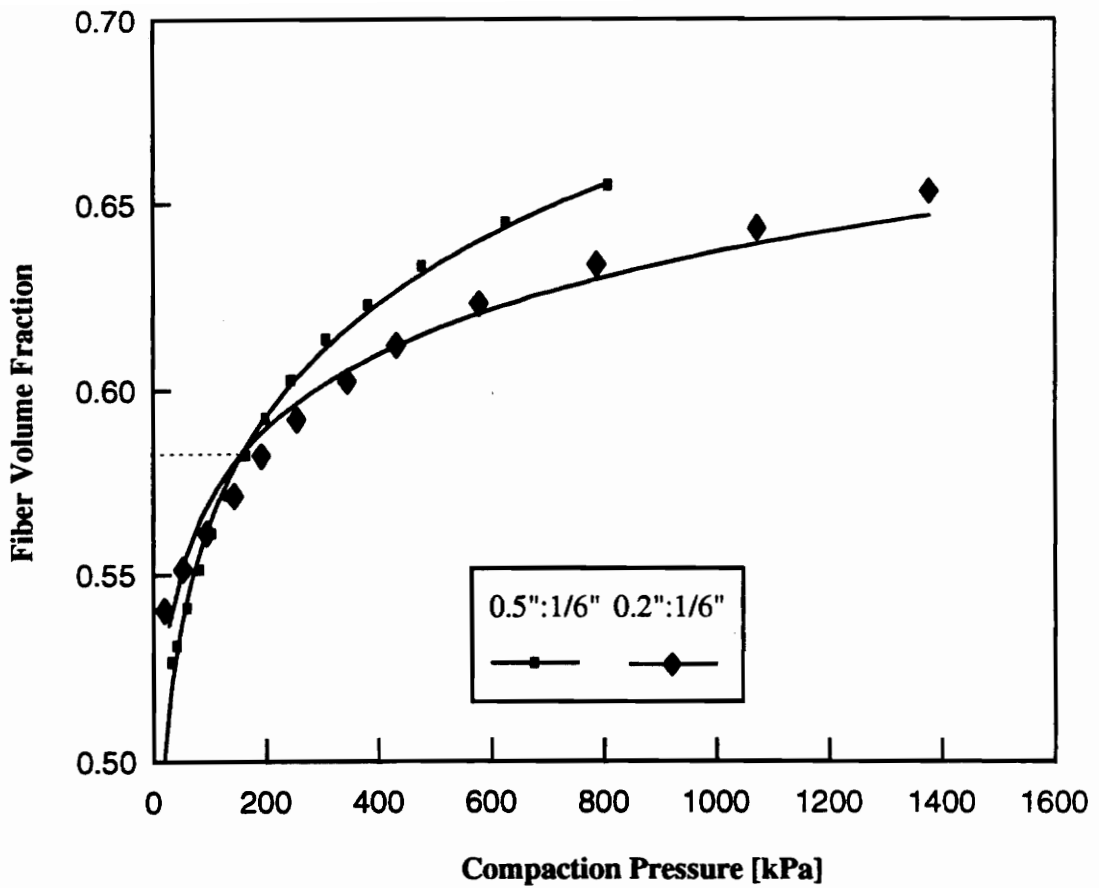


Figure 5.17:Fiber volume fraction versus compaction pressure. Comparisons between preforms with different stitch spacing and a stitch pitch of 1/6\"/>

fiber volume fraction can be attributed to the intersecting compaction curves in Figure 5.10. The constants for the regression model are presented in Table 5.3.

Results for the in-plane, normal to the stitching direction, permeability are presented in Figures 5.18 and 5.19. For a specified stitch spacing, the preforms with a higher stitch pitch have a lower in-plane permeability. The preforms with a 1/8" pitch offer a greater resistance to the flow of fluids than preforms with a 1/6" pitch. Figures 5.20 and 5.21 are bar graph plots of the in-plane permeability at specific fiber volume fractions obtained from data in Figures 5.18 and 5.19, respectively. Again these curves clearly show the effects of stitch pitch on the in-plane permeability measured normal to the stitching direction.

The through-the-thickness permeability as a function of fiber volume fraction for multiaxial warp knit preforms with different stitching parameters are presented in Figure 5.22. It can be seen that the through-the-thickness stitching tends to increase the permeability. This could be attributed to channel formation around a stitching thread in the thickness direction created by the penetration of the stitching needle. However, preforms with the highest density do not necessarily have the highest permeability. Figure 5.23 shows that the 0.2" stitch spacing preforms, with stitch densities of 30 and 40 penetrations/inches² have a lower permeability compared to the 0.5" stitch spacing preforms with stitch densities of 12 and 16 penetrations/inches². This surprising result can best be answered by taking a closer look at the dry preforms

Table 5.3 : Constants for the Permeability Fit Equation

Material Type	Test Conducted	Number of Plies/Tubes Used	Constant 'a' (in m²)	Constant 'b'
Multiaxial Warp Knit Preform Batch`95 (Unstitched)	Along Knitting	70	1.2 E-14	-11.35
	Normal to Knitting	70	8.4 E-15	-10.85
	Through-the-Thickness	70	1.0 E-16	-14.15
Multiaxial Warp Knit Preform Stitched Batch`95 (0.5":1/6")	Along Stitching	70	6.8 E-15	-12.84
	Normal to Stitching	70	3.8 E-15	-12.22
	Through-the-Thickness	70	1.7 E-14	-7.43
Multiaxial Warp Knit Preform Stitched Batch`95 (0.5":1/8")	Along Stitching	70	1.8 E-14	-11.07
	Normal to Stitching	70	3.5 E-15	-11.95
	Through-the-Thickness	70	2.0 E-14	-7.77
Multiaxial Warp Knit Preform Stitched Batch`95 (0.2":1/6")	Along Stitching	70	1.6 E-15	-15.42
	Normal to Stitching	70	8.2 E-16	-14.92
	Through-the-Thickness	70	4.9 E-15	-8.86
Multiaxial Warp Knit Preform Stitched Batch`95 (0.2":1/8")	Along Stitching	70	2.7 E-15	-14.77
	Normal to Stitching	70	7.7 E-16	-14.95
	Through-the-Thickness	70	5.0 E-15	-9.42

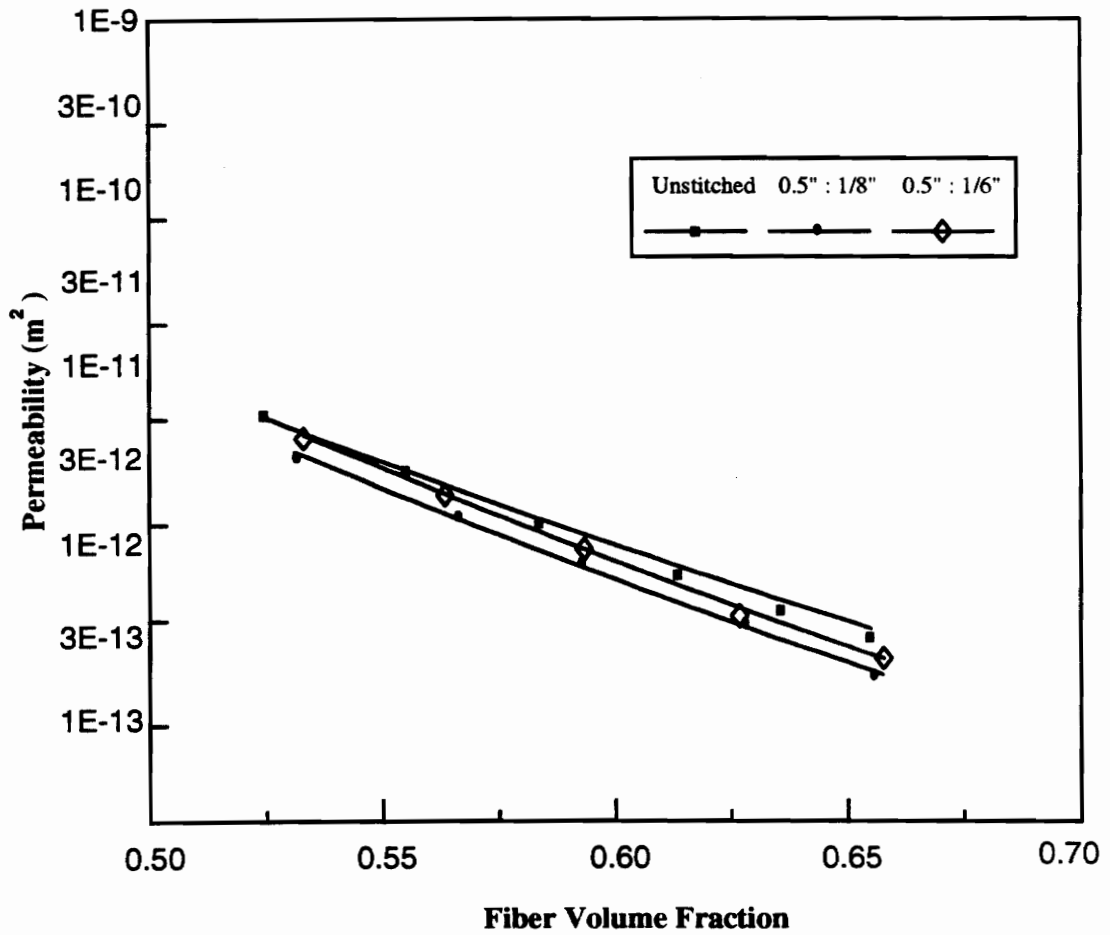


Figure 5.18: In-plane permeability as a function of fiber volume fraction for multi-axial warp knit preforms measured normal to the stitching direction.

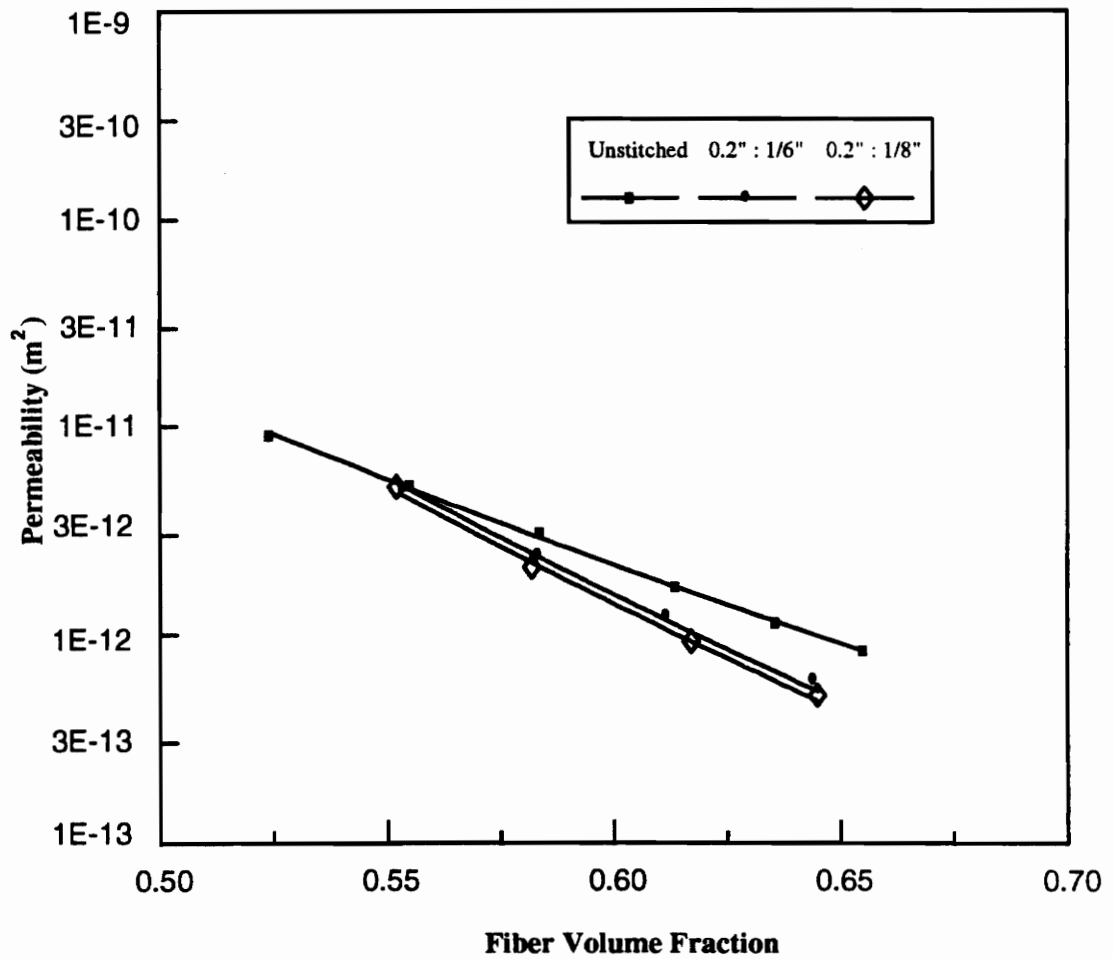


Figure 5. 19: In-plane permeability as a function of fiber volume fraction for multi-axial warp knit preforms measured normal to the stitching direction.

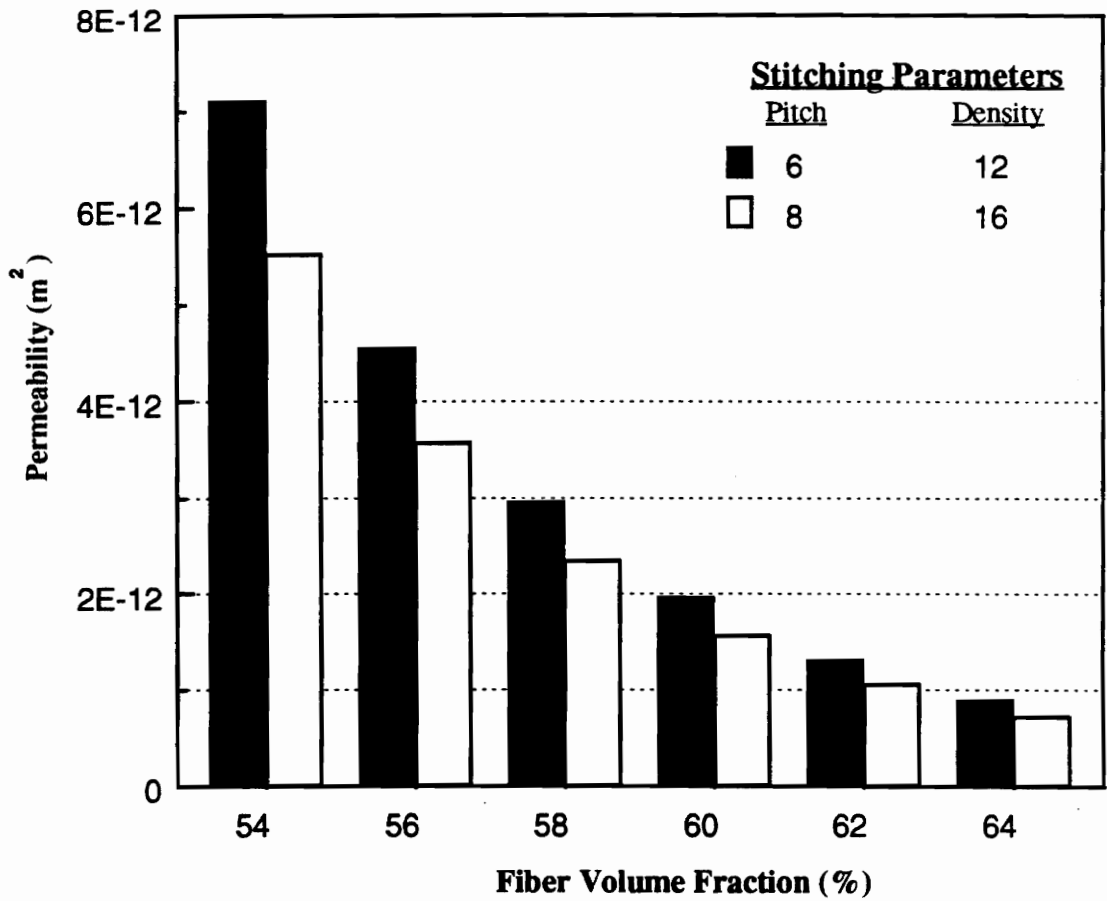


Figure 5.20: Bar graph comparison of in-plane, normal to the stitching direction permeability of preforms with a 0.5" stitch spacing at specific fiber volume fractions.

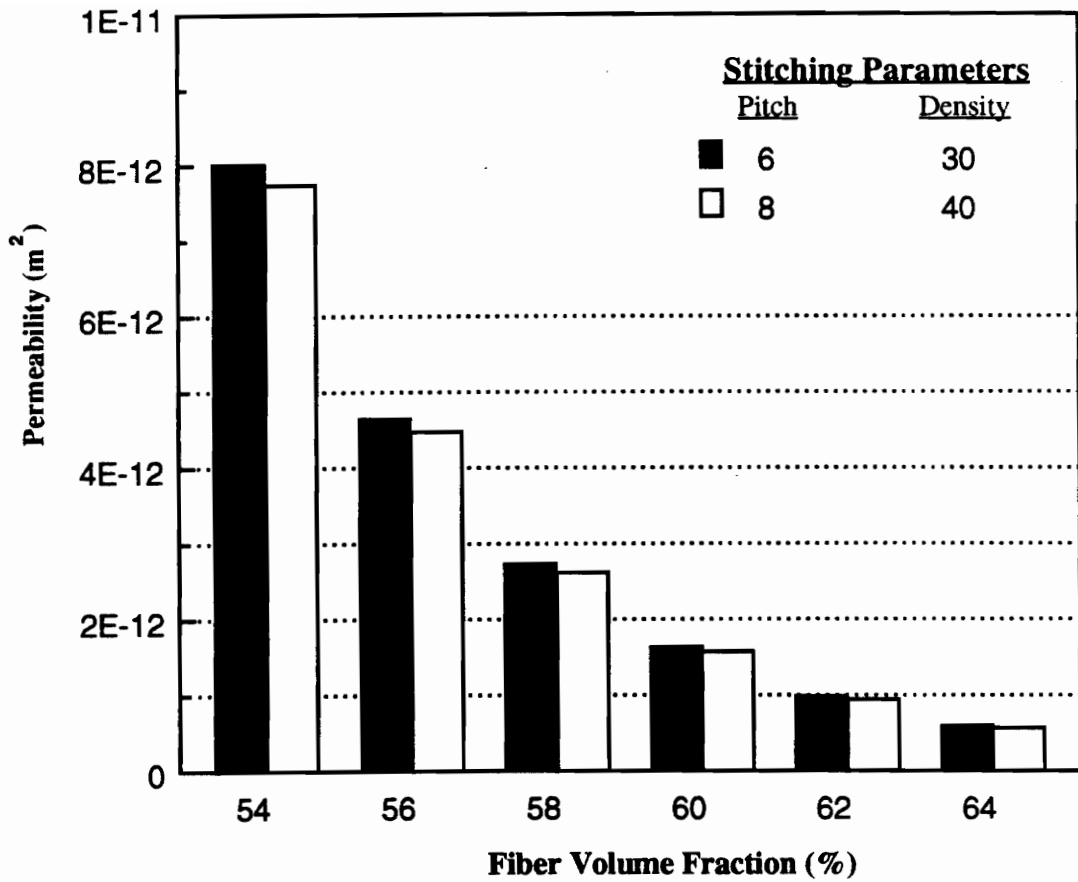


Figure 5.21: Bar graph comparison of in-plane, normal to the stitching direction permeability of preforms with a 0.2" stitch spacing at specific fiber volume fractions.

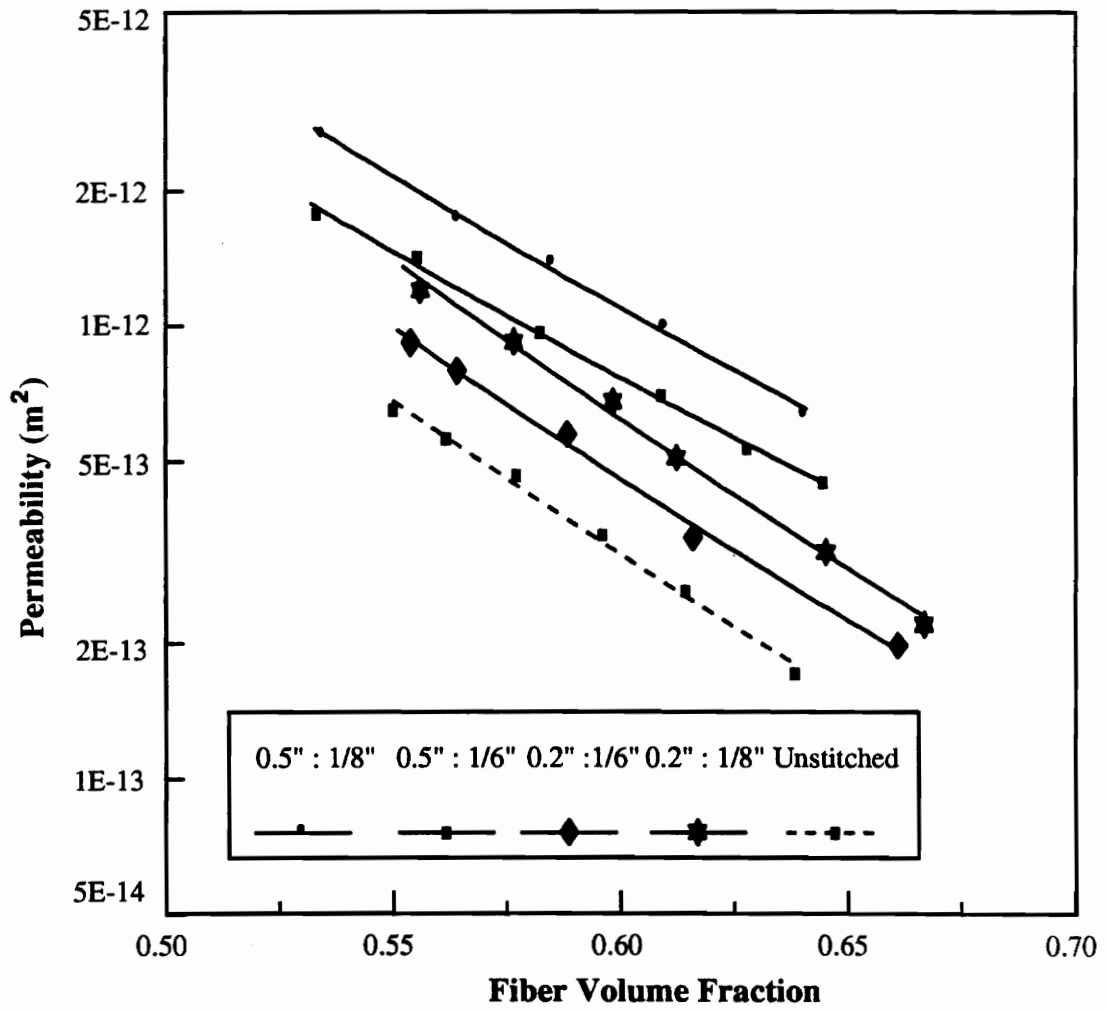


Figure 5.22: Through-the-thickness direction permeability as a function of fiber volume fraction for multi-axial warp knit preforms.

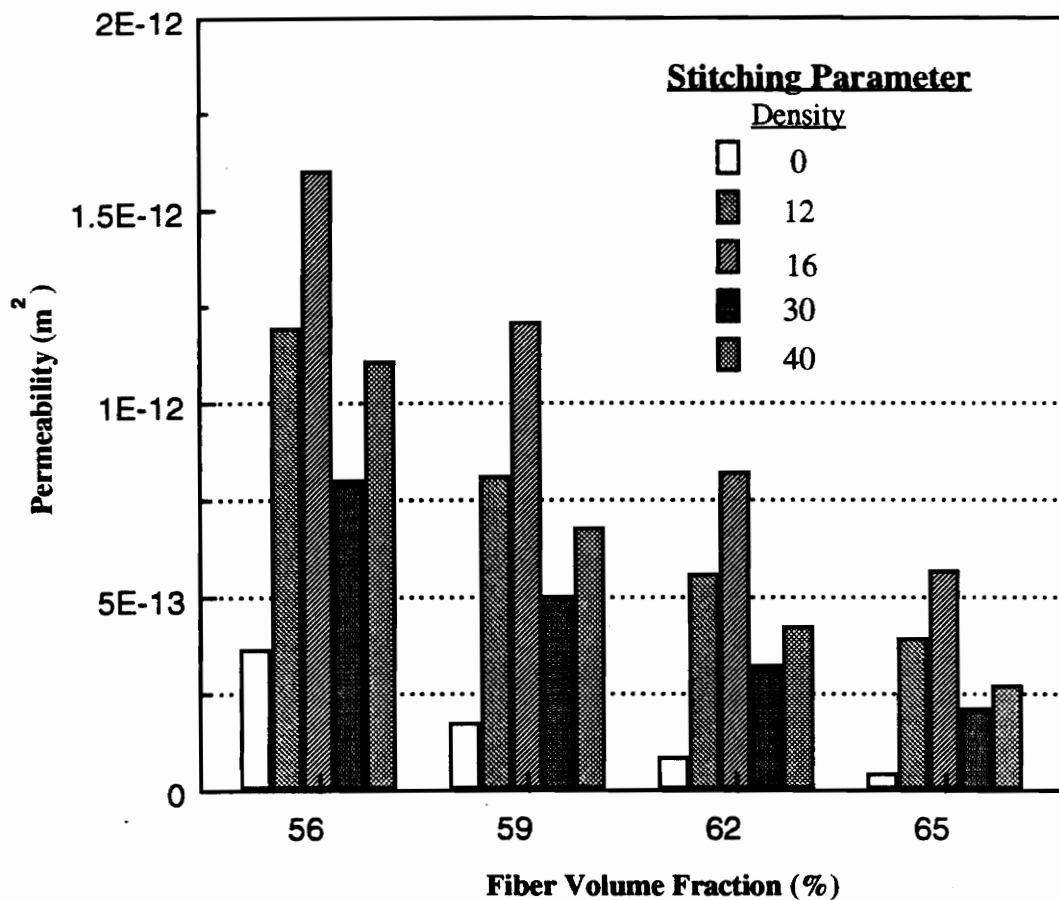


Figure 5. 23: Through-the-thickness direction permeability plots of multi-axial warp knit preforms at specific fiber volume fractions. The numbers in the legend stand for the penetrations per square inch

and studying the microstructure of the individual tows in the preform. Figures 5.24 and 5.25 show the region around a stitch, looking down the top, of preforms with a 1/8" stitch pitch and stitch spacing of 0.5" and 0.2", respectively. The photographs were taken using a camera mounted Wild M3Z microscope. In the case of the preform with 0.5" spacing, the tows are cleanly separated apart, especially the +45° ones and a clear region around the stitch is formed. For the preform with 0.2" spacing, the tows are held tightly together thereby restricting their movement and consequently reducing the size of the open region around the stitch. Figures 5.26 and 5.27 show the same region around the stitch looking from the bottom of the preform with a stitch spacing of 0.5" and 0.2", respectively. This is the region where the stitching thread is made to loop around the runner thread which runs along the bottom surface. Once again, the preform with a 0.5" stitch spacing shows a clean separation of the tows whereas the preform with a 0.2" stitch spacing shows large amounts of fiber damage because of the tight stitching. Figures 5.28 and 5.29 are photographs of composite specimens taken with a Nikon Epiphot microscope. The section studied is around a stitch. The specimens were cut out from cured, 70-ply multiaxial warp knit preform composite panels with stitch spacings of 0.5" and 0.2" and a stitch pitch of 1/8" fabricated by the resin film infusion (RFI) molding process. The micrographs clearly show a larger resin rich area around the stitch of the preform with a 0.5" stitch spacing, compared to the preform with a 0.2" stitch spacing. Figures 5.30 and 5.31 show microphotographs of sections between two stitches of panels with 0.5" and 0.2" stitch spacings. It can be seen that there exists considerable tow distortion at the ply

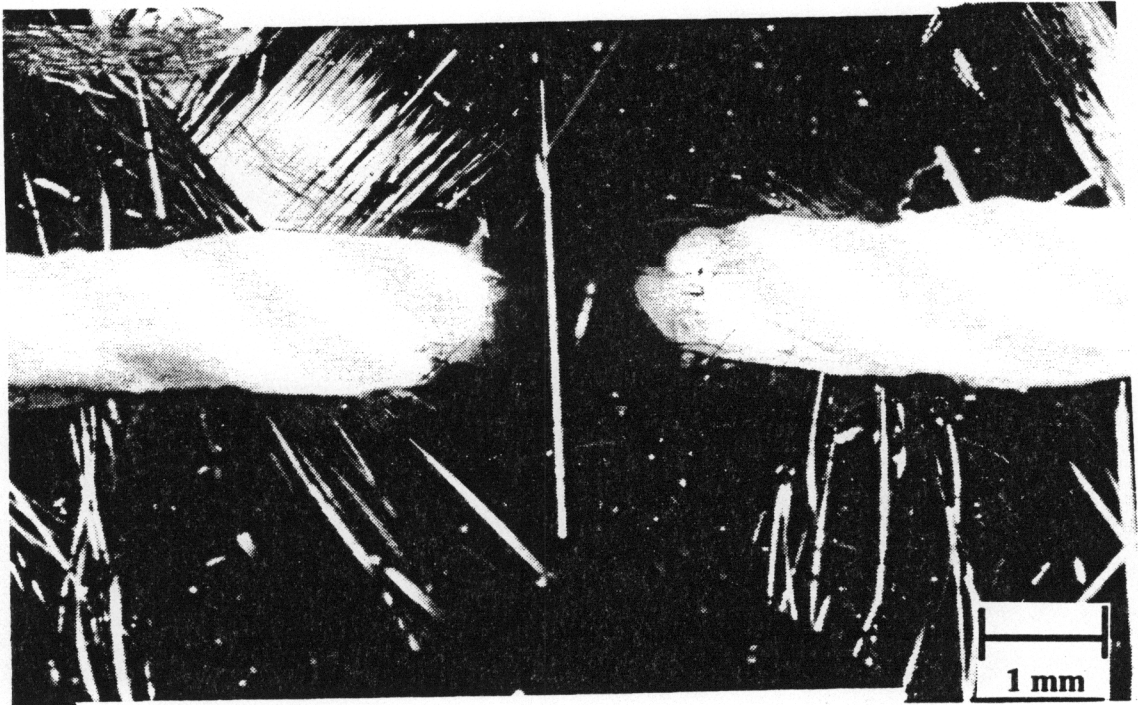


Figure 5.24: Optical micrograph of the area around a stitch of a preform with 0.5" stitch spacing and 1/8" stitch pitch. Magnification used is indicated by the scale bar.

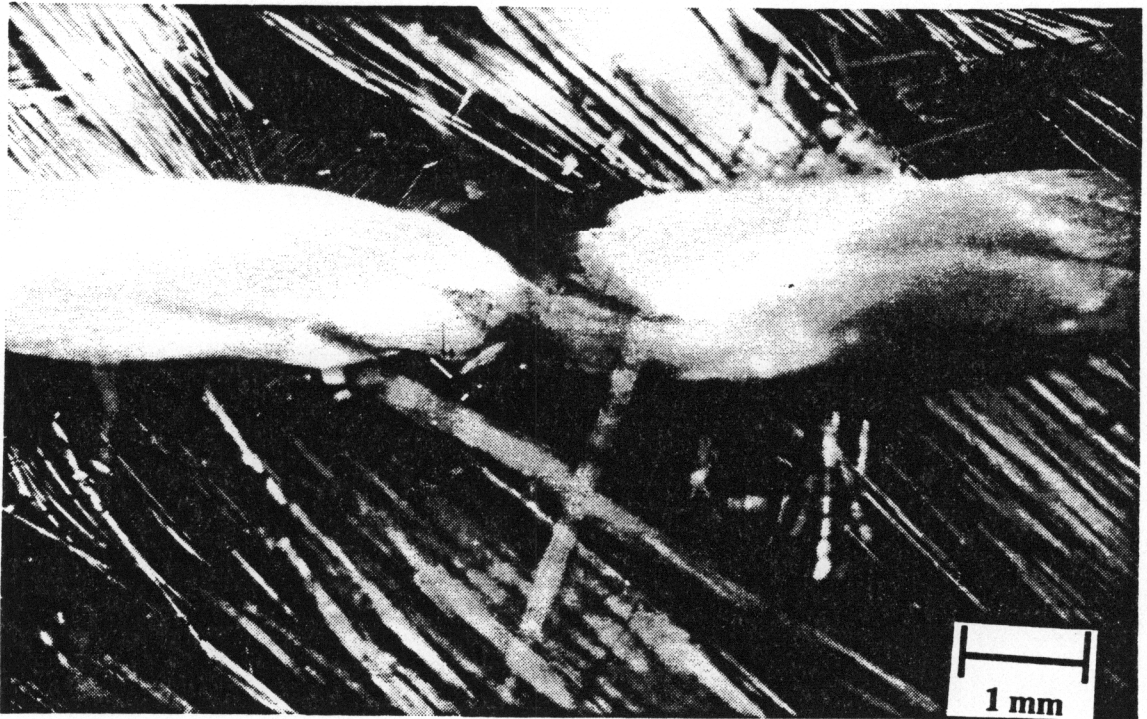


Figure 5.25: Optical micrograph of the area around a stitch of a preform with 0.2" stitch spacing and 1/8" stitch pitch. Magnification used is indicated by the scale bar.

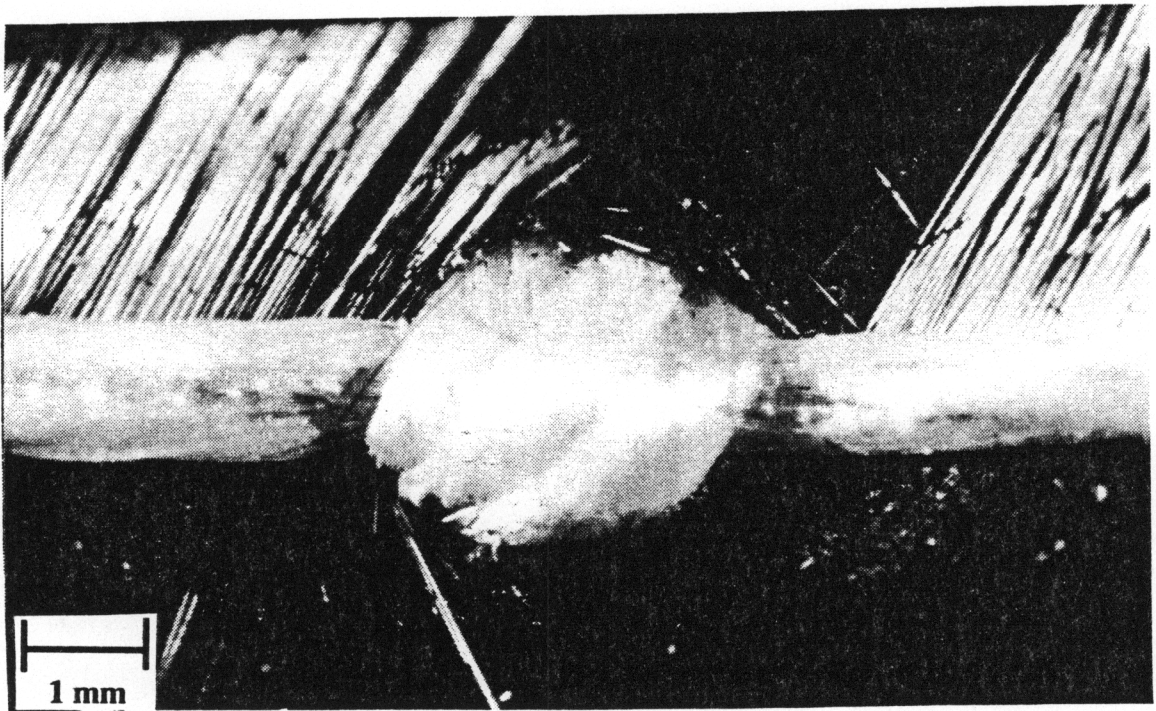


Figure 5.26: Optical micrograph of the area around a stitch looking from the bottom of a preform with 0.5" stitch spacing and 1/8" stitch pitch. Magnification used is indicated by the scale bar.

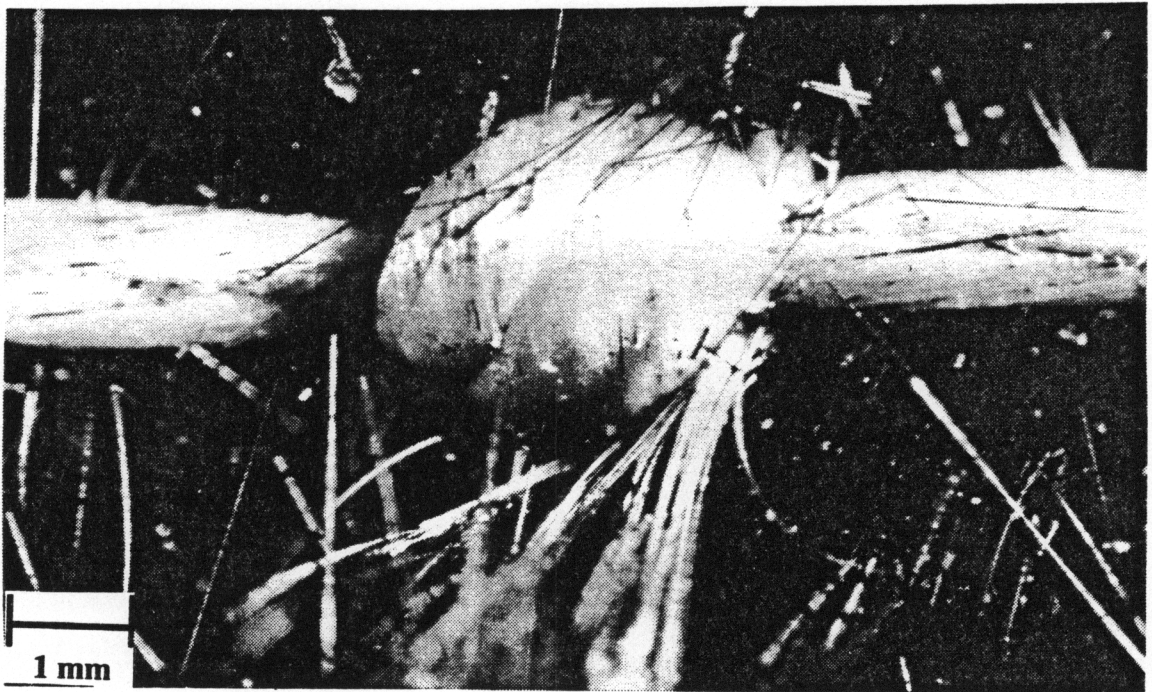


Figure 5.27: Optical micrograph of the area around a stitch looking from the bottom of a preform with 0.2" stitch spacing and 1/8" stitch pitch. Magnification used is indicated by the scale bar.

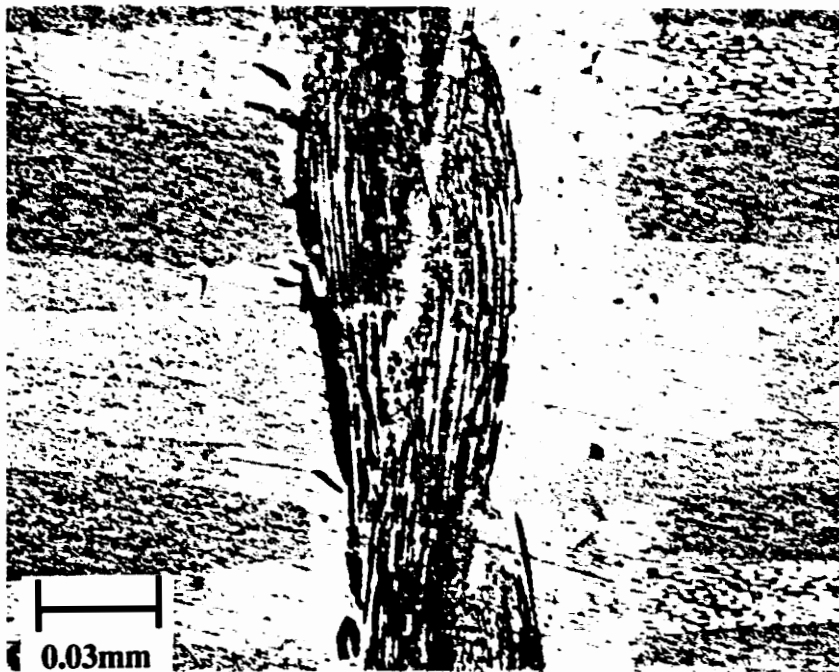


Figure 5.28: Photograph taken on the Nikon Epiphot around a stitch of a preform with 0.5" stitch spacing and 1/8" stitch pitch

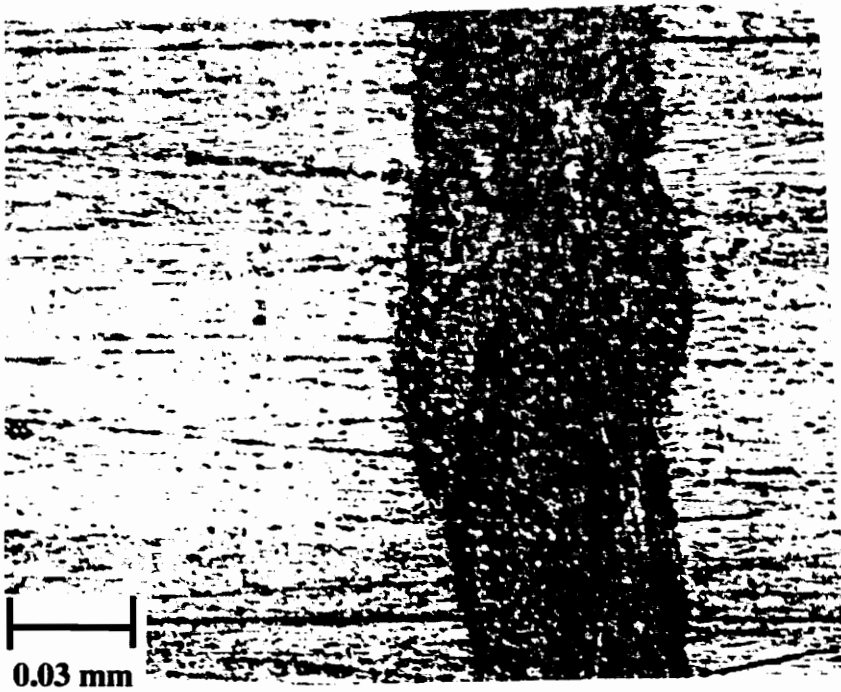


Figure 5.29: Photograph taken on the Nikon Epiphot around a stitch of a preform with 0.2" stitch spacing and 1/8" stitch pitch

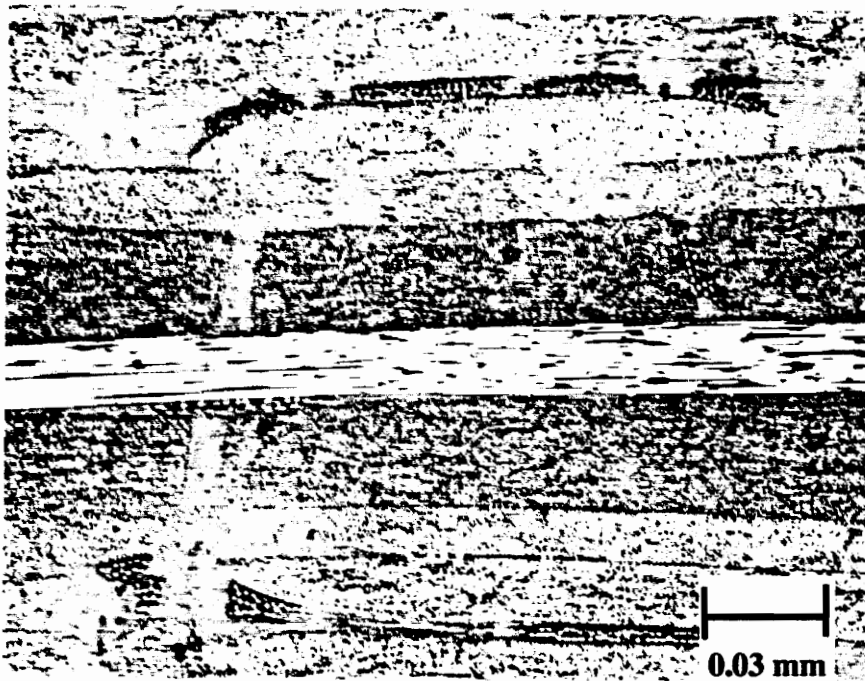


Figure 5.30: Photograph taken on the Nikon Epiphot between two stitches of a panel with 0.5" stitch spacing and 1/8" stitch pitch.



Figure 5.31: Photograph taken on the Nikon Epiphot between two stitches of a panel with 0.2" stitch spacing and 1/8" stitch pitch.

level in the preform with 0.5" stitch spacing, while the preform with the 0.2" stitch spacing is highly compacted. The region around the stitch will be referred to as the "nip" region. This region contains misaligned fiber tows that are bunched together. Figure 5.32 shows a schematic diagram of the "nip" region. The $\pm 45^\circ$ plies are the most affected by this phenomenon, and since 45% of the plies in the multiaxial warp knit fabric consist of tows in these directions, this effect could be significant. It is speculated that stitching causes two things to happen. Firstly, openings are created around the stitch as the fibers are pushed away when the stitching needle penetrates the preform. Secondly, the fibers are distorted and misaligned in the region between two rows of stitching. The extent to which both of them can occur depends on the stitch spacing, stitch pitch and tension of the stitching thread. The situation could also be visualized as a problem concerning a beam on supports subjected to a load. The distance between the supports, analogous to the stitch spacing, determines the extent to which the beam or tows can deflect or move. Therefore, the larger the stitch spacing, the greater the movement of the fiber tows between two rows of stitching. The amount of bunching of tows around the stitch region however, depends on both the stitch pitch and the tension used on the thread during the stitching operation. Therefore, for a given stitch spacing, the 1/8" pitch will always have a higher permeability than the 1/6" pitch.

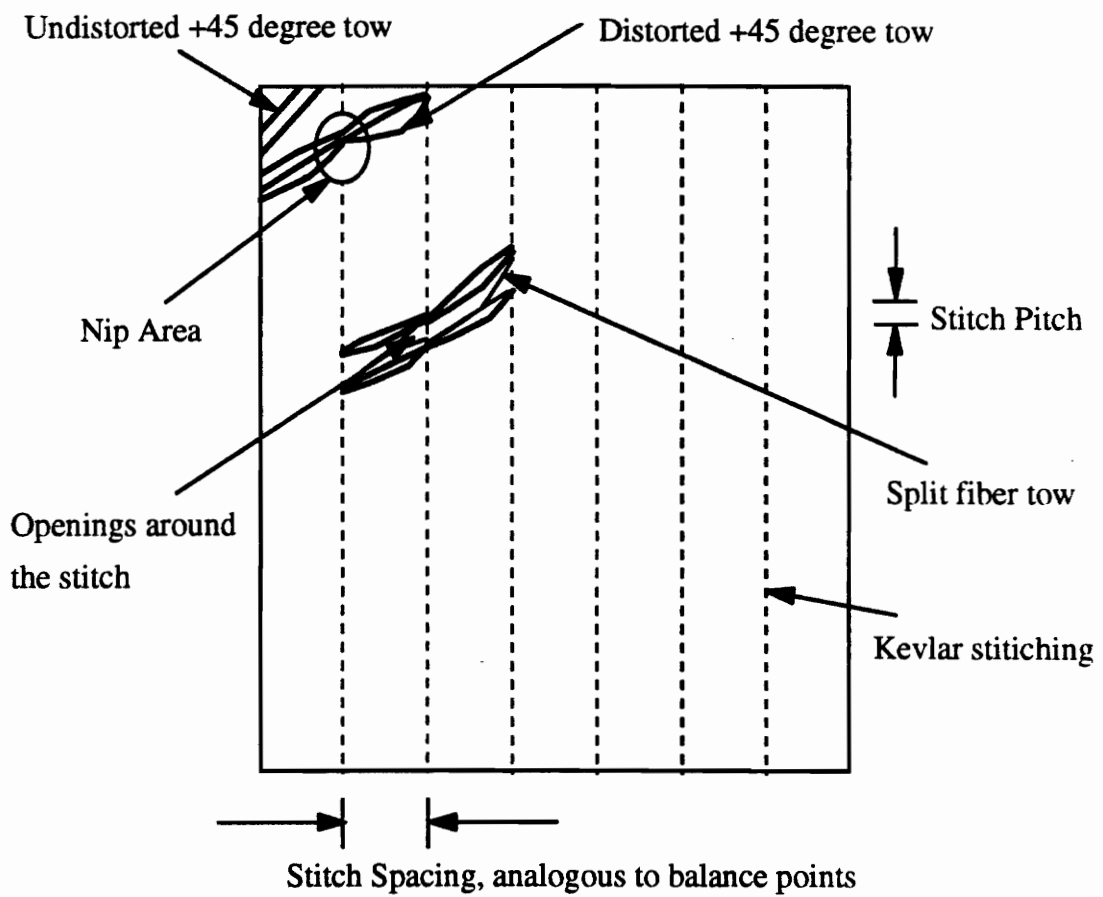


Figure 5.32: Schematic diagram of the misalignment in the individual fiber tows caused by stitching.

5.5 BRAIDED PREFORMS

A detailed description of the braided preforms along with the test procedures has been outlined in Section 3.3. Two sets of preforms were tested in order to study the effects of braiding angle and thickness on permeability and compaction.

5.5.1 Braiding Angle

In order to study the effects of braiding angle on permeability and compaction, triaxially braided preforms with braiding angles of $\pm 60^\circ$ and $\pm 70^\circ$ were tested. The areal weights of the preforms are given in Table 3.1. Figure 5.33 is the plot of fiber volume fraction as a function of compaction pressure for both the preforms. The constants of the power law model are given in Table 5.2. The $0\pm 60^\circ$ braided preform is seen to require a larger compaction load as compared to the $0\pm 70^\circ$ to achieve the same fiber volume fraction. However, at higher fiber volume fractions ($v_f > 0.63$), both curves tend to merge. A possible reason for this could be because of the well conforming architecture that results during braiding. This conforming architecture results in excellent “nesting”. Nesting, as the word indicates, is the process by which fiber tows in individual plies pack upon the application of an external load. Therefore, at higher fiber volume fractions, both preforms have nested extremely well and therefore exhibit almost the same compaction loads.

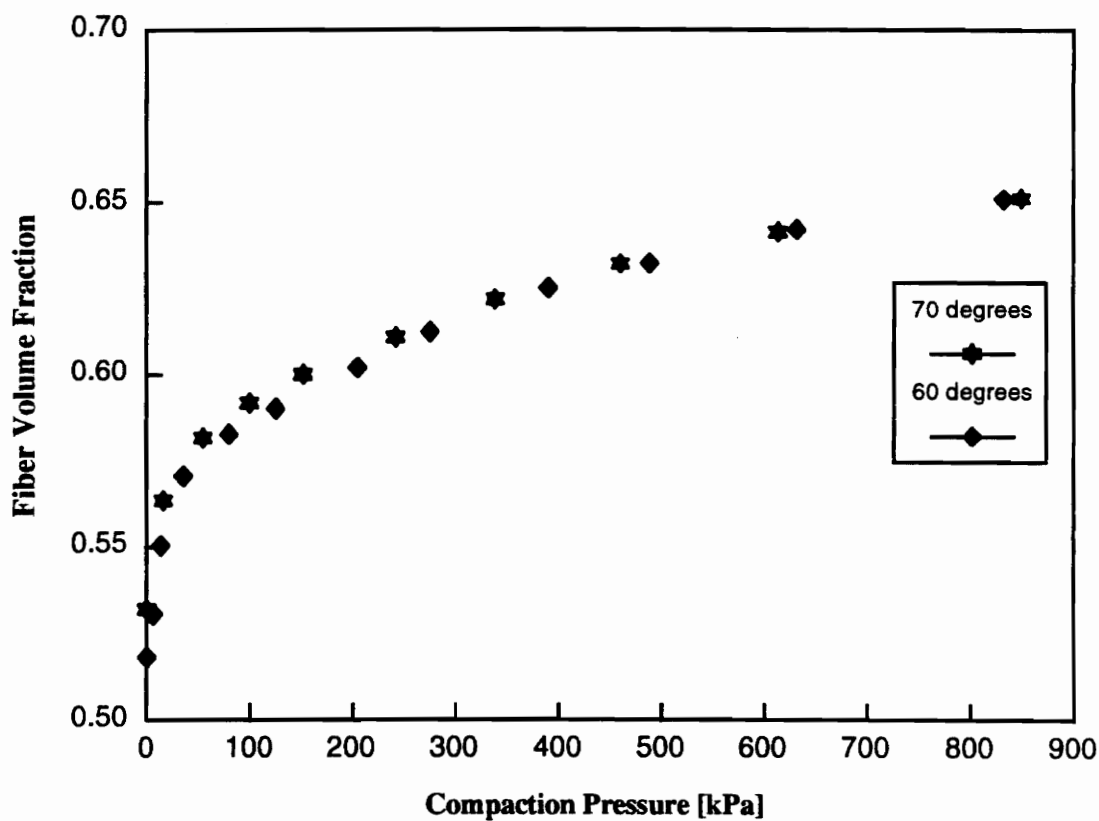


Figure 5.33: Fiber volume fraction as a function of compaction pressure for preforms with 60 and 70 degree braiding angles.

Figure 5.34 is a plot of in-plane permeability, in the along the stitching direction, as a function of fiber volume fraction. The constants of the power law regression model are given in Table 5.4. The $0\pm 60^\circ$ preform is seen to have a much higher permeability compared to the $0\pm 70^\circ$ preform over the range of fiber volume fractions measured. Figure 5.35 is a plot of the permeability as a function of fiber volume fraction measured normal to the stitching direction. The permeability for the $0\pm 60^\circ$ preform is just slightly higher than permeability for the $0\pm 70^\circ$ preform. Figure 5.36 is a plot of the through-the-thickness permeability as a function of fiber volume fraction for both the preforms. The 70° preform has a higher initial compaction at fiber volume fractions less than 56% which results in a lower permeability. Above 56% fiber volume fraction, the permeability of the 70° preform is higher than the permeability of the 60° preform.

5.5.2 Thickness Effects

Figure 5.37 is a plot of fiber volume fraction as a function of compaction pressure for both the thick and thin braided preforms. The thick and thin braided preforms consisted of 14 and 4 braid tubes, respectively. Both preforms had a braiding angle of $0\pm 60^\circ$. The areal weights of the preforms are given in Table 3.1. From the compaction curves it is evident that there is a significant thickness effect for the braided systems. Both preforms have the same initial fiber volume fraction. The thin

Table 5.4: Constants for the Permeability Fit Equation

Material Type	Test Conducted	Number of Plies/Tubes Used	Constant 'a' (in m²)	Constant 'b'
Braided Preform 0°±60°	Along Stitching	10	1.6 E-15	-18.86
	Normal to Stitching	10	2.5 E-15	-11.91
	Through-the-Thickness	10	2.6 E-17	-16.55
	Along Stitching	4	1.5 E-15	-15.14
	Normal to Stitching	4	8.0 E-16	-14.89
	Through-the-thickness	4	5.7 E-14	-5.47
	Along Stitching	14	4.2 E-17	-23.22
	Normal to Stitching	14	8.2 E-17	-20.02
	Through-the-thickness	14	1.8E-15	-11.25
	Along Stitching	9	1.8 E-18	-32.52
Braided Preform 0°±70°	Normal to Stitching	9	3.0 E-16	-18.52
	Through-the-thickness	9	2.4 E-16	-12.77

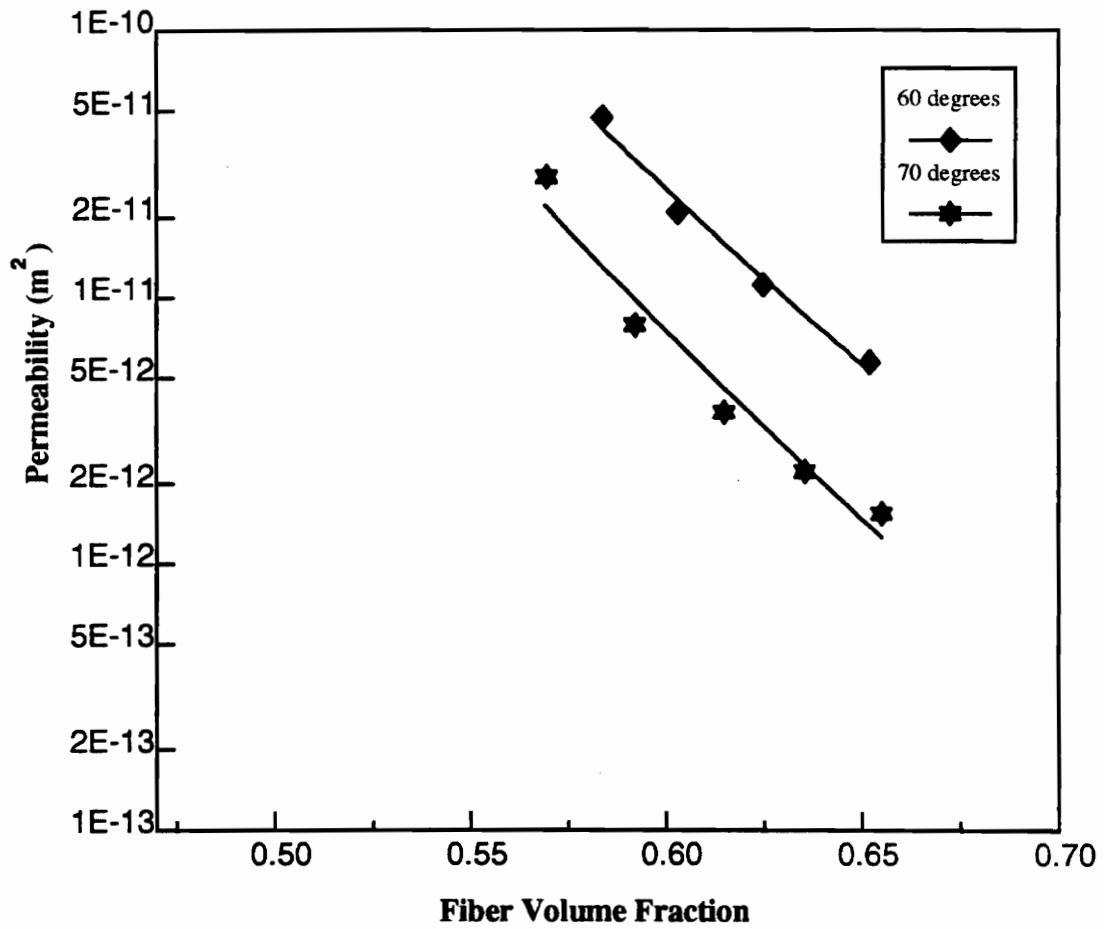


Figure 5.34: In-plane permeability as a function of fiber volume fraction for the braided preforms measured along the stitching direction. Legend indicates braiding angle.

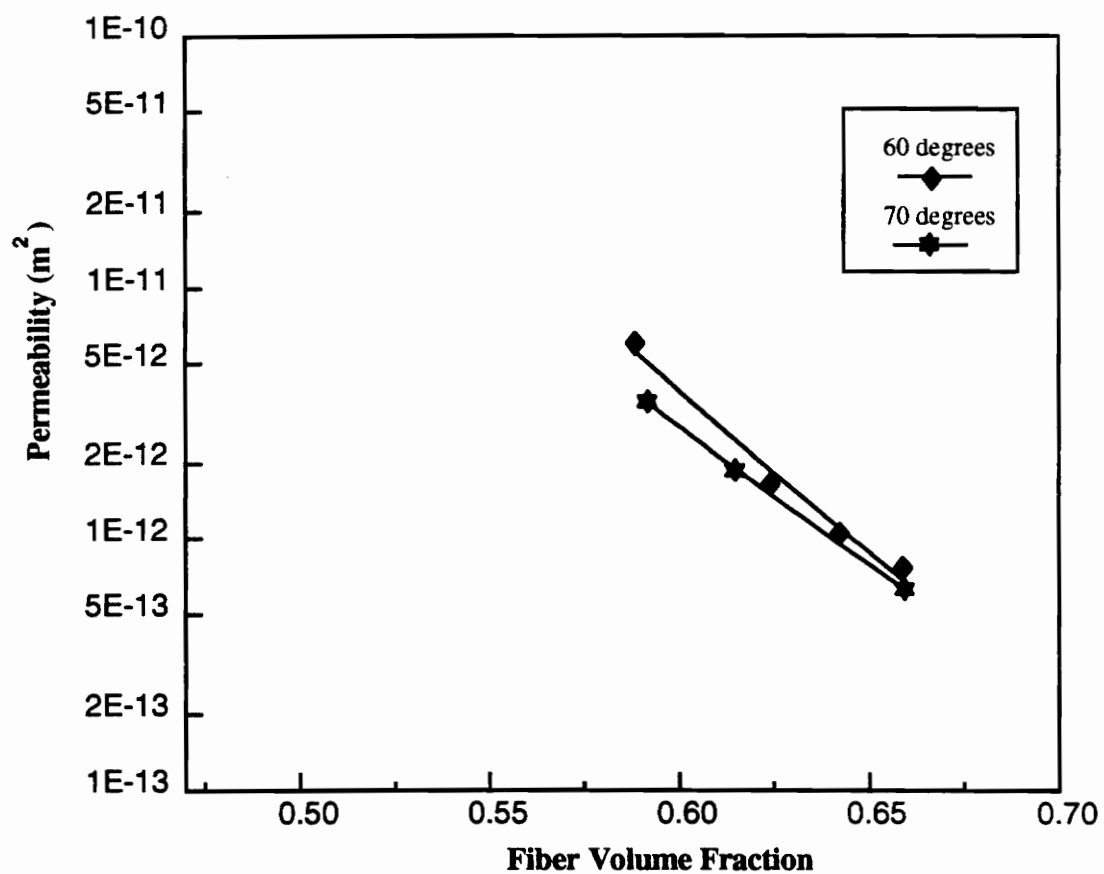


Figure 5.35: In-plane permeability as function of fiber volume fraction for the braided preforms measured normal to the stitching. Legend indicates braiding angle.

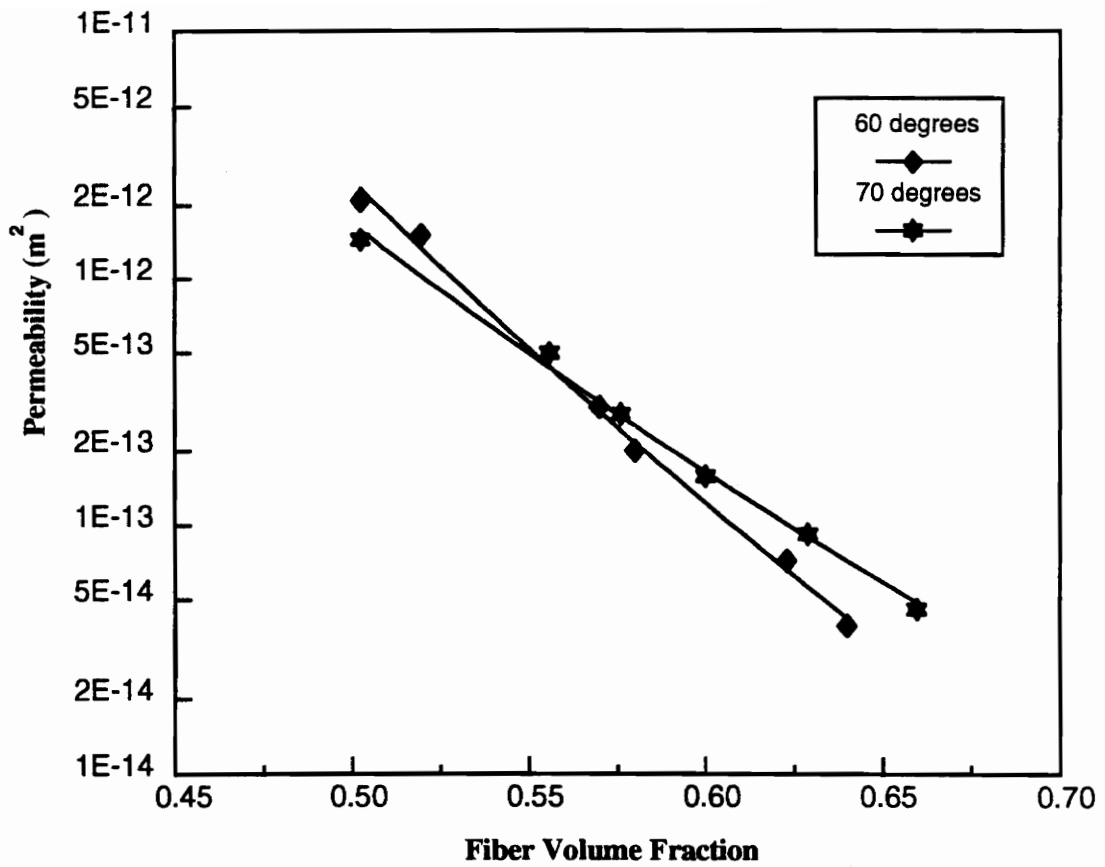


Figure 5.36: Through-the-thickness permeability as function of fiber volume fraction for the braided preforms. Legends indicate the braiding angle.

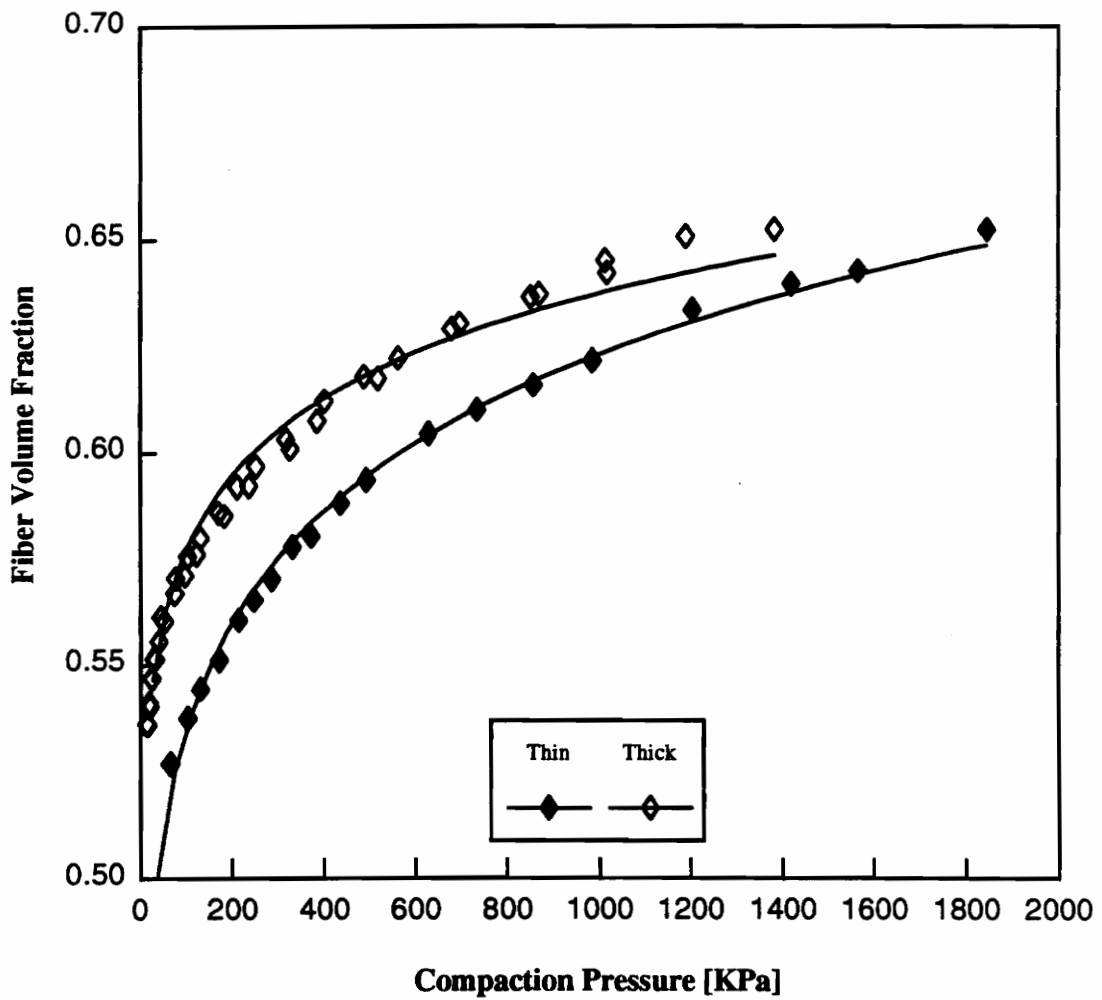


Figure 5.37: Fiber Volume Fraction as a function of compaction pressure for thick and thin braided preforms. Braiding angle was 60 degrees.

preform is seen to require a much higher compaction pressure to achieve the same fiber volume fraction as compared to the thick preform.

Figure 5.38 is a plot of the in-plane, along the stitching direction, permeability as a function of fiber volume fraction. The thick preform has a higher permeability compared to the thin preform. However, the drop in permeability with increasing fiber volume fraction is greater for the thick preform. This could be attributed to the nature of their individual compaction curves. At very high fiber volume fractions both the preforms exhibit the almost the same permeability. Figure 5.39 shows a plot of the in-plane, normal to the stitching direction, permeability as a function of fiber volume fraction. Once again the thick preform is seen to exhibit a higher permeability as compared to the thin preform. The through-the-thickness permeability behavior is shown in Figure 5.40. At low fiber volume fractions, both preforms have almost the same permeability. However, as the fiber volume fraction increases, the thick preform has a lower permeability as compared to the thin preform. The constants of the power law regression are given in Table 5.4.

5.6 SIZING EFFECTS ON PERMEABILITY

The mechanical properties of composites are largely affected by the properties of the interface between the fiber and the matrix. Poor fiber-matrix adhesion caused due to several reasons has been the primary reason. Fiber manufacturers, will use a

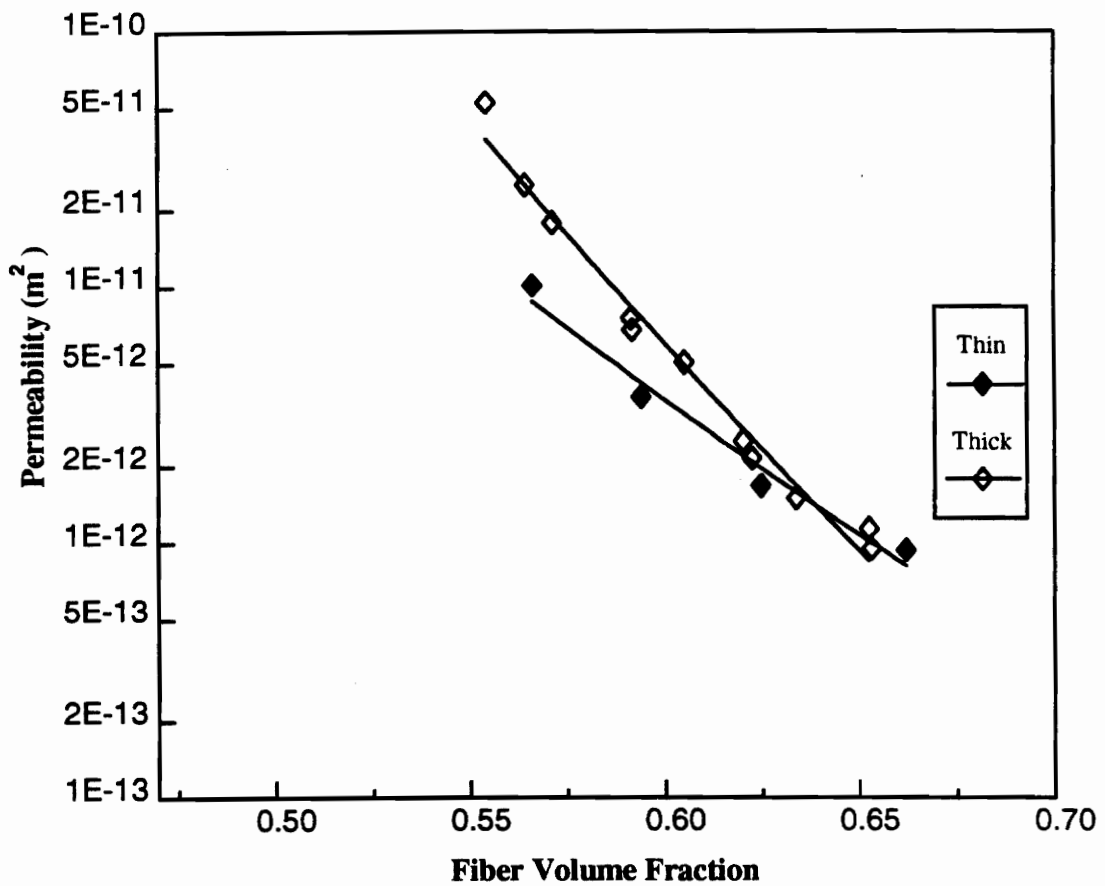


Figure 5.38: In-plane permeability as function of fiber volume fraction for thick and thin braided preforms measured along the stitching direction.

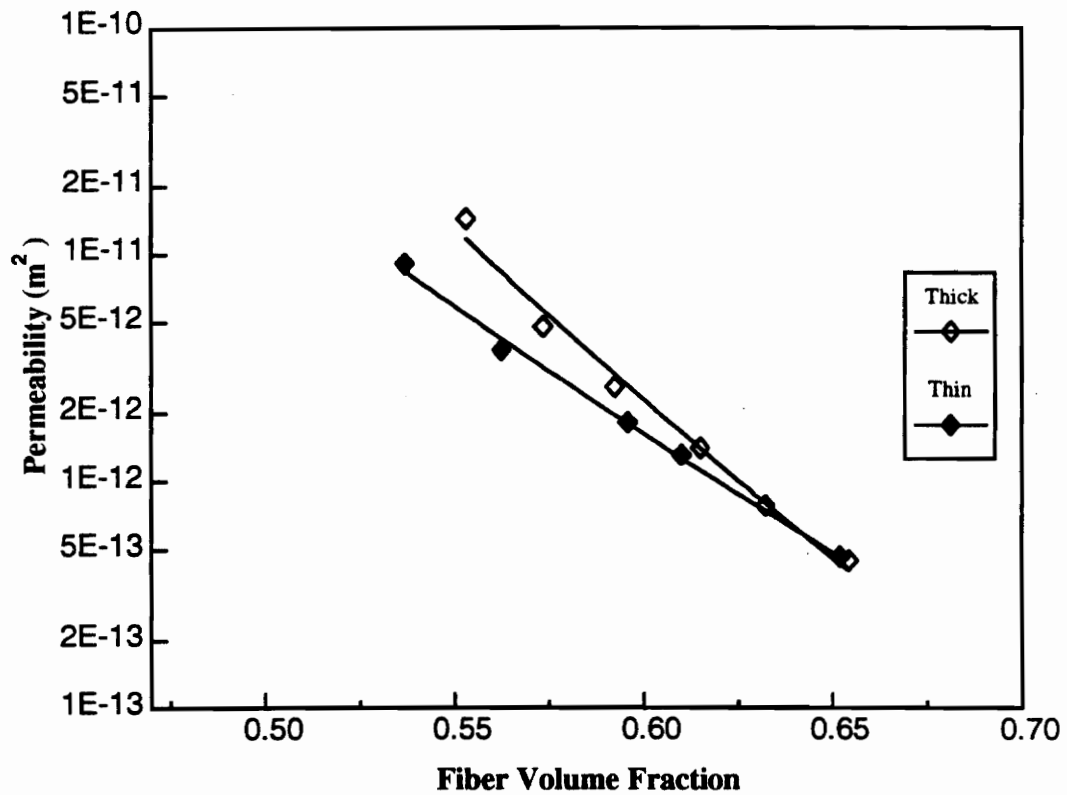


Figure 5.39: In-plane permeability as function of fiber volume fraction for thick and thin braided preforms measured normal to the stitching direction.

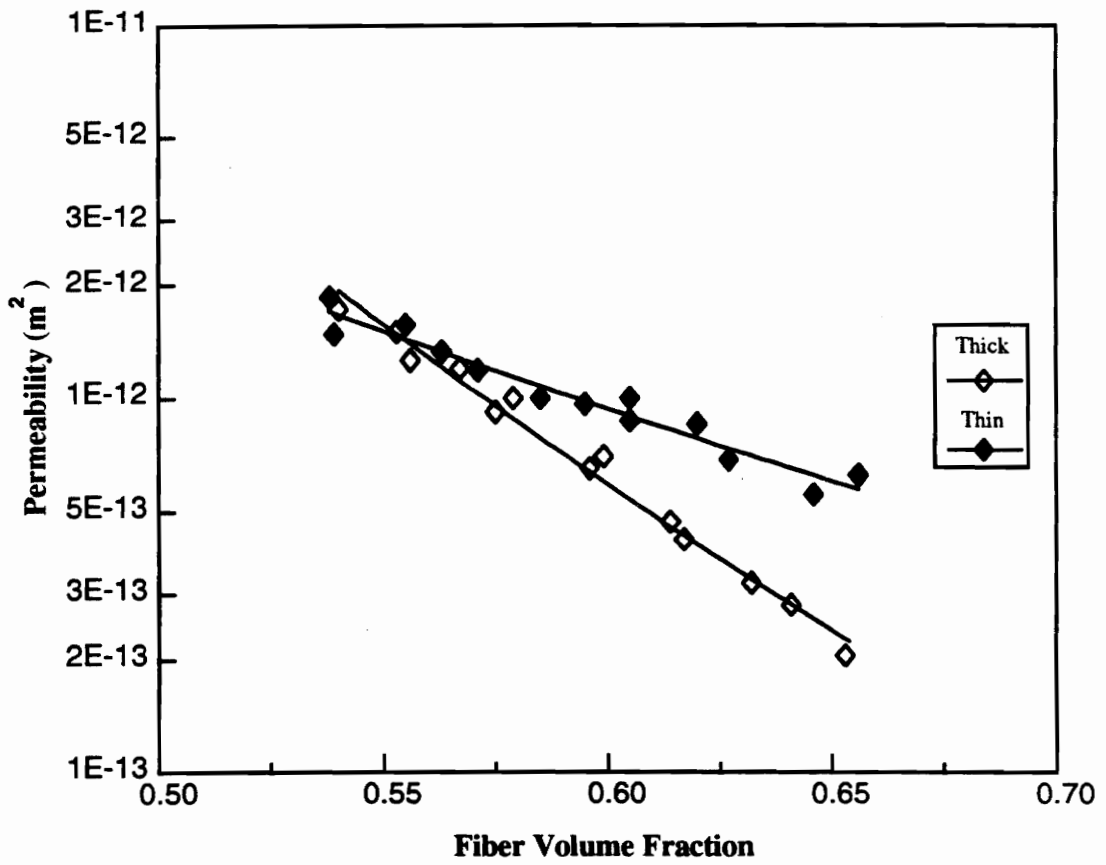


Figure 5.40: Through-the-thickness permeability plot for the thick and thin braided preforms.

fiber surface treatment agent or sizings to enhance the adhesion between the fiber and the resin. The sizing agents depend on the type of resin to be bonded to the fiber and are more than often proprietary. Two systems were examined in this study and the results obtained are presented in the following sections.

5.6.1 AS-4 Carbon Fiber

A plain weave, unsized AS-4 carbon fabric was tested along with another batch of plain weave AS-4 carbon fabric with proprietary 'W' sizing. Figures 5.41 and 5.42 show plots of in-plane permeability in the warp and fill directions, respectively. 10 plies of fabric were used in the tests. Table 5.5 presents the constants for the power law regression model. It is seen that sizing tends to increase the permeability in both directions. Figure 5.43 is a plot of in-plane permeability, in the warp and fill directions, as a function of fiber volume fraction for the unsized fabric. The curves are seen to lie close to each other as expected for a plain, balanced weave fabric with equal number of fill yarns as compared to warp yarns.

5.6.2 Glass Fiber

A batch of 7781, 8 harness satin weave E-glass fabrics with F-16 and F-72 finishes were tested. The results of the various tests performed on this system are presented in Figures 5.44 - 5.47. The fabric had an extremely glossy appearance because of the finish, and was extremely thin and fragile. It therefore, posed a lot of

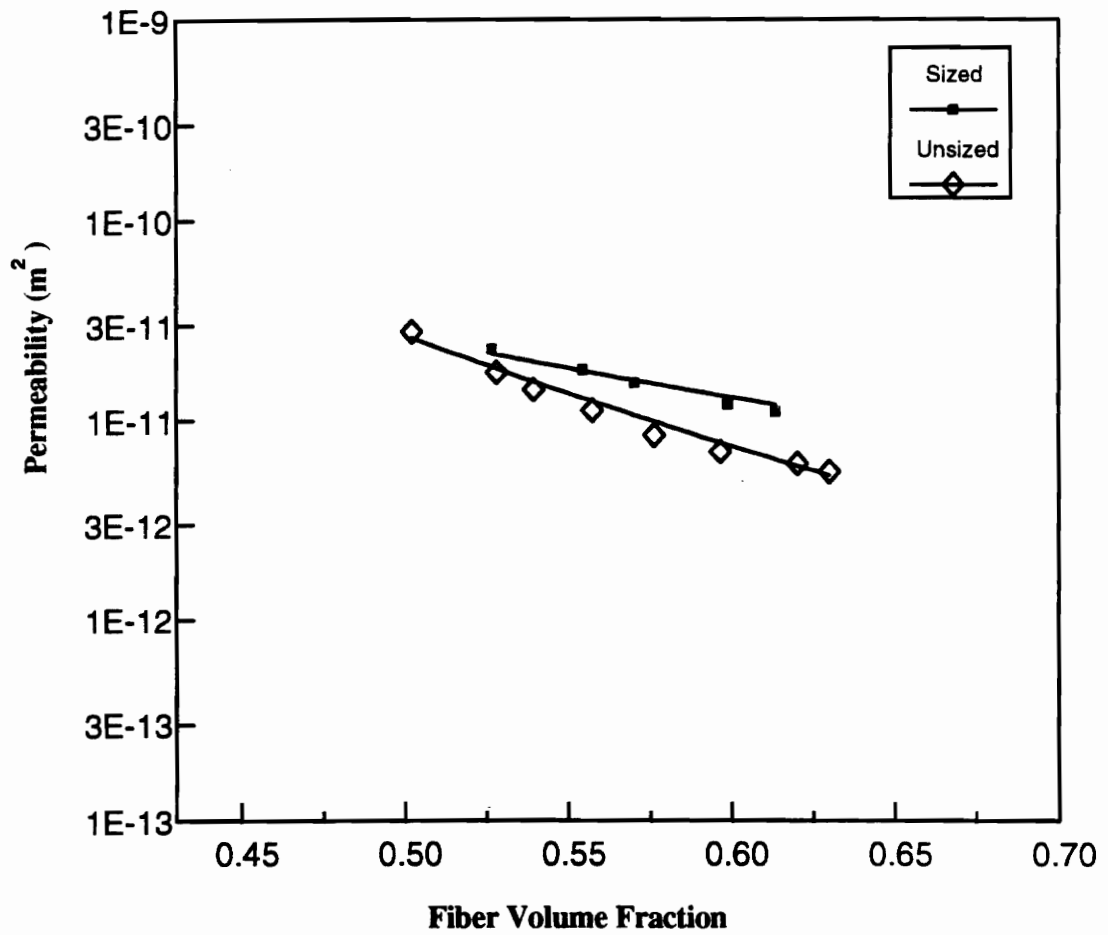


Figure 5.41: In-plane, warp direction permeability as a function of fiber volume fraction for 'W' sized and unsized AS4 fabric.

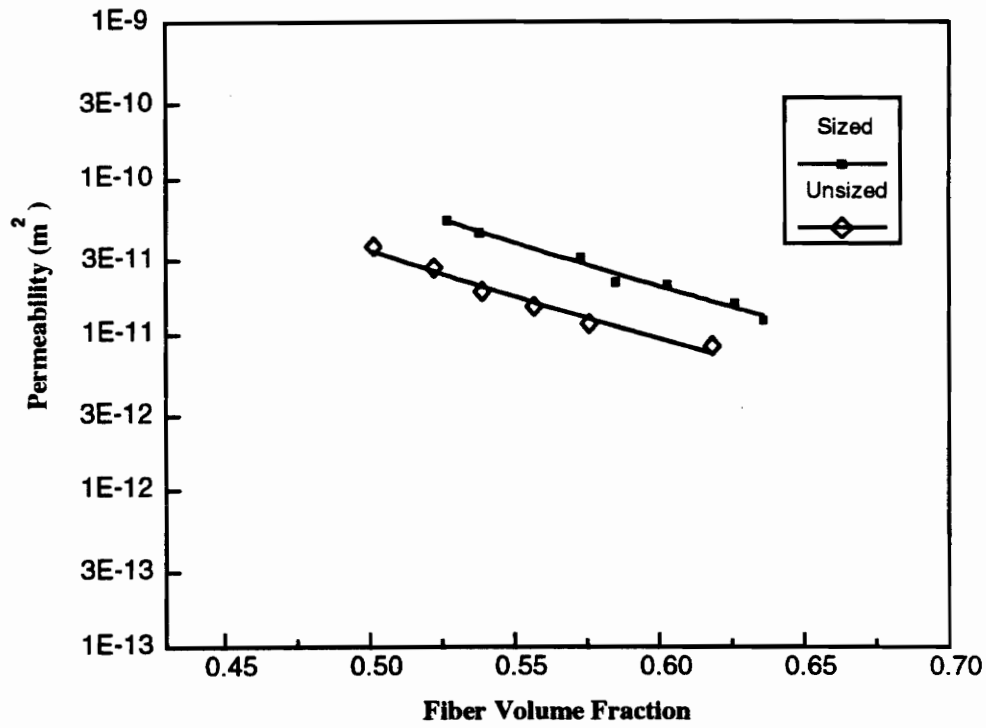


Figure 5.42: In-plane, fill direction permeability as function of fiber volume fraction for 'W' sized and unsized AS4 fabric.

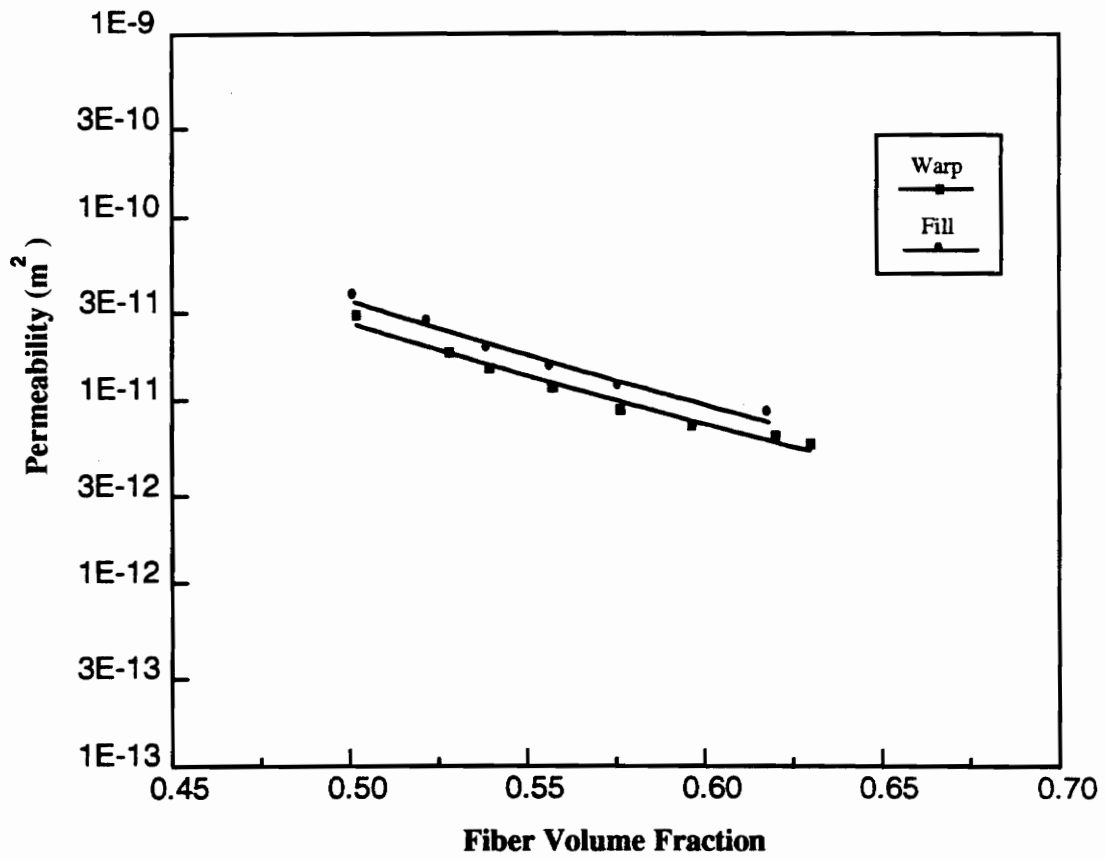


Figure 5.43: In-plane permeability as function of fiber volume fraction for unsized AS4 fabric.

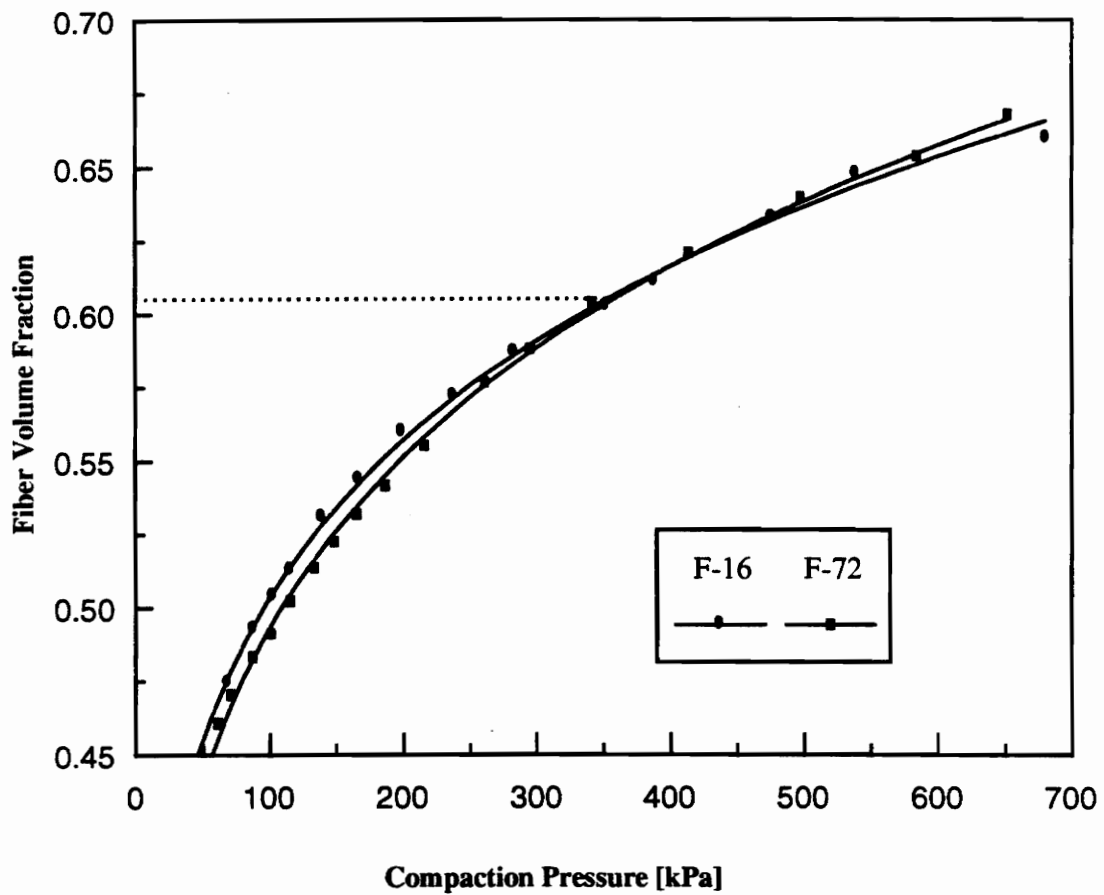


Figure 5.44: Fiber volume as a function of compaction pressure for F16 and F72 finished 7781 E-glass fabrics.

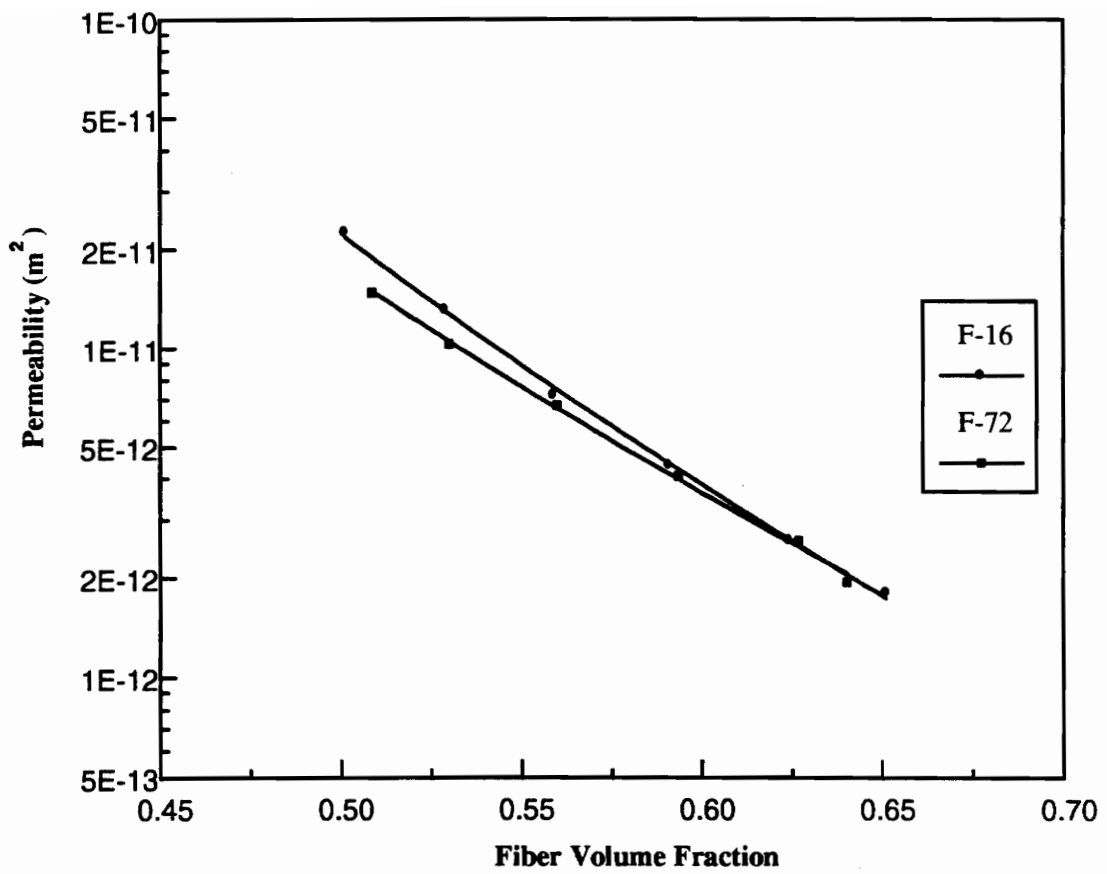


Figure 5.45: In-plane permeability plots for finished E- glass fabrics measured in the warp direction.

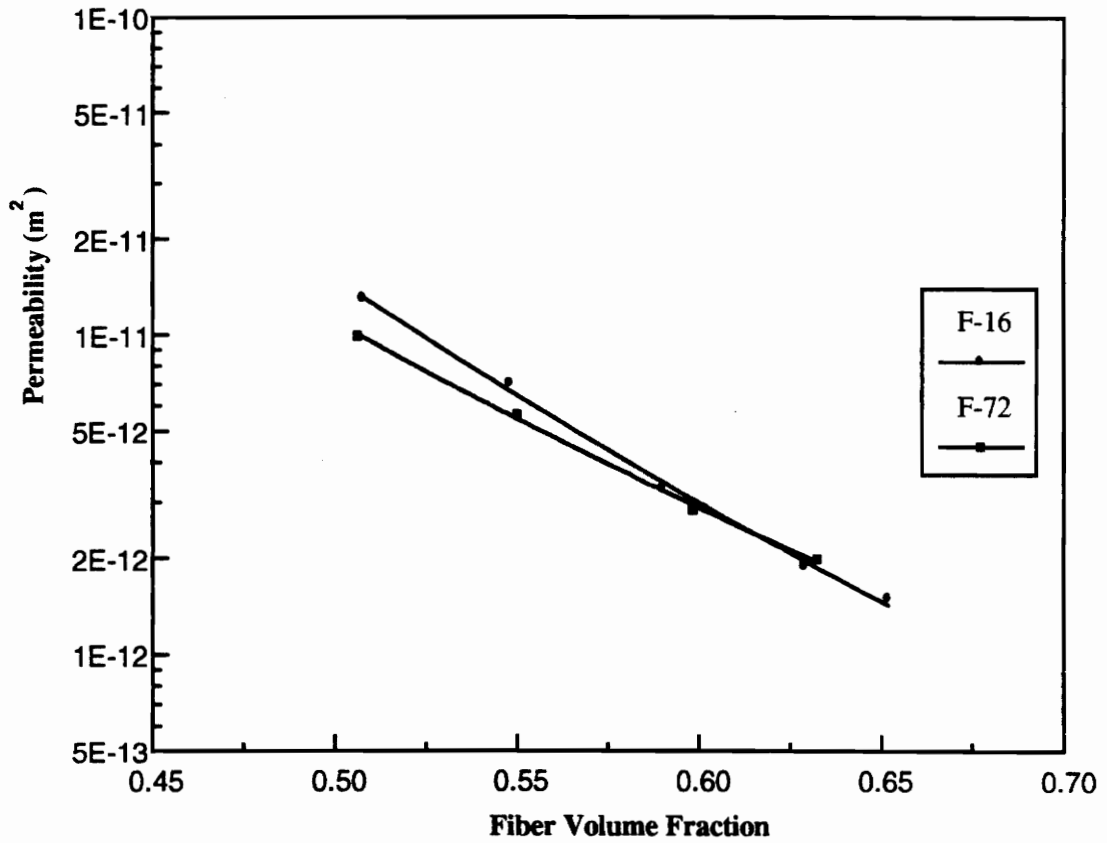


Figure 5.46: In-plane permeability plots for finished E-glass fabrics measured in the fill direction.

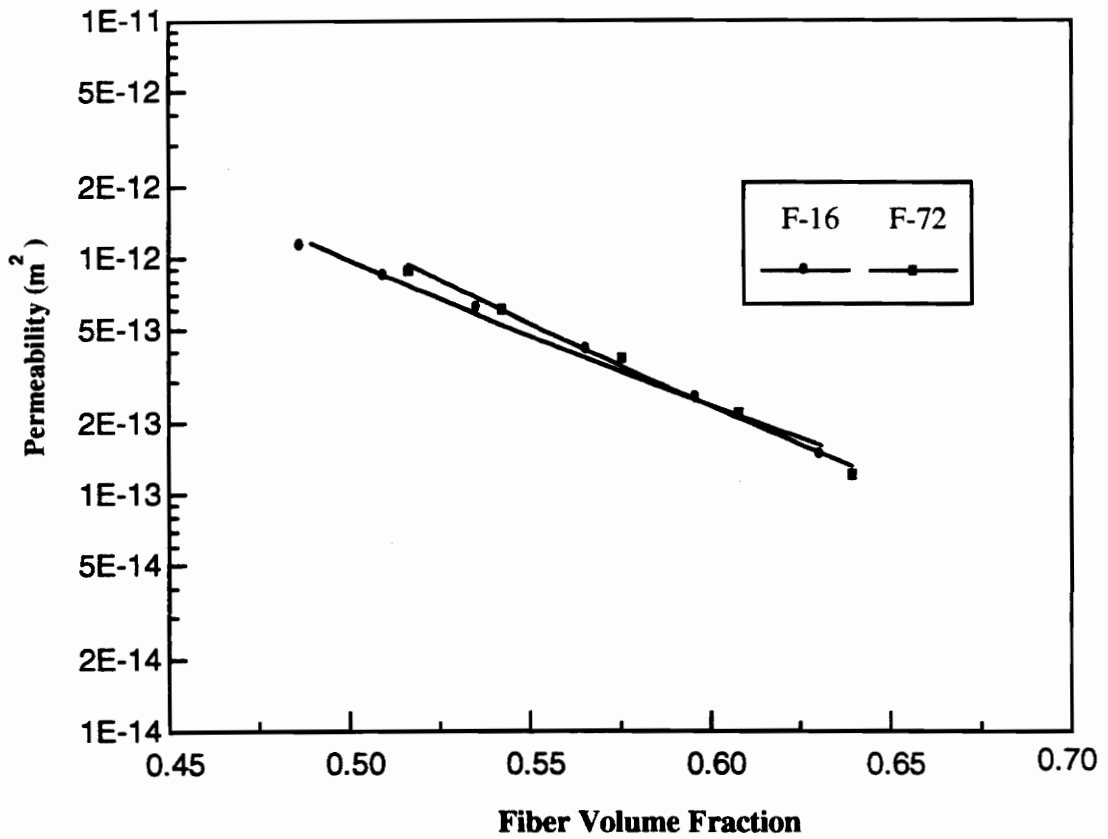


Figure 5.47: Through-the-thickness permeability as a function of fiber volume fraction for finished E-glass fabrics.

Table 5.5: Constants for the Permeability Fit Equation

Material Type	Test Conducted	Number of Plies Used	Constant 'a'[*] (in m²)	Constant 'b'[*]
AS 4 Fabric Unsize	Warp	10	2.0 E-13	-6.99
	Fill	10	2.4 E-13	-7.17
AS 4 Fabric 'G' Sized	Warp	10	5.3 E-13	-4.91
	Fill	10	2.4 E-12	-4.05
Glass Fabric 'F 16' Finish	Warp	16	5.0 E-13	-5.62
	Fill	16	2.7 E-14	-9.67
	Through-the-Thickness	16	4.3 E-15	-7.82
Glass Fabric 'F 72' Finish	Warp	16	4.4 E-14	-8.61
	Fill	16	6.7 E-14	-7.34
	Through-the-Thickness	16	2.1 E-15	-9.23

Note:

* The fit equation for the constants is $Permeability = a * (Fiber Volume Fraction)^b$

difficulty in cutting and handling and resulted in excessive fraying of the fiber tows from the edges. 16 plies of the fabric were used in all the tests. The constants of the power law regression for the compaction tests are reported in Table 5.2. The compaction curves are seen to lie very close to each other with the load required to compact the F-72 fabric being slightly higher than that required for the F-16 fabric.

The in-plane permeability plots (Figures 5.45 and 5.46) for the fabric with the F-16 finish is higher in both the warp and fill directions. This may be due to the fact that it takes less pressure to compact the F-16 finished fabric to a given fiber volume fraction compared to the F-72 fabric (Figure 5.44). The through-the-thickness permeability plot is presented in Figure 5.47. The through-the-thickness permeabilities for the two finished fabrics are quite similar. The constants of the power law regression for the permeability tests are presented in Table 5.5.

Chapter 6

CONCLUSIONS AND FUTURE WORK

The focus of this research was to characterize different fabrics and preforms and determine the compaction and permeability responses as a function of fiber volume fraction. These responses are of particular importance in resin transfer molding, resin film infusion molding and other similar manufacturing processes as resin is made to infiltrate a dry preform compacted to the desired fiber volume fraction.

It was also an objective of this research to understand the effects of through-the-thickness stitching on the compaction and permeability behavior of multiaxial warp knit preforms.

A brief statistical study was also conducted to try and calculate confidence bounds about the least squares regression curve of the steady state permeability measurements and compare that with the advancing front permeability measurement.

6.1 CONCLUSIONS

The fiber volume fraction and in-plane and through-the-thickness permeabilities of multiaxial warp knit preforms with different stitching densities were measured as a function of compaction pressure. The densities varied from zero, an unstitched material, to 40 penetrations per square inch. From the compaction data, it

was observed that the compaction curve had two regions. An initial linear region and the non-linear region at higher fiber volume fractions. The initial fiber volume fraction increased with an increase in stitching density. It was also seen that increase in stitching density, resulted in significantly higher pressures being required in order to achieve the same fiber volume fraction as compared to a similar unstitched preform.

The stitching pitch was seen to have a major influence on the in-plane permeability. For a given stitch spacing, the preform with the higher stitch pitch had a higher along the stitching direction permeability. However, normal to the stitching, the preform with the smaller stitch pitch had the higher permeability. In the through-the-thickness direction, the stitched preforms had a higher permeability as compared to the unstitched preform. However, in the stitched preforms the preform with the larger stitch spacing was seen to have a higher permeability as compared to the preform with the smaller stitch spacing. For a given stitch spacing however, increasing the stitch pitch was seen to result in a higher permeability.

Compaction and permeability tests were performed on 2-D, triaxially braided preforms. The braiding angle was $0^{\circ}\pm 60^{\circ}$. Preforms consisting of 4 and 14 tubes were studied in order to assess the effects of thickness. It was seen that the thin preform required a larger amount of pressure to compact it down to the same fiber volume fraction as compared to the thick preform. The in-plane permeability was seen to be higher for the thick preform compared to the thin preform except at very high fiber volume fractions where they were almost the same. The through-the-thickness

permeability was almost the same for both preforms at low fiber volume fractions. However, at higher volume fractions, the thin preform was seen to have a higher permeability compared to the thick preform.

The statistical study indicated that the steady state permeability data obtained lay between a 50% confidence bound. However the advancing front infiltration pressure data when compared to the steady state measurements, tended to at times move below the lower confidence bound.

Tests were performed on glass fabrics with different finishes and sized and unsized carbon fabrics. The sized fabrics showed higher values of permeability compared to the unsized fabrics.

6.2 FUTURE WORK

Tests should be directed more to the individual 7 ply sub units that make up the preform. A complete understanding of this unit could then be used in trying to understand the effects of stacking up these base units and then finally introducing the effects of stitching.

Perform tests on multiaxial warp knit preforms with a wider range of stitching densities in order to develop a better correlation between stitching density and permeability and compaction.

Develop a more elaborate statistical approach in studying permeability. It is clear that there are several factors that influence the reproducibility of permeability measurements.

REFERENCES

- [1] Becker, W, "Tooling for Resin Transfer Molding", presented at the Resin Transfer Molding Clinic for Aerospace Industry, Los Angeles, CA., (April 1992)
- [2] Darcy, H, *Les Fontaines Publiques de la Villa de Dijon*. Dalmont: (1856)
- [3] Gauvin, R. and M.Chibani. "The Modelling of Mold Filling in Resin Transfer Molding." *International Polymer Processing*, Vol 1, pp.42-46 (1986)
- [4] Molnar, J.A., L.Trevino and L.J.Lee. "Mold Filling in Structural RIM and Resin Transfer Molding." 44th Annual Conference, Composites Institute, SPI (1989)
- [5] Fracchia, C.A. and C.L. Tucker III. "Simulation of Resin Transfer Mold Filling." presented at the 6th Annual Meeting, Nice, France, Polymer Processing Society, (1990)
- [6] Gebart, B.R., L.A. Strombeck and C.Y. Lundemo. "Permeability of Reinforcement Materials for RTM." presented at the 6th Annual Meeting , Nice, France, Polymer Processing Society, (1990)
- [7] Carman, P.C. "Fluid Flow Through Granular Beds", *Trans. Intl. Chemical Eng.*, (1937), Vol 15, pp.150-166
- [8] Gutowski, T.G., Z. Cai, S.Bauer, D.Boucher, J.Kingery and S. Wineman. "Consolidation Experiments for Laminate Composites", *Journal of Composite Materials*, (1987), Vol. 21, pp.650-669
- [9] Kim, Y.R, S.P.McCarthy, J.P.Fanucci, S.C.Nolet, and C.Koppernaes. "Resin Flow Through Fiber Reinforcements During Composite Processing." in L.D.Michelove et al. (eds.), 22nd International SAMPE Technical Conference, SAMPE, Covina, Ca., (1990), pp.709-723
- [10] Skartsis, L., J.L. Kardos, and Khomami. "Resin Flow Through Fiber Beds During Composite Manufacturing Processes. Part I: Review of Newtonian Flow Through Fiber Beds. *Polymer engineering and Science*, (Mid-November 1986), Vol.26, No. 20, pp.1434-1441
- [11] Gauvin, R. and M. Chibani. "Analysis of Composites Molding with Woven and Non Woven Reinforcements", *Proceedings of the 45th Annual Conference February 12-15, 1990*, Composites Institute, Society of the Plastics Industry, (1990) Session 9F

- [12] Greve, B.N. and J.K.Soh. "Directional Permeability Measurement of Fiberglass Reinforcements", *Polymer Composites for Structural Automotive Applications*, (1990), pp.101-113
- [13] Parnas, R.S. and F.R. Phelan, Jr. "The Effects of Heterogeneities in Resin Transfer Molding Preforms on Mold Filling", in J. Stinson, R. Adsit, and F. Gordaninejad (eds.), *36th International SAMPE Symposium*, SAMPE, Covina, Ca., Vol. 36, No. 1, (April 15-18, 1991), pp.506-520
- [14] Phelan, Jr., F.R. "Modeling of Microscale Flow in Fibrous Porous Media", *Advanced Composite Materials: New Developments and Applications: Proceedings of the 7th Annual ASM/ESD Advanced Composites Conference*, ASM International, Materials Park, Ohio, (1991), pp.175-185
- [15] Sadiq, T., R. Parnas, and S. Advani, "Experimental Investigation of Flow in resin Transfer Molding", in T.S. Reinhart et al. (eds.), *24th International SAMPE Technical Conference*, SAMPE, Covina, Ca., (1992), pp.T660-T674
- [16] Berdichevski, A. and Z. Cai. "Preform Permeability Predictions by Self Consistent Method and Finite Element Simulation", *Polymer Composites*, Vol.14, No.2 (April 1993), pp.132-143
- [17] Astrom, B.T., R.B. Pipes, and S.G. Advani, "On Flow Through Aligned Fiber Beds and it's Applications to Composite Processing", *Journal of Composite Materials*, Vol.26, (1992), pp.1351-1373
- [18] Gauvin, R., A. Kerachni, and B. Fisa, "Variations of Mat Surface Density and it's Effects on Permeability Evaluation for RTM Modeling", *Journal of Reinforced Plastics and Composites*, Vol.13, (1994), pp.371-383
- [19] Batch, G.L. and S. Cumiskey, "Multilayer Compaction and Flow in Composites Processing", *Proceedings of the 45th Annual Conference*, February 12-15, 1990, Composites Institute, Society of the Plastics Industry, (1990), Session 9A
- [20] Pearce, N. and J. Summerscales, "The Comperessibility of a Reinforcement Fabric", *Composites Manufacturing*, Vol 6, Number 1, (1995), pp.15-21
- [21] Adams, K.L., B. Miller, and L. Rebenfeld, "Forced In-Plane Flow of an Epoxy Resin in Fibrous Networks", *Polymer Engineering and Science*, Vol. 26, No.20, Mid-November (1986), pp.1434-1441
- [22] Lam, R.C. and J.L. Kardos, "The permeability of Aligned and Cross-Plied Fiber Beds During Processing of Continuous Fiber Composites", *Proceedings of the American Society for Composites 2nd Technical Conference*, (1988), pp.3-11

- [23] Adams, K.L. and L. Rebenfeld, "In-plane flow of fluids in fabrics: structure/flow characterization", *Journal of Textile Research*, Vol.57, (1987), pp.647-654
- [24] Molnar, J.A., L. Trevino, and L.J. Lee, "Mold Filling in Structural RIM and Resin Transfer Molding", *Proceedings of the 44th Annual Conference*, February 6-9, 1989, Composites Institute, Society of the Plastics Industry, (1989), Session 20A
- [25] Wang, J.T., C.H. Wu, and L.J. Lee, "In-Plane Permeability Measurement and Analysis in Liquid Composite Molding", *Polymer Composites*, Vol.15:No.4, (1994), pp.278-288
- [26] Loos, A.C. and M.H. Weideman, "RTM Process Modeling for Advanced Fiber Architectures", *Advanced composite Materials: New Dvelopments and Applications: Proceedings of the 7th Annual ASM/ESD Advanced Composites Conference*, ASM International, Materials Park, Ohio, (1991), pp.209-216
- [27] Wu, C.H, T.J. Wang, and L.J. Lee, "Trans-Plane Fluid Permeability Measurement and it's Applications in Liquid Composite Molding", *Polymer Composites*, Vol.15, No.4, (1994), pp.289-296
- [28] Foley, M.F. and T. Gutowski, "The Effect of Process Variables on Permeability in the Flexible Resin Transfer Molding (FRTM) Process", *23rd International SAMPE Technical Conference*, SAMPE, Covina, Ca, (1991), pp.326-340
- [29] Ahn, K.J., J.C. Seferis, and J.C. Berg, "Simultaneous Measurements of Permeability and Capillary Pressure of Thermosetting Matrices in Woven Fabric Reinforcements", *Polymer Composites*, Vol.12, No.3, (June 1991), pp.146-152
- [30] Peterson, R.C. and R.E. Robertson, "Flow Characteristics of Polymer Resin Through Glass Fiber Preforms in Resin Transfer Molding", *Advanced Composite Materials: New Developments and Applications: Proceedings of the 7th Annual ASM/ESD Advanced Composites Conference*, ASM International, Materials Park, Ohio, (1991), pp.203-208
- [31] Dave, R. and S. Houle, "The Role of Permeability During Resin Transfer Molding", *Proceedings of 4th Technical American Society for Composites Conference: Composite Materials Systems*, (1990), pp.539-547
- [32] Williams, J.G., C.E.M Morris, and B.C. Ennis, "Liquid Flow Through Aligned Fiber Beds", *Polymer Engineering and Science*, Vol.14, No.6, (June 1974)
- [33] Cercon, L., "Optimizing Fiber Wetout for Composites Manufacturing", *Polymer Composites*, Vol.12, No.2, (April 1991), pp.81-86

- [34] Madhu, S.M. and L.T. Drzal, "Fiber matrix Adhesion and it's effects on Composite Mechanical Properties: I. Inplane and Interlaminar Shear Behavior of Graphite /Epoxy Composites", *Journal of Composite Materials*, Vol.25, (August 1991), pp.932-957
- [35] Madhu, S.M. and L.T. Drzal, "Fiber matrix Adhesion and it's effects on Composite Mechanical Properties: II. Longitudinal (0°) and Transverse (90°) Tensile and Flexure Behavior of Graphite/Epoxy Composites", *Journal of Composite Materials*, Vol.25, (August 1991), pp.958-991
- [36] Madhu, S.M. and L.T. Drzal, "Fiber matrix Adhesion and it's effects on Composite Mechanical Properties: IV. Mode I and Mode II Fracture Toughness of Graphite /Epoxy Composites", *Journal of Composite Materials*, Vol.26, No.7, (1992), pp.936-968
- [37] Munjal, A.K. and P.F. Maloney, "Braiding for Improving Performance and Reducing Manufacturing Costs for Aerospace Applications", 22nd International SAMPE Technical Conference, November 6-8, (1990), pp.1231-1242
- [38] Dow, M. and D. Smith, "Damage Tolerance Composite Materials Produced by Stitching Carbon Fabrics", *Proceedings of the 21st International SAMPE Technical Conference*, Atlantic City, N.J, (1989)
- [39] Morales, A., "Structural Stitching of Textile Preforms", 22nd International SAMPE Technical Conference, November 6-8, (1990), pp.1217-1229
- [40] Farley, G.L., "A Mechanism Responsible for Reducing Compression Strength of Through-the-Thickness Reinforced Composite Material", *Journal of Composite Materials*, Vol.26, No.12, (1992), pp.1784-1795
- [41] Farley, G.L., and L.C. Dickinson, "Removal of Surface Loop from Stitched Composites Can Improve Compression and Compression-after-Impact Strengths", *Journal of Reinforced Plastics and Composites*, Vol.II, (1992), pp.633-641
- [42] Shim, S.B., K. Ahn, and J.C. Seferis, "Flow and Void Characterization of Stitched Structural Composites Using Resin Film Infusion Process (RFIP)", *Polymer Composites*, Vol.15, No.6, (1994), pp.453-463
- [43] Fingerson, C. J., "Verification of Three-Dimensional Resin Transfer Molding Process Simulation Model", *Master's Thesis*, Virginia Polytechnic Institute and State University, 1995
- [44] Weideman, H. M., "An Infiltration Model for Manufacture of Fabric Composites By The Resin Infusion Process", *Master's Thesis*, Virginia Polytechnic Institute and State University, 1991

- [45] Pastore, M.C., "Quantification of Processing Artifacts in Textile Composites", *Composites Manufacturing*, No.4 (1993), pp.217-226
- [46] Hammond, V.H., "Verification of a Two-Dimensional Infiltration Model for the Resin Transfer Molding Process", Master's Thesis, Virginia Polytechnic Institute and State University, (1993)
- [47] Koopmans, L.H., "Introduction to Contemporary Statistical Methods", 2nd edition, PWS Publishers, (1987), pp.302

Vita

Kandathil Eapen Verghese “Nikhil” was born on March 11, 1971, to Mary and Kandathil V. Verghese in Calcutta, India. He grew up in different towns in northern India and attended public school at Lawrence School in Lovedale, Ooty. In 1989 he graduated from school and joined Manipal Institute of Technology in the fall of 1989 to study engineering. Mr. Verghese graduated with a first class with distinction in 1993, with a Bachelor of Science degree in Mechanical Engineering from Mangalore University, standing 2nd in a batch of 200. Nikhil then joined VPI&SU in the fall of 1993 to pursue a Master of Science degree in Materials Science and Engineering with a focus on processing of polymer matrix composites. He graduated with his Masters in February of 1996. As of this writing, Nikhil is pursuing his doctoral work in the Materials Engineering and Science department at VPI.

Verghese
(25th March 1996)